# TARGETTING OF DISTINCT CILIARY PKD2 COMPLEXES IN CHLAMYDOMONAS REINHARDTII

by

#### POULOMI DAS

(Under the Direction of Karl F. Lechtreck)

#### **ABSTRACT**

Chlamydomonas PKD2 localizes into two distinct ciliary compartments (zones). In the distal cilium, PKD2 anchors mastigoneme in two rows. The distal PKD2 is stably connected to axoneme making it a stationary complex. The proximal cilium has more mobile PKD2 complex as it hops on-off from axoneme. Pull-down of detergent soluble PKD2 complex recognized a novel protein SIP, a single pass transmembrane protein. SIP has homology with the first transmembrane helix (TMH) of PKD2 and is part of both distal and proximal PKD2 complexes as sip knock-out has reduced ciliary PKD2 and no mastigoneme rows. Proximity labeling by PKD2-miniTurbo recognized a distally distinct protein, MST3, a 5-TMH protein like PKD2 with an incomplete PKD domain. The PKD domain of MST3 is predicted to be completed by SIP. In mst3 knockout strain distal PKD2 is largely absent. Another study via cryo-EM also discovered MST3 as the central backbone of mastigonemes. MST3 has a large extracellular domain adorned with numerous MST1 glycoproteins. Thus, MST3 is unique to the distal PKD2 complex.

Chlamydomonas Genome scanning and domain predictions gave seven more gene hits whose gene products are 5-TMH proteins like MST3. All the seven proteins are

predicted to form complex with SIP. Mass-spectrometry analysis showed that three out of the seven hits are ciliary proteins. To access, if the ciliary proteins are indeed a part of PKD2 interactome, endogenously tagged PKD2-mNG<sup>CRISPR</sup> strain has been established as a tool to generate knockouts of the respective proteins. One out of the three knock-outs, *scv (scavenger)*, showed phenotypic defect in PKD2-mNG as it lacks the proximal PKD2. Endogenously tagged SCV-mNG localizes to the proximal cilia. Thus, SCV is a part of the proximal PKD2. Double knock-out *mst3 scv*PKD2-mNG reveals the abruption of both PKD2-mNG zones with only few randomly dotted PKD2-mNG moving via IFT (intraflagellar transport) indicating that MST3 and SCV are the distal and proximal zonal markers, respectively, for the specific PKD2 targeting. This study revealed a surprising heterogenicity of PKD2 complexes in cilia of *Chlamydomonas*. Thus, SIP, MST3 and SCV are established as novel interactors of PKD2 in *Chlamydomonas*.

INDEX WORDS: PKD2, mastigoneme, IFT, TMH, SCV, CRISPR

Targetii	ng of	distinct	ciliary	PKD2.c	omplexes	in Chlo	amydomonas	reinhardtii
Iuigoni	15 01	arstinet	CILICITY	111020	Ompienes		iniyaonionias	I Cillian airi

by

## Poulomi Das

Integrated Masters in Biology (Major) and chemistry (Minor),
National Institute of Science Education and Research (NISER), India, 2019

A Dissertation Submitted to the Graduate faculty of the University of Georgia in

Partial Fulfillment for the Requirements of Degree

Doctor of Philosophy

Athens, Georgia

2025

©2025

Poulomi Das

All Rights Reserved

# Targeting of distinct ciliary PKD2 complexes in Chlamydomonas reinhardtii

by

## **POULOMI DAS**

Major Professor: Committee: Karl F. Lechtreck Jacek Gaertig Silvia Moreno PengPeng Bi Xiarong Lin

Electronic Version Approved: Ron Walcott Vice Provost for Graduate Education and Dean of the Graduate School The University of Georgia May 2025

# DEDICATION

To my parents.

#### **ACKNOWLEDGEMENTS**

I am very grateful to my major professor Dr. Karl F. Lechtreck for his kind guidance and immense support. He has always been a positive inspiration for me. His openness and acceptance for the ideas put forth by me has always helped me to grow as a researcher and learn new things. The project is a huge blessing to me because the way it got unfolded has enabled me to discover my biggest findings till date. Along with imparting research skills, Karl also has taught me to have a kind outlook in life.

My strongest point of my life are my parents. They are the biggest cheer leaders. My mother has been my role model and most of the bed time stories told by her included the biography of inspiring personalities. My mother is my best friend. My parents gave the best education to me and fulfilled all my wishes. Since my childhood, I have always been a dedicated and a hardworking person. All the teachings from my parents have made it clear from very early on that we should be honest and true to our work. Honesty towards work make life the liveliest and most rewarding one. Throughout my thesis writing period, my parents also stayed on video calls with me to give me company.

I am very thankful to all my committee members Dr. Jacek Gaertig, Dr. PengPeng Bi, Dr. Silvia Moreno and Dr. Xiaron Lin for all the research inputs and guidance. I will always be grateful to Jacek because he helped me during my Masters days in India, and inspired me to join UGA.

I got the best set of lab members and the warmest company while working. A special thanks to all of my labmates: Gui Zhang, Jin Dai, Peiwei liu, Jack Butler, Oranti Ahmed Omi,

Jenna wingfield, Keiwei Liu, Kang Sun, Tara Mallik, Sunita Sharma and Sneha. Jin Dai has been the best senior. I am thankful to my school friends and NISER friends for their support.

All the people who came across my USA stay definitely played a role whether major or minor and has enabled me to get to this point where I have completed my journey on a very satisfied note with a huge smile on my face and a bag full of memories to cherish for life.

# TABLE OF CONTENTS

Page
ACKNOWLEDGEMENTSv
LIST OF TABLESx
LIST OF FIGURESxi
CHAPTER
1 INTRODUCTION AND LITRETURE REVIEW1
1.1 Cilia1
1.2 Structure of cilia
1.3 Intraflagellar transport
1.4 Ciliary signalling14
1.5 Mechanosensation and chemosensation: conserved functions of cilia21
1.6 Ion channels of cilia: TRP- A super family22
1.7 Polycystin: Mechanosensor
1.8 Mastigoneme: An additive clue of mechanosensation29
1.9 References 32
2 The PKD2-related protein Small Interactor of PKD2 (SIP) promotes assembly and
ciliary entry of <i>Chlamydomonas</i> PKD245
2.1 Abstract
2.2 Introduction
2.3 The two PKD2 regions are established early during cilia regeneration50

	2.4 Efficient assembly of PKD2-NG into the distal region requires de novo
	assembly of cilia
	2.5 Identification of Small Interactor of PKD2 (SIP) as a novel PKD2-associated
	protein
	2.6 The PKD2-mastigoneme complex increases the efficiency of the ciliary beat
	57
	2.7 Discussion
	2.8 Materials and Methods67
	2.9 Acknowledgements
	2.10 Figure with legends
	2.11 Tables86
	2.12 Supplementary Data89
	2.13 References
3	Targeting of distinct ciliary PKD2 complexes in Chlamydomonas reinhardtii105
	3.1 Abstract
	3.2 Introduction
	3.3 Proximity labeling identified MST3 as a PKD2-associated protein111
	3.4 MST3 is required for PKD2 localization to the distal cilium112
	3.5 Assembly of PKD2 in the proximal cilium requires the PKD2-like protein
	Scavenger
	3.6 Discussion
	3.7 Materials and Methods119

	3.8 Figure with legends
	3.9 Tables
	3.9 References 137
4	Conclusions and Future Directions
	4.1 Summary of dissertation
	4.2 SIP: A novel single pass transmembrane protein
	4.3 MST3: A 5-TMH protein of distal PKD2 complex141
	4.4 Generation of a biological tool: g1 PKD2-mNG <sup>(CRISPR)</sup> 142
	4.5 TRP proteins in sub-ciliary compartments
	4.6 Future directions in PKD2 targeting
	4.7 References

# LIST OF TABLES

	Page
Table 2.1: List of strains used in this study	86
Table 2.2: List of primers	87
Table 2.3: List of anti-bodies	88
Table S1: Mass spectrometry of PKD2-NG immune-isolates.	96
Table S2: Distribution and conservation of SIP	98
Table 3.1: List of strains used in this study	131
Table 3.2: List of primers	133
Table 3.3: List of anti-bodies	136

# LIST OF FIGURES

Page
Figure 1.1: Structure of cilia and flagella6
Figure 1.2: The intraflagellar transport
Figure 2.1: PKD2 regions develop early during ciliogenesis
Figure 2.2: Assembly of PKD2 into distal region of <i>pkd2</i> cilia need de novo assembly78
Figure 2.3: Ciliary presence of the PKD2-mastigoneme complex80
Figure 2.4: SIP is required for proteolytic cleavage of PKD282
Figure 2.5: Loss of PKD2-mastigoneme complexes reduces the efficiency of the ciliary beat84
Figure S1: The PKD2-NG cell body pool89
Figure S2: identification of SIP as a PKD2 interactor90
Figure S3: Anti-bodies to SIP and MST192
Figure S4: Analysis of swimming velocity using the Length Analysis Tool plugin in ImageJ93
Figure 3.1: PKD2-miniTurbo rescues mastigonemes in the <i>pkd2</i> strain
Figure 3.2: MST3 is required for distal PKD2 assembly
Figure 3.3: SCV is required for proximal PKD2 assembly
Figure 4.1: Proposed design principle of PKD2

#### CHAPTER 1

#### INTODUCTION AND LITRETURE REVIEW

#### 1.1 Cilia

Cilia were first described by Anthony Van Leeuwenhoek in 1675 due to their motility via the use of light microscopy, making them the oldest reported cell organelle. He described cilia as 'incredibly thin feet, or little legs, which move very nimbly. The term cilium stands for eyelash in Latin (Beales & Jackson, 2012). Cilia can be divided into two kinds depending on their motility i.e, motile and immotile cilia. The immotile cilium (singular) is popularly called primary cilium (PC). The 19<sup>th</sup> and 20<sup>th</sup> century, light microscopy did not allow the study the fine structure of cilia due to the limitation in its resolution that was around the diameter of cilia. The arrival of electron microscopy solved the issue of the resolution, now providing atomic structures of many ciliary structures and complexes. Structural analysis, together with cilia genetics, biochemistry and in vivo imaging, brought rapid progress to the field of ciliary research (Satir, 2017).

Motile cilia are evolutionary conserved whip-like organelles which can propel the fluid around them resulting in either fluid current or cell movement, and sometimes both activities are observed (Lindemann & Lesich, 2021). Motile cilia in protists are being used to swim and to feed. The fresh water alga *Chlamydomonas reinhardtii* has two motile cilia at the apical region of its cell body which are beat in whip-like waveform to move itself through the liquid (Wan & Jékely, 2020; Wei et al., 2024). Mammalian cilia play diverse roles: Cilia on epithelial cells remove mucus and debris out of lungs, nodal cilia twirl to generate a leftward flow of fluid and

that causes the establishment of the left-right symmetry, and sperm have a single cilium helping it to move (Bustamante-Marin & Ostrowski, 2017; Kuek & Lee, 2020; Rosenfeld, 2019).

Primary or immotile cilia lack the capability of generating motion due to absence of important structures needed for movement. Primary cilia are found on most of the cells in mammalian bodies and function as sensory organelles for detecting extracellular cues and integrating and processing intracellular and extracellular signals (Anvarian et al., 2019). For example, outer segments of rods and cones, which consist of modified primary cilia are filled with photoreceptor molecules (Spencer et al., 2020). During embryonic development, primary cilia at the nodes sense the leftward flow caused by the motile nodal cilia, resulting in the upregulation of left-specific genes (Yoshiba et al., 2012). Primary cilia in kidney prevent cyst formation likely by sensing the fluid flow (Yoder, 2007). Other functions of primary cilia include hosting or participating in several signaling pathways such as Hedgehog (Hh), Wingless (Wnt), Notch, receptor tyrosine kinase (RTKs), transforming growth factor-b (TGF-b), and Hippo(Saternos et al., 2020).

The functions of cilia are determined by their protein constitutions. Proteomic analysis showed cilia is made up of more than 1,000 proteins(Yuan & Sun, 2013). These proteins constitute of three major categories: structural units, signalling units and transporting units. Ciliary structural components are the building blocks and a large number of them are involved in axonemal motility. Many signaling proteins, including GPCRs and channels are enriched in cilia. A third group of abundant ciliary components are intraflagellar transport (IFT) proteins, which shuttle ciliary building blocks to assemble and maintain cilia.

#### 1.2 Structure of Cilia

The main structural element of cilia is the central axoneme, a strand of microtubules (MTs) in the center, which is surrounded by the ciliary membrane, a specialized portion of the plasma membrane (Garcia et al., 2018). The ciliary membrane has different lipid and protein compositions as compared to the plasma membrane (Garcia et al., 2018). Electron microscope (EM) recognized that the axoneme of motile cilia typically has 9 + 2 microtubule arrangements whereas primary cilia mostly have 9 + 0 axoneme (Soares et al., 2019). The 9 + 2 axoneme consists of 9 sets of doublet MTs surrounding a central pair (CP) which is missing in the immotile cilia. The doublet microtubules are made up of one complete microtubule with 13 protofilaments (A tubule) and an incomplete second microtubule, the B tubule with 10 protofilaments, attached to the side of the A tubule. The MTs have their plus ends to be oriented towards the tip. The axonemal microtubules are the tracks for ciliary protein transport. The base of cilia is known as the basal body and has differently arranged MTs with 9 sets of triplet MTs (Mizuno et al., 2012). Moving from the basal body to the axoneme the triplet MTs transforms into doublet and this zone of change is called the transition zone. Transition zone is the control point which regulates the entry and exit of soluble and membrane proteins into and from cilia, respectively. Even if the ciliary matrix and membrane are direct continuations of the cytosol and the plasma membrane respectively, the cilium is considered a separate organelle due to its restricted entry and unique environment (Gonçalves & Pelletier, 2017; Reiter et al., 2012).

Basal bodies: Basal bodies are barrel-like microtubular structures located near the cell surface that provide the template for the nine-fold symmetry upon which the cilium is built.

They are structurally similar to centrioles, which in G1 phase of the cell cycle or during

quiescence, migrate to the plasma membrane converting into the basal bodies of cilia (Breslow & Holland, 2019). In multiciliated cells, basal bodies may also form *de novo*. Basal bodies like centrioles are quasi-cylindrical structures of about 500 nm in length with a diameter of 200-300 nm, consisting of nine microtubule triplets, i.e., A-, B- and C-tubules (Kilburn & Winey, 2008). The basal bodies determine the structure and diameter of the axoneme, which is nearly the same in all motile cilia. Within the triplets, the A tubule is complete with 13 protofilaments, while the B and the C tubules are incomplete with 10 protofilaments. During ciliogenesis, A and B tubules elongate, forming the axonemal DMTs whereas the C tubules terminate at the distal end of the basal bodies. Basal bodies have an intricate cartwheel structure. The basal body is anchored and stabilized by the fibrous structures (distal striated fibers, lateral fibers, proximal fibers), and the four microtubule rootlets extending inside the cell body(Dutcher & O'Toole, 2016; Wingfield & Lechtreck, 2018). At the distal end, basal bodies are linked via the transitional fibers (TFs) to the apical plasma membrane. The basal bodies and TFs function as docking sites for IFT proteins for beginning the transport into cilia (Reiter et al., 2012).

The transition zone: The end of C-tubules of basal body and the emergence of transition fibers mark the beginning of the transition zone (TZ), which is believed to function as the ciliary gate, serving as a control point for regulating the entry and exit of proteins (Park & Leroux, 2022). It functions as a diffusion barrier, allowing the free passage of smaller proteins whereas the transfer of larger proteins and protein complexes, such as the multi-megadalton IFT trains is thought to be regulated, probably by processes analogous to nuclear transport. The TZ contains the nine DMTs but not the CP, which only initiates more distally. In the TZ, the Y-linkers connect the DMTs to the ciliary membrane and terminate in particles embedded in the

ciliary membrane (i.e., the ciliary necklace as identified by freeze fracture electron microscopy) (Szymanska & Johnson, 2012; Wang et al., 2022). There are three main transition zone modules that are necessary for the gating functions: the MKS module, the NPHP module, and the CEP290 module. Disruptions in these structures lead to Meckel-Gruber Syndrome (MKS), Nephronophthisis (NPHP), Joubert syndrome (JBTS), or other ciliopathies indicating a critical role of the TZ for ciliary function (Barker et al., 2014; Sang et al., 2011).

The axoneme: The axoneme is the main part of cilia and is located outside of the cell body. The axoneme consists of MTs and various associated protein complexes. The axoneme from most of the species has a 5-to-10 um length and an ~300-nm diameter (Ishikawa, 2017). Most species—from the green algae *Chlamydomonas* to humans—share a similar ultrastructure of axoneme in motile cilia. Nine MTDs encircle two singlet microtubules (the CP). This architecture is called the "9+2" axonemal structure. An MTD consists of one complete cylindrical microtubule (A-tubule) and one incomplete tubule (B-tubule) attached to the A-tubule and originates from a triplet microtubule in the basal body (centriole). Adjacent MTDs are connected by dyneins and dynein regulatory complex (DRC) (nexin), whereas the MTD and the CP are linked by radial spokes (RS). The radial spokes (RSs) emerge from the DMTs and convene onto the CP. It is thought that mechanical or electrostatic interactions between the CP and the RS regulate the activity of axonemal dyneins (Antony et al., 2021; Oda et al., 2015). Dyneins, RSs, and the DRC form a regular 96-nm periodicity through the MTDs. This periodic repeat is determined by two coiled-coil proteins, FAP59 and FAP172, proved by elongation of the periodicity by lengthening these proteins. Nine MTDs show pseudo ninefold symmetry. Different from cytoplasmic dynein, there are several axonemal dynein isoforms. These dyneins

are composed of outer dynein (ODAs) and inner dynein arms (IDAs). The ODAs are required for maintaining cilia beat frequency, whereas the IDAs determine the beat pattern (Olbrich et al., 2015; Yamamoto et al., 2021). Within the 96-nm periodic unit, there are four ODAs with 24-nm spacing. One IDA consists of eight axonemal dynein molecules, whereas one ODA is either heterodimer or heterotrimer. Each proximal end of the axoneme (1 μm or less) has no dynein or RS. Recent advancements in microtubule inner proteins (MIPs) may provide new insights into this process(Ishikawa, 2017). Cryo-electron microscopy (cryo-EM) revealed that some of these proteins protrude to the sur\face of the DMTs, potentially providing anchors for the various axonemal substructures docked to the surface of the DMTs (Ichikawa et al., 2017; Ma et al., 2019).

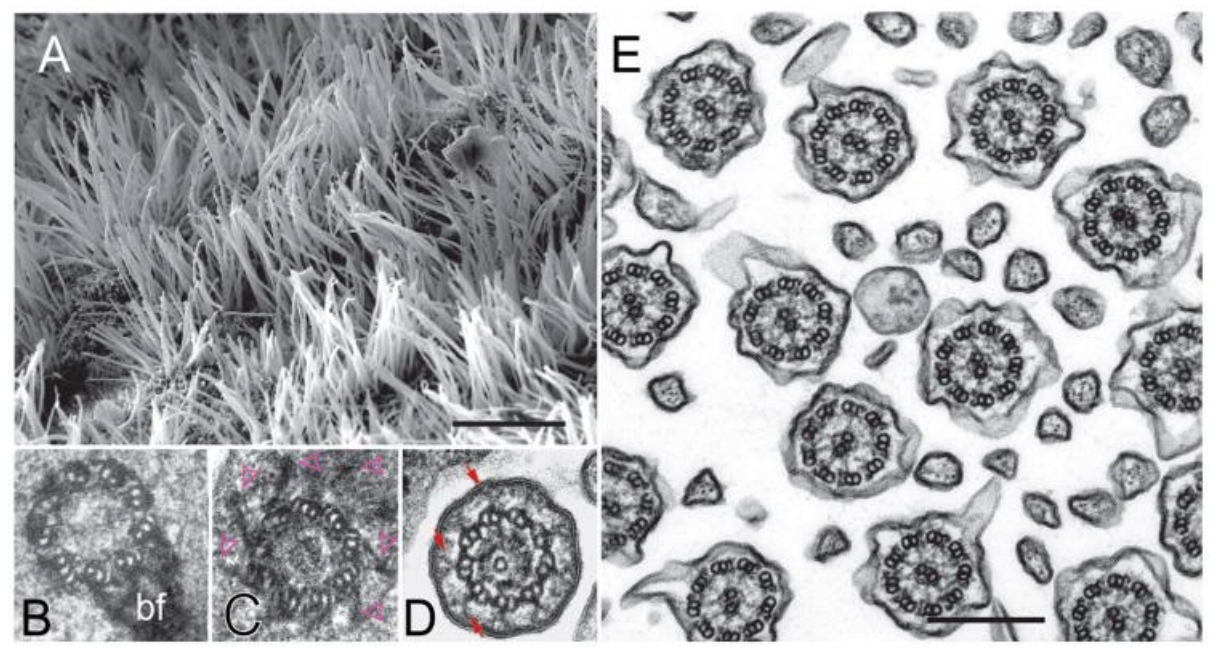


Figure 1.1) Structure of cilia and flagella:

A) Scanning micrograph showing the ciliated epithelium lining the ventricular system of the brain in mouse.

B-D) Thin sections showing the proximal region of the basal body (B) with the attached basal foot (bf), a more distal section with the paddle-wheel like transitional fibers (C, arrowheads), and the transition zone (D) in cross-sections. In D, note the Y-shaped connectors (arrows) linking the doublet microtubules to the ciliary membrane.

E) Micrograph showing airway cilia with typical 9+2 axonemes in cross-section. Bars =  $10 \mu m$  (A) and 250 nm (E) (Lechtreck et al., 2017).

The ciliary tip: The most distal segment of the cilia also called the ciliary tip is marked by the termination of the B-tubules of the DMTs in most cilia. This segment contains the singlet zone where only A-tubules are present (and the motile cilia also contain the CP)(Legal et al., 2023). The length of the singlet zone varies among species and cilium types (Fisch & Dupuis-Williams, 2011). In *Chlamydomonas*, the singlet zone is very short compared to the entire cilium, but lengthens during mating (Mesland, 1976; Morris & Scholey, 1997). The cilia of amphid channel neurons in *Caenorhabditis elegans* (*C. elegans*) have long singlet zone and is dependent on the homodimeric kinesin motor OSM-3(Bae & Barr, 2008). In primary cilia, the singlet zone runs for the major portion, while the A-tubules may also terminate far before the tip of the cilia; the outer microtubules bundle more closely that results in prevention of the occupancy of the CP, and the diameter of the primary cilia gradually decreases approaching the tip(Sun et al., 2019). At the ends of the CP and the A-/B-tubules, capping proteins are present for stabilization of the microtubule ends (Legal et al., 2023; Louka et al., 2018).

The ciliary membrane: The ciliary membrane is connected to the plasma membrane through the periciliary membrane, which is invaginated and surrounds the proximal region of the cilium. Despite being continuous with the cell body plasma membrane, the screening done at the TZ results in very distinct identity of proteins and lipids in ciliary membrane (Garcia et al., 2018). The ciliary membrane is rich in sterols and saturated fatty acids, indicating a higher

concentration of lipid rafts. This composition induces anchorage and enrichment of certain membrane or membrane-associated proteins, including those having myristoylation or palmitoylation(Emmer et al., 2010). The best studied examples of ciliary proteins include the autosomal dominant polycystic kidney disease (ADPKD) gene products polycystin-1 (PKD1; OMIM: 601313) and polycystin-2 (PKD2; OMIM: 173910), which form a cilium-localized heterodimeric receptor-cation channel complex necessary for obstructing cystogenesis, and the Sonic Hedgehog (SHH) co-receptor Patched-1 (PTCH1) and the class F GPCR, smoothened (SMO), which accumulate in cilia in the absence and presence of SHH, respectively (Boucher & Sandford, 2004; Yue et al., 2014). These membrane signalling proteins can be expressed normally in absence of cilia but can no longer function properly, leading to characteristic fibrocystic features (in the case of ADPKD) or patterning defects (in the case of SHH signalling defects) observed in patients with ciliopathies (Bergmann et al., 2018). Intriguingly, even within the cilium itself, domains of protein organization may exist. Recent advances in cilia-targeted proximity-labelling and proteomics approaches have expanded the repertoire of cilia-localized receptors, ion channels and downstream effectors (Mill et al., 2023; Nachury & Mick, 2019). This composition may also change in response to external signalling cues and/or mutations in specific ciliopathy disease genes, for example, BBS genes (Reiter & Leroux, 2017). During ciliary membrane protein import the IFT-A subcomplex binds to the TUBBY domain proteins TULP3 and TUB, which regulate the ciliary localization of a broad range of integral membrane proteins, including GPCRs and polycystins (Badgandi et al., 2017; Hong et al., 2021). Thus, the ciliary membrane is very crucial in communication. Secretion of ectosomes from the membrane is required either to initiate intracellular communications or to remove excess ciliary content(Ye et al., 2018).

## Specialized ciliary subcompartments

Primary cilia in numerous cell types have a specialized periaxonemal subcompartment called inversin compartment (INVc). INVc proteins are well conserved in vertebrates. An INVc-like region containing an INVS homologue has even been described in sensory neuronal cilia in Caenorhabditis elegans (Warburton-Pitt et al., 2014). INVc is located near the proximal end of cilia i.e., close to the basal bodies. This compartment is essentially made up of four proteins INVS, ANKS6, NEK8 and NPHP3 and they assemble into a novel structure called fibrilloid. Three fibrilloids constitute the INVc. These four proteins form an epistatic relationship among each other to build the compartment. INVS connects to ANK6-NEK8 complex, NEK8 determine the density of ANK6-NEK8 and high density of NEK8-ANK6 is required to localize and concentrate NPHP3. INVS is the core component of the fibrilloids that determine their length and placement. NPHP3 forms connection with the membrane. NEK8 is the only active member having enzymatic activity and it has two substrates: PC-2, an ion channel and ANK6.ANK6 is an interactor of NEK8 but it is also an activator of NEK8 to phosphorylate PC-2 and thus is involved in kidney function. The special point of INVc is its compartmentalization without membrane. The function of this compartment is not known but defect or loss of its constituents cause left-right asymmetry defect and kidney disease. Delving into the compartment will be helpful to understand its role in development, left-right asymmetry and prevention of cysts in kidney (Bennett et al., 2020).

#### FAP93: Proximal compartment

One special protein has been identified at the proximal zone of cilia named FAP93. The specialty of this protein is the correlation between length of FAP93 domain (amount of area covered by FAP93) and ciliary length which is directly proportional to each other. FAP93 localizes in the proximal 1.03  $\mu$ m of axoneme in steady cilia. The short cilia mutants like *pf9-2*, *pf28* have smaller area covered by FAP93 i.e.,  $0.48 \pm 0.13 \mu$ m and long cilia mutant like *lf-5* has doubled the length of FAP93 domain i.e.,  $1.45 \pm 0.43 \mu$ m.

The function of FAP93 is not known. Ciliary translocation of FAP93 is majorly independent of intraflagellar transport. Assembly of FAP93 occurs slowly because of its asymmetric and sequential assembly on only a subset of the nine outer DMT but eventually covering all of the nine. It is hypothesized that mechanism of FAP93 assembly is interconnected to the ciliary length determining signalling pathway(s). Exploring FAP93 has potential to crack the factors involved in ciliary length determination (Hwang et al., 2024).

*Motor proteins forming sub-compartments:* 

Many ciliary motor proteins localize in unique positions along the cilia and do not follow a repeated pattern which leads to distinguished and defined regional compositions. For example, different ODAs like dynein axonemal heavy chains; DNAH11 and DNAH9 organize into proximal and distal zones of cilia, respectively, leading to clear demarcations. DNAH11, being in proximal area, helps in ciliary bending and DNAH9 helps in structural integrity. (Dougherty et al., 2016). ODA10 and ODA5 in *Chlamydomonas* cilia also localize in a unique very proximal

flagellar domain (initial 2-3 µm of cilium) and is necessary for ciliary beat initiation. ODA10 very specifically interacts only with the DMT1 in the proximal area (Dutcher, 2020). One of the novel inner arm dynein, DHC11, localizes exclusively to the proximal cilia (Yagi et al., 2009). The trypanosomes paralogues of dynein chain1 (DC1) and two paralogues of DC3 form a proximal docking complex and a distal docking complex, respectively, and are needed for waveform initiation (Edwards et al., 2018). Thus, motor proteins can recognize and dock onto their specified proteins without any membranous separation and help in ciliary motility.

All these sub compartments formed by INVc, FAP93 and all the motor proteins are of different length (along the cilium). There are no clearly specialized proximal and distal regions separations rather multiple and partial overlapping regions co-exist.

# 1.3 Intraflagellartransport (IFT)

Proteins cannot be synthesized within the cilium, and so all materials required to build cilia are synthesized in and transported from the cell body. A monumental characteristic of cilia is that they are assembled and maintained by the active motility process known as intra flagellar transport (IFT) (Bhogaraju et al., 2013; Ishikawa & Marshall, 2017). IFT machinery selects components to assemble, move them to the desired position, and regulates them to control the size of final ciliary structure. IFT is a bidirectional protein transport system inside cilia- carrying ciliary components from the cell body to the tip of cilia and returning the products of turnover back to the cell body from cilia (Bertiaux et al., 2018; Sun et al., 2019).

IFT was first discovered as the bidirectional movement of granule-like particles (socalled "IFT trains") along the cilium of the biflagellate green alga Chlamydomonas by using differential interference contrast (DIC) microscopy (Kozminski et al., 1993). The IFT system has since been shown to be expressed in most ciliated organisms, including humans. The "railroad tracks" for IFT, the DMTs, point their minus ends towards the cell, and their plus ends towards the ciliary tip. IFT is a motor-based multi-megadalton shuttle responsible for transporting proteins in and out of the cilia. Two different microtubule motors drive IFT: Kinesin-2 drives IFT trains toward the tip of the axoneme known as anterograde IFT, and cytoplasmic dynein 2 drives IFT trains toward the minus ends of the microtubules i.e., the base of the axoneme known as retrograde IFT. The canonical anterograde IFT motor is heterotrimeric kinesin-2, which consists of two heterodimerized kinesin-2 motor subunits and an accessory subunit, kinesin-associated protein (KAP). The retrograde IFT motor cytoplasmic dynein 2 is a multiprotein complex comprising of four different subunits: a heavy chain, a light intermediate chain, an intermediate chain, and a light chain. IFT trains were first isolated from Chlamydomonas cilia and were found to consist of two large complexes, termed IFT complex A and complex B (Cole et al., 1998; Piperno & Mead, 1997). IFT complexes A and B are loosely associated and seem to move together within the cilium, but they have distinct functions. IFT complex B is involved in anterograde transport with kinesin and is necessary for the assembly and maintenance of cilia. In most cases, mutation or knockdown of IFT complex B proteins results in absent or very short cilia (Brazelton et al., 2001; Follit et al., 2010; Haycraft et al., 2003; Pazour et al., 2000). At the ciliary tip, anterograde IFTs disassemble during the turnaround event, unloading the dyneins that were carried along in an inhibitory conformation, and reassembling on to the unlocked dyneins for retrograde transport. In contrast, IFT complex A is required for the retrograde transport that returns proteins to the cell body for turnover, but it does not appear to be necessary for ciliary assembly. For example, cilia can assemble with a mutation in an IFT complex A protein but have

abnormal bulges containing accumulated IFT complex B proteins. Anterograde IFTs travel on the B tubules, while the retrograde IFTs travel on A tubules, which probably helps to avoid collision between trains moving in opposite direction. In total, there are 22 identified IFT proteins, including 6 IFT-A proteins (IFT43, IFT121, IFT139, IFT122, IFT140, IFT144, the latter 3 forming the IFT-A core), 10 IFT-B core (IFT-B1) proteins (IFT22, IFT25, IFT27, IFT46, IFT52, IFT56, IFT70, IFT74, IFT81, IFT88), and 6 IFT-B peripheral (IFT-B2) proteins (IFT20, IFT38, IFT54, IFT57, IFT80, IFT172) (Cole et al., 1998; Taschner and Lorentzen, 2016). IFT-A and IFT-B complexes arrange in separate tandem repeats to form the IFT "train" structure, appearing as elongated electron densities between the DMTs and the ciliary membrane (Jordan et al., 2018; Kozminski et al., 1993; Rogowski et al., 2013). IFT trains may also appear stationery within the cilia, reaching a length of 700 nm, although it is unclear how and why this occurs(Stepanek & Pigino, 2016). In primary cilia, certain signalling events require the translocation of signaling proteins to switch between on and off states (Nachury & Mick, 2019). Inhibition of IFT disrupts these signaling events and leads to more detrimental effects on the whole organism level. In contrast with binding directly to cargoes, IFT also utilizes cargo adaptors for protein binding and transport (Lechtreck, 2015). Cargo adaptors are themselves cargoes of IFT, binding to IFT components, while serving as scaffolds to connect other cargoes for shuttling in or out of the cilia. So far, a few cargo adaptors have been identified. The BBSome is a protein complex named after the Bardet-Biedl Syndrome, a rare genetic disorder characterized by polydactyly, retinal degeneration, and obesity(Zaghloul & Katsanis, 2009). As an IFT cargo adaptor, its functions are related to the transport of membrane associated proteins such as PLD, as well as membrane proteins including GPCRs (Berbari et al., 2008; Craft et al., 2015; Lechtreck et al., 2009). Other cargo adaptors include the IFT-A adaptor Tulp3 for transporting membrane proteins (Badgandi et al., 2017; Mukhopadhyay et al., 2010), ODA16 for transporting ODA (Ahmed et al., 2008), IDA3 for transporting IDA (Hunter et al., 2018), and etc.

In the absence of IFT, ciliogenesis is completely blocked (Cole et al., 1998; Huang et al., 1977). In primary cilia, certain signaling events requires the translocation of signaling proteins to switch between on and off states (Nachury and Mick, 2019). Inhibition of IFT disrupts these signaling events and leads to more detrimental effects on a whole organism level (see below) (Ocbina and Anderson, 2008; Pazour et al., 2000).

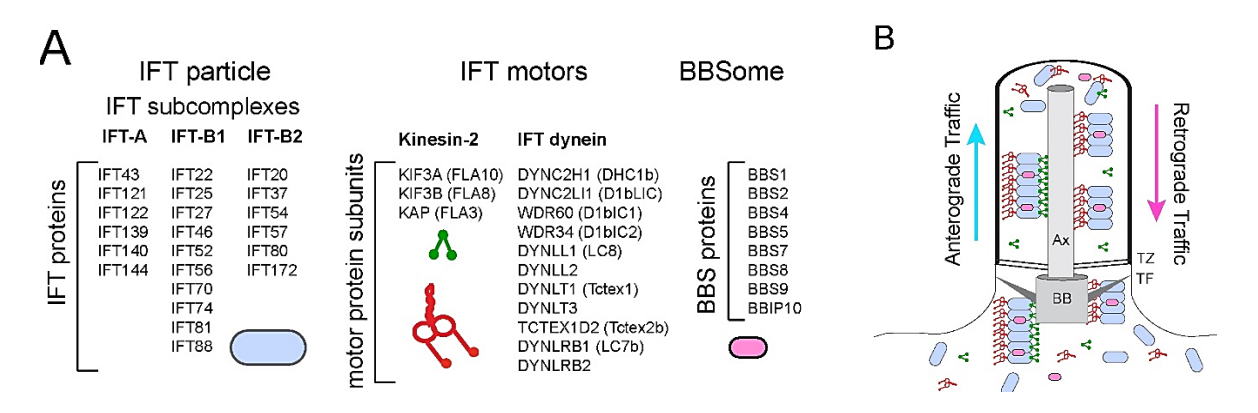


Figure 1.2) The Intraflagellar transport:

- A) Composition of IFT particles, IFT motors, and the BBSome. For the motors, the mammalian protein names are shown; the *Chlamydomonas* protein names are listed in the brackets.
- B) Schematic presentation of IFT. Ax, axoneme, TZ, transition zone, TF, transition fibers, BB, basal body.(Lechtreck et al., 2017)

# 1.4 Ciliary signalling

Primary cilium is a tapered cylindrical projection present on almost every cell type in our bodies functioning as sensory organelles. Ciliary signaling is a process that involves the transmission of environmental cues to cells through primary cilia(Pala et al., 2017). They serve as critical mediators of certain types of intercellular communication and are important signaling

hubs. This sensory capacity of PCs relies on coordinated trafficking and temporal localization of specific receptors and associated signal transduction modules in the cilium(Anvarian et al., 2019; Hsiao et al., 2012). Some of the best-established ciliary pathways are – G protein-coupled receptors, Hedgehog, WNT, receptor tyrosine kinase, TGFβ/BMP and polycystins signalling. These pathways have critical roles in diverse areas of development and physiology(Christensen et al., 2017; Gopalakrishnan et al., 2023; Morthorst et al., 2018). Dysfunctions of signalling pathways in primary cilia give rise to a pleiotropic group of diseases and syndromic disorders termed as ciliopathies because of its involvement in so many pathways. Ciliopathies impact several organs negatively during embryonic development as well as in postnatal life (Guemez-Gamboa et al., 2014; Morthorst et al., 2018). Well studied pathways in cilia are described below.

# Ciliary GPCR signalling

GPCRs are transmembrane proteins functioning as receptors that sense a broad range of cues, including light and peptide ligands. The human genome encodes approximately 800 functional GPCRs, divided into class A (rhodopsin), class B (secretin and adhesion), class C (glutamate) and class F (Frizzled and Smoothened (SMO))(Yang et al., 2021).

In recent studies, more than 30 GPCRs are found to be localized in primary cilia. Numerous GPCRs and their downstream effector molecules localize in cilia on a variety of mammalian cell types(Anvarian et al., 2019; Mykytyn & Askwith, 2017; Schou et al., 2015). GPCRs are trafficked by TULPs in cilia and removed by BBSome only after their activation. GPCRs are also released from cilia tips as ectosomes. GPCRs on plasma membrane and cilium signal differently(Ye et al., 2018). Canonical signal transduction through GPCRs is mediated by

activation of heterotrimeric G proteins composed of three associated subunits,  $G\alpha$ ,  $G\beta$ , and  $G\gamma$ . Upon activation, GPCRs are phosphorylated at specific sites within their intracellular domains. Few of the ciliary GPCRs and their signalling are discussed below:

Primary cilia of epithelia of bile ducts (cholangiocyte) are enriched of two different GPCRs — purinergic receptor P2Y12 (P2RY12) and G-protein coupled bile acid receptor 1 (GPBAR1, also known as TGR5), as well as the cAMP signalling proteins, suggesting that cholangiocyte cilia mediate cAMP signalling in response to biliary factors. Primary cilia in cholangiocyte provide mechanosensory, chemosensory and osmosensory functions to regulate its proliferation(Masyuk et al., 2008).

Polycystic liver disease is a ciliopathy, characterized by the formation of fluid-filled hepatic cysts that originate from cholangiocytes. The presence or absence of cilia effect GPBAR1 signalling differently. Activation of GPBAR1 on non-ciliated cholangiocytes induces increased cellular proliferation, whereas activation of GPBAR1 on ciliated cells leads to decrease in cellular proliferation(Anvarian et al., 2019; Zhang et al., 2021). Thus, ciliary GPCRs are involved in controlling long-term energy homeostasis(Cassioli & Baldari, 2019; Paolocci & Zaccolo, 2023).

GPCRs also localize on neuronal cilia and failure of GPCRs to make their way to neuronal cilia disrupt its signalling. GPCRs contribute in regulating metabolic homeostasis of neurons. MC4R (GPCR) localizes in neural cilia and mutations in MC4R cause obesity in humans and impair its ciliary localization. Thus, GPCRs have are very crucial as defects in GPCRs cause plethora of syndromes with abolishment of their normal localization and impacted signaling.

## Hedgehog signalling

Embryo development requires various signalling pathways for formation of tissues and organs. One of the pathways is hedgehog signalling. In vertebrate HH signal transduction pathway localizes in primary cilium and is involved in proliferation and patterning of diverse organs(Bangs & Anderson, 2017; Jing et al., 2023). The final transcriptional output of canonical HH signalling cause intracellular activation or basal repression of pathway targets in the presence or absence of HH morphogens, respectively.

Defects in IFT disrupt sonic hedgehog (SHH) signalling. GLI is a transcription factor regulating HH pathway. Activation of the SHH pathway by formation of the GLI transcriptional activator (GLIA) and basal repression of the SHH pathway by GLI transcriptional repressor (GLIR) are both dependent on the primary cilium(Murdoch & Copp, 2010; Niida et al., 2021). Studies indicate that suppressing the Hedgehog (HH) pathway is just as crucial as activating it for tissue homeostasis. Different tissues express SHH at various developmental stages and disruption of GPR161 causes premature SHH signaling(Jing et al., 2023). This sudden onset of SHH pathway is associated with defects in limb and skeletal morphogenesis, cell proliferation, and medulloblastoma formation(Jing et al., 2023).

Additional ligands of the HH family includes desert (DHH) and Indian (IHH) hedgehog, which also operate via primary cilia but in a tissue-specific manner, such as in cells of the testis and in growth plate chondrocytes, respectively(Kim et al., 2015).

## WNT signalling

WNT signalling is a network of pathways that coordinate a multitude of cellular events over a lifespan. WNT ligands consist of secreted lipoproteins often activating frizzled receptors of the class F GPCRs. Two main pathways are the canonical WNT-β-catenin and the non-canonical WNT-planar cell polarity (PCP)(Komiya & Habas, 2008; Liu et al., 2022). In canonical pathway, WNT ligands bind frizzled to stabilize cytoplasmic β-catenin and regulate gene expression affecting cell proliferation and survival. The WNT-PCP pathway controls cell morphology, migration, and division through various receptor combinations and signaling events(Yang & Mlodzik, 2015).

Various components of the WNT pathway are found in primary cilia, and there is evidence suggesting that cilia play a role in regulating WNT signaling, despite conflicting views in the literature. Studies initially linked WNT signaling to primary cilia through nephrocystin-2 (NPHP2) and DVL1-mediated activation. Depletion of NPHP2 in *X. laevis* disrupted convergent extension, implying a role in WNT-PCP signaling. NPHP2 was also found to control fibroblast polarity and cell motility through ciliary WNT pathways(Anvarian et al., 2019). A zebrafish mutant lacking ift88 still showed normal WNT target gene expression, suggesting primary cilia may be redundant in WNT signaling (Corbit et al., 2008; Tran et al., 2014). Overall, the exact role of primary cilia in regulating WNT signaling remains uncertain.

# Ciliary RTK signalling

Many growth factors and hormones exert their effects through Receptor Tyrosine Kinases (RTKs), which make up a large family of over 50 enzyme-linked receptors. RTKs can be

categorized into different classes based on their structure, domain organization, and their need for co-receptors in signal transduction. They are often activated by dimerization, leading to the activation of their tyrosine kinase domains and subsequent phosphorylation of specific tyrosine residues. This activation triggers a cascade of signaling pathways involving various adaptors and effector proteins. RTKs play a crucial role in downstream signaling components such as ERK1/2, p38, JNK, PI3K-AKT-mTOR, and others(Ségaliny et al., 2015; Tomuleasa et al., 2024). Specific RTK subtypes, including PDFGRα, IR, and IGFIR, operate within primary cilia to regulate cell and tissue processes. Two isoforms of PDGF receptors, PDGFRα and PDGFRβ, function as homodimers or heterodimers. Mutations in these receptors are linked to various diseases including cancer. PDGFRα is mainly found in primary cilia. RTKs can crosstalk with other receptor systems and signal through various proteins to control cellular responses(Koefoed et al., 2014).

## TGFβ/BMP signalling in primary cilia

The TGFβ superfamily includes a range of ligands that signal through receptor complexes to regulate cellular processes in development and tissue homeostasis. Canonical signaling involves phosphorylation and activation of R-SMAD transcription factors, forming complexes that enter the nucleus for gene expression(Wu et al., 2024). Non-canonical pathways like NF-κB, Rho-like GTPases, and PI3K-AKT pathways also play a role in cellular responses. Receptor internalization through clathrin-mediated and caveolin-mediated endocytosis influences TGFβ/BMP signaling outputs. Clathrin-mediated endocytosis supports SMAD2/3 signaling by anchoring to endosomes, while caveolin-mediated endocytosis inhibits TGFβ/BMP signaling

through receptor degradation. The function of SARA in R-SMAD activation and gene expression may vary between cell types(Tsukazaki et al., 1998).

The primary cilium plays a key role in coordinating the balanced output of TGFβ/BMP signaling. Studies have shown active TGFβ signaling in the primary cilium, with receptors accumulating at the ciliary base region upon ligand stimulation. Activation of SMAD2/3 and ERK1/2 occurs at the ciliary base, influencing various cellular responses such as heart development, differentiation of stem cells, and bone formation(Koefoed et al., 2014). Primary cilia regulate TGFβ-mediated R-SMAD activation in adipose progenitor differentiation and counteract endothelial-to-mesenchymal transition. Shortening of primary cilia by TGFβ signaling is associated with epithelial-to-mesenchymal transition in kidney cells and impaired mechanosensation in osteoblasts(Zhong & Dong, 2024). Overall, primary cilia play diverse roles in fine-tuning TGFβ signaling to control cellular responses in different processes.

#### Polycystin signalling

Another essential signalling pathway linked to cilia is mediated by the polycystin complex. Inherited defects in polycystin signalling cause polycystic kidney disease (PKD). Polycystins are transient receptor potential (TRP) channel proteins that localize and are likely functioning at the ciliary membrane of the kidney epithelial cells that line the nephrons(Ong & Harris, 2005). Polycystins are integral membrane proteins, synthesized in the endoplasmic reticulum and are matured in the Golgi. After leaving the Golgi, polycystins become localized in cell–cell junctions, extracellular vesicles and, prominently, at the ciliary membrane(Hu & Harris, 2020). Although the best understood function of polycystins is in limiting growth of kidney

tubule epithelial cells, polycystin family proteins also function in vertebrate left–right axis patterning (Esarte Palomero et al., 2023). These functions of PKD2 are dependent on their capability to respond to mechanosensation and chemosensation (described below).

#### 1.5 Mechanosensation and chemosensation: conserved functions of cilia

Primary cilia, of which there is only one on each cell, have primarily sensory functions (as receptors for chemical, mechanical, or other signals) (Berbari et al., 2009; R. Ferreira et al., 2019). Cilia are known for bridging communication between environment and cells. The external cues can be primarily categorized into two kinds i.e., mechanical and chemical. The response generated in a cell or tissue(s) due to mechanical cue or force is called mechanosensation whereas response arising due to chemicals is called chemosensation. The quality of mechanosensation is determined by the force exerted on the cilia as well as ciliary length (Resnick & Hopfer, 2007). Whereas the sensitivity of a chemoreceptor is characterised by its binding affinity for the ligand, as well as its association/dissociation kinetics (Endres & Wingreen, 2009). The role of cilia in mechanosensation and chemosensation is exemplified by its conserved presence across varied ranges of organisms in different tissues whose functional and physical attributes is dependent on sensing external stimuli.

For example, primary cilia in endothelial cells lining blood vessels function as mechanosensors that sense blood flow and mediate angiogenesis in zebrafish. Osteocyte primary cilia respond to mechanical stress to control osteogenic and bone-resorptive responses, as well as to regulate cartilage development (Claude-Taupin et al., 2022; Malone et al., 2007; Yuan & Yang, 2016). Motile cilia in cells of respiratory tract always beat consistently regardless of viscous load, to propel mucus along the tract(Bloodgood, 2010). Motile cilia can improve their chemosensitivity by increasing their capture rate of ligands (Hickey et al., 2021). Motile cilia of

mammalian respiratory epithelium exhibit mechanosenation as well as chemosensation. They have bitter-taste sensory receptors and bitter compounds increase intracellular Ca<sup>2+</sup> concentration tha results into faster ciliary beating frequency. Cerebrospinal fluid-contacting neurons (S-CSF-cNs) requires motile cilia to perform critical mechanosensory functions (Orts-Del'Immagine et al., 2020). These examples of a variety of cilia needing to respond to external cues for normal functional maintenance glorifies the critical importance of mechanosensation and chemosensation. A large family of channel proteins depending on mechanical force and chemical cues are described below (Bezares-Calderón et al., 2020).

#### 1.6 Ion Channels of Cilia: TRP -A super family

One of the essential factors involved in the sensory characteristics of cilia are ion channels. The ion channels on primary and motile cilia are different from each other. Calcium ion (Ca2+) signaling is central for controlling how cilia move and responds to external signals (Phua et al., 2015). Patch clamping has shown that primary cilia generates calcium signalling waves as a response to mechanical stress (Sherpa et al., 2019). The resting calcium concentration in cilia is higher than that in the cytoplasm, which indicates that compartmentalized calcium concentration is regulated by ion channel (Du Toit, 2014). The predominant channels on primary cilia belong to polycystin family (e.g., PKD2, PKD2-L1), but other channels on or near cilia have also been reported that include other TRPs such as TRPM4 and TRPV4, as well as the calcium-activated chloride channel ANO1. Several TRP proteins (e.g., TRPM4, TRPV4, TRPC1, and PKD2) have been proposed as ciliary ion channels.

Motile cilia like those on ependyma are majorly autonomous motors without significant regulation by the few voltage-gated calcium (Ca<sub>V</sub>) channels present in their membranes. Catsper is a Ca<sup>2+</sup> ion channel which localizes in the membrane of sperm flagella. Catsper channel is distributed in four rows resulting into a pattern called race stripes. This is involved in chemotaxis and sperm motility (Sun et al., 2017). TRP channels have also been reported on motile cilia. TRP channels are described in detail below.

## Transient Receptor Potential (TRP) channels in Cilia

TRP channels are a grand family of multifunctional signalling molecules with many roles in physiology and sensory perception(Zhang et al., 2023). These are expressed in a wide range of organisms as well as variety of tissues. Therefore, TRP channels have been implicated in numerous diseases, including hereditary disorders caused by defects in genes encoding TRP channels (TRP channelopathies. Thus, targeting TRP proteins by drugs can be used as strategy to prevent or treat diseases. TRP channel has a similar architecture to other ion channels i.e., the presence of a six-transmembrane helix topology (named S1, S2, S3, S4, S5 and S6) with a reentrant loop between S5 and S6 that forms the channel pore(Cao et al., 2013; Yu & Catterall, 2004). These channels tetramerize to a 24-helix functional protein complex(Hellmich & Gaudet, 2014).

Most TRPs are polymodal channels, so-called coincidence detectors that are activated by both physical (temperature, voltage, pressure and tension) and chemical stimuli. Some TRPs function as non-selective cation channels in the plasma membrane; others regulate Ca<sup>2+</sup> release in intracellular organelles. TRPs have functional modulators, e.g. phosphoinositides (Nilius et al.,

2008), or quaternary ammonium ions (Jara-Oseguera et al., 2008) and venom toxins (Siemens et al., 2006) and response towards them is conserved across ion channel families.

This large group has sequence and topological differences and, on their basis, TRPs are divided into seven subfamilies: group 1 with five subfamily members (TRPC, TRPV, TRPM, TRPN, and TRPA), and group 2 with two subfamilies (TRPP and TRPML)(Zhang et al., 2023; Zheng, 2013). The sole architecture is the presence of six transmembrane helices (sometimes less than or more than 6 are also encountered) and permeability to cations. TRPA, TRPV, and TRPC channels contain ankyrin repeat sequences in their intracellular N-terminal structural domains, whereas TRPC and TRPM subfamilies possess a proline-rich "TRP structural domain" in the C-terminal region near the transmembrane segment. Group 2 channels also have high sequence homology in their transmembrane structural domains and are only distally related to the genes of group 1 channels because they contain a large extracellular domain between transmembrane helices.

Multiple transient receptor potential channels are found in cilia and are involved in ciliary processes. Few of the examples are described below:

• TRPV4 is present in ciliated epithelial cells of mammalian female reproductive organs and ciliated cells in airway epithelia. TRPV4 channels are responsible for sensing and responding to mechanical stress, heat, acidic pH, endogenous ligands, and synthetic agonists such as 4α-phorbol 12,13-didecanoate (4α-PDD). TRPV4 participates in the coupling of fluid viscosity changes to ciliary beat regulation and in cell volume regulation. TRPV4 is an important piece in the signaling cascade of Ca<sup>2+</sup> entry pathway(Arniges et al., 2006; Arniges et al., 2004).

- TRPA1 localizes in the tips of the stereocilia in the bullfrog and TRPN1 is the main transduction channel of frog stereocilia(Corey et al., 2004; Shin et al., 2005).
- TRP11 is present in the proximal part of cilia in green algae *Chlamydomonas* and is known to be involved in numerous mechanosensations (Oshima et al., 2023).
- that regulates ciliary calcium concentration and thereby ciliary signalling(Du Toit, 2014). Cells depleted of PKD1L1 and PKD2L1 by siRNA and Pkd211—/— mouse embryonic fibroblasts (MEFs) showed reduced ciliary calcium currents compared with wild type, suggesting that PKD1L1 and PKD2L1 initiate ciliary calcium transduction. Other TRPP like PKD2 is present in cilia of nephrons and blood vessels and take part in responding to fluid flow which result in Ca2+ signalling. The mechanosensation of PKD protein will be discussed in detail(AbouAlaiwi et al., 2009).

# TRP and hetero/homo complexes:

TRP proteins form oligomers i.e., either homomer or heteromer for achieving functional completion. Initially on the basis of primary structure, TRP channel complexes have been assumed to be tetramers because of its resemblance with the *Shaker* K<sup>+</sup> channel, which is known to be tetrameric(Hellmich & Gaudet, 2014). Tetrameric structure for a number of TRP channel family members, including TRPC1(Barrera et al., 2007), TRPC3(Mio et al., 2007), TRPV1, TRPV5 and TRPV6 (Kedei et al., 2001), and TRPM2A (Maruyama et al., 2007) have been established by usage of variety of structural and functional techniques. Atomic force microscopy showed that TRPP2 assembles a homo-tetramer and that TRPP2 and TRPC1 form a heterotetramer with a 2:2 stoichiometry and an alternating subunit arrangement (Kobori et al.,

2009). TRPV5 and TRPV6 are unique in terms of their high calcium selective nature. Therefore, they have a significant contribution in calcium homeostasis in the body. TRPV5 and TRPV6 have high sequence homology (~75%) at the amino acid level and this easily leads to formation of homo-tetrameric and heterotetrameric functional units in epithelia (van de Graaf et al., 2006). Similar to TRPV5 and TRPV6, TRPM6 and TRPM7 also share high sequence homology and hence both have the ability to form functional heterotetrameric channels (Li et al., 2006). Intriguingly, data have been presented indicating that TRPP2 exists in the plasma membrane as a trimer, which is then able to interact with polycystin-1 to form a heteromer with a 3:1 stoichiometry (Yu et al., 2009). PC-1 is a well-known interactor of PC-2 (TRPP-2).

## 1.7 Polycystins and mechanosensation

The genes which are responsible for causing autosomal dominant polycystic disease (ADPKD) are PKD1 and PKD2 and belong to a subclass of TRP family. PKD1 and PKD2 encode PC-1 and PC-2 respectively. ADPKD is a ciliopathy and evidence from patients and animal models have suggested that Ca<sup>2+</sup> signalling is an important factor in pathogenesis of ADPKD. The mouse embryo node and the LRO of zebrafish embryos, which are required for left–right asymmetry of body morphology, the Ca2+ transients responding to mechanical stimuli in cilia and the cytoplasm are lost in the absence of PC-2(Babu & Roy, 2013; Qian et al., 1997; Sherpa et al., 2019). These observations suggest that polycystins in Cilia are required to respond to the mechanical cues and generate the downstream signalling pathways for proper functioning (Besschetnova et al., 2010; Xiao & Quarles, 2010).

*Molecular features of polycystins:* 

PC-1 is a megadalton-sized receptor-like protein, having 11 transmembrane helices and an extensive extracellular N-terminal fragment (NTF) containing several annotated domains, including a C-type lectin (CTL) domain and the G-protein-coupled receptor autoproteolysisinducing (GAIN) domain (Hardy & Tsiokas, 2020). PC-1 has characteristic features of both a channel and a receptor, acting as a receptor for WNT ligands (Kim et al., 2016). PC-2 belongs to the TRP channel family and has conserved structure across species. PC-2 comprises six transmembrane regions. The extracellular tetragonal opening for polycystin (TOP) domain of PC-2 is situated between transmembrane regions 1 and 2, functioning as the putative 'lid' for the channel (Giamarchi et al., 2010; Ha et al., 2020; Shen et al., 2016). PC-2 mediates the movement of Ca2+ and monovalent cations (Na+ and K+) across membranes (Liu et al., 2018). Indeed, mutations in the TOP domain and those affecting the channel permeability are hotspots for pathogenic mutations (Grieben et al., 2017; Su et al., 2018). Lipid bilayer nano-discs and purification of polycystins from human embryonic kidney (HEK) has shown that PC-1 and PC-2 form heterotetramers with a 1:3 stoichiometry. Polycystins are widely distributed membrane proteins within primary cilia. PC-1 and PC-2 have been reported in primary cilia of radial glial cells (RGC). Neuronal progenitor (NPC) are the early RGC and PC-1/PC-2 complex regulate its proliferation because loss of function of PC1 or PC-2 leads to uncontrolled growth (Winokurow & Schumacher, 2019).

Working Models of polycystin in Cilia:

Polycystins are localized in cilia across wide ranges of species. PC-2 is expressed in cilia of green algae *Chlamydomonas* and is present in distinct pattern forming two rows, and the rows are divided into proximal mobile and distal stationary zones(Liu et al., 2020). Zebrafish PC-2 are

localized in sensory cells associated with mechanotransduction, for example of the ear, the lateral lone organ and the olfactory placodes(Choi et al., 2022). In Caenorhabditis elegans, the homologs of PC-1 (LOV-1) and PC-2 (PKD-2) localize to the cilia of sensory neurons. PC-2 mediates mating in nematodes (Wang et al., 2014) where mechanical stimulation triggers the release of PC-2-carrying extracellular vehicles (EVs) from cilia tips and periciliary membranes during mating (Wang et al., 2021). The mechanical stimuli applied to the male worms is directly proportional to the release of PC-2-containing EVs (Yang et al., 2020). This evidence from model organisms appears to reveal the mechanosensory properties of polycystins. Applying fluid flow on renal cell cilia causes Ca<sup>2+</sup> signalling and the strength of Ca<sup>2+</sup> change is dependent on PC-1 and PC-2(Drummond, 2011). A mechanosensation model has thus been proposed about polycystin complex helping understand the polycystin signalling at molecular level. The model describes that the mechanical force applied on the flexible extracellular domains of PC-1 brings conformational changes in the polycystin complex which results in regulation of PC-2 channel activity(Ha et al., 2020).

Apart from this mechanical model, a ligand-receptor model also exists for polycystin pathway. According to this model a portion of the extracellular N-terminus of PKD2, either in uncleaved or cleaved form acts as a ligand for PC-2 channel to get activated(Padovano et al., 2020). Recently, it has been demonstrated that the CTL domain containing N-terminus part of PC-1 is enough to activate PC-2 (Ha et al., 2020). In this scenario, the fluid flow brings the two proteins closer for the channel activity. Both the working models need to be tested further, and both ethe models can work synergistically together.

# 1.8 Mastigonemes: An additive clue of mechanosensation

Mastigonemes are minute projections looking like "hair on cilia" as they form rows on the surface of one or both flagella of some unicellular ciliates (Bouck 1969; Bouck, 1971; Brooker, 1965; Fischer, 1894; Tran et al., 2022). Mastigonemes have been reported first in the 19th century via light microscopy (Bouck 1969; Fischer, 1894), and they can be divided into two groups based on their morphology: tubular and non-tubular. Tubular mastigonemes are found on the anterior flagellum of heterokont organisms, which have two flagella of unequal length. Tubular mastigonemes are stiff and straight and are ~1 μm in length. Protists usually use the flagellum with tubular mastigonemes as the locomotory flagellum (Bouck, 1971). Tubular mastigonemes can further be subdivided into two categories: bipartite and tripartite. Bipartite mastigonemes encase typical morphological components like a tubular shaft and several fine terminal filaments. For example, flagella in Acronema sippewissettensis have bipartite mastigonemes (Teal et al., 1998). Tripartite mastigonemes have a morphology similar to bipartite mastigonemes, with the addition of a basal region. Such tripartite mastigonemes can be observed in Paraphysomonas butcheri(Pennick & Clarke, 1972).

Non-tubular mastigonemes are thin and flexible filament like and with lesser diamater than tubular. These mastigonemes are found on the surface of both Chlamydomonas flagella in two rows(Witman et al., 1972). Chlamydomonas mastigoneme is the best described one. They consist of polymers of glycoprotein mastigoneme 1(MST1, also known as mastigoneme-like protein 1) which contain four cysteine-rich epidermal growth factors (EGF)-like domains (Blackman et al., 2011; Liu et al., 2020). MST1 is a part of the interacteractome of Chlamydomonas PC-2 homolog, with the latter anchoring mastigonemes on the axoneme (Liu et al., 2020). The proximal end of the mastigoneme is buried in a loose carbohydrate coat around

the flagellum called the glycocalyx, which is required for flagella-dependent whole-cell gliding motility (Bloodgood, 2010). Additionally, the distal region of non-tubular mastigonemes terminates with a much thinner filament, suggesting a delicate tip structure.

The proposed function of mastigonemes is that of increasing the effective surface of the flagellum (Brennen, 1976; Holwill & Peters, 1974; Jahn & Bovee, 1965; Namdeo et al., 2011). Tubular mastigonemes are needed in controlling the direction of cell motion. Smooth flagella have shown to push the cell body and move in opposite direction to the flagella waveform. While flagella with rigid mastigonemes on its surface pull the cell body and moves in direction of the flagella waveform(Bouck, 1971; Kamennaya et al., 2022). The ability to move in the direction of the waveform is given by the rigidity in the tubular mastigonemes as it allows the key thrust as described via mathematical modelling(Namdeo et al., 2011). Paraphysomonas vestita, a golden alga, has rigid mastigonemes which on encountering food changes the flagellar beating pattern resulting in the food particles being moved towards the ingestion area. This indicates that mastigonemes are involved in flagellar mechanosensation (Amador et al., 2020; Tottori & Nelson, 2013). The non-tubular mastigonemes being flexible in nature helps in whole cell gliding as reported in Peranema trichophorum (Amador et al., 2020). Another example of organisms with this kind of mastigonemes is *Chlamydomonas*. Here, the mastigonemes being loosely attached to the flagella keep on shedding when the cell is allowed to glide due to facing friction from the surface and this loss of mastigoneme results in slower swimming rate as compared to a normal cell(Liu et al., 2023; Liu et al., 2020). The same slow swimming phenotype is replicated in *Chlamydomonas* which are null in MST-1 protein that naturally inhibits the typical mastigoneme rows on the flagellar surface. This confirms that non-tubular mastigonems have a role in motility too(Das et al., 2023).

Non-tubular mastigonemes also determine the flagellar localization of other proteins like PC-2 in *Chlamydomonas* as the lack of mastigonemes changes the PC-2 localization and enrichment(Das et al., 2023; Liu et al., 2020). Impacting the ciliary presence of another channel protein as well the motility rate indicates that the non-tubular mastigonemes are responsible for performing either a mechanosensory role or function like a ligand-receptor complex.

It is remarkably interesting to note that the characteristic mechanosenation in cilia can be connected to the polycystin-mastigoneme complexes.

- AbouAlaiwi, W. A., Takahashi, M., Mell, B. R., Jones, T. J., Ratnam, S., Kolb, R. J., & Nauli, S. M. (2009). Ciliary polycystin-2 is a mechanosensitive calcium channel involved in nitric oxide signaling cascades. *Circ Res*, 104(7), 860-869. <a href="https://doi.org/10.1161/circresaha.108.192765">https://doi.org/10.1161/circresaha.108.192765</a>
- Amador, G. J., Wei, D., Tam, D., & Aubin-Tam, M. E. (2020). Fibrous Flagellar Hairs of Chlamydomonas reinhardtii Do Not Enhance Swimming. *Biophys J*, *118*(12), 2914-2925. <a href="https://doi.org/10.1016/j.bpj.2020.05.003">https://doi.org/10.1016/j.bpj.2020.05.003</a>
- Antony, D., Brunner, H. G., & Schmidts, M. (2021). Ciliary Dyneins and Dynein Related Ciliopathies. *Cells*, *10*(8). <a href="https://doi.org/10.3390/cells10081885">https://doi.org/10.3390/cells10081885</a>
- Anvarian, Z., Mykytyn, K., Mukhopadhyay, S., Pedersen, L. B., & Christensen, S. T. (2019). Cellular signalling by primary cilia in development, organ function and disease. *Nat Rev Nephrol*, *15*(4), 199-219. https://doi.org/10.1038/s41581-019-0116-9
- Arniges, M., Fernández-Fernández, J. M., Albrecht, N., Schaefer, M., & Valverde, M. A. (2006). Human TRPV4 channel splice variants revealed a key role of ankyrin domains in multimerization and trafficking. *J Biol Chem*, *281*(3), 1580-1586. <a href="https://doi.org/10.1074/jbc.M511456200">https://doi.org/10.1074/jbc.M511456200</a>
- Arniges, M., Vázquez, E., Fernández-Fernández, J. M., & Valverde, M. A. (2004). Swelling-activated Ca2+ entry via TRPV4 channel is defective in cystic fibrosis airway epithelia. *J Biol Chem*, 279(52), 54062-54068. https://doi.org/10.1074/jbc.M409708200
- Babu, D., & Roy, S. (2013). Left-right asymmetry: cilia stir up new surprises in the node. *Open Biol*, *3*(5), 130052. <a href="https://doi.org/10.1098/rsob.130052">https://doi.org/10.1098/rsob.130052</a>
- Badgandi, H. B., Hwang, S. H., Shimada, I. S., Loriot, E., & Mukhopadhyay, S. (2017). Tubby family proteins are adapters for ciliary trafficking of integral membrane proteins. *J Cell Biol*, 216(3), 743-760. https://doi.org/10.1083/jcb.201607095
- Bae, Y. K., & Barr, M. M. (2008). Sensory roles of neuronal cilia: cilia development, morphogenesis, and function in C. elegans. *Front Biosci*, *13*, 5959-5974. https://doi.org/10.2741/3129
- Bangs, F., & Anderson, K. V. (2017). Primary Cilia and Mammalian Hedgehog Signaling. *Cold Spring Harb Perspect Biol*, 9(5). https://doi.org/10.1101/cshperspect.a028175
- Barker, A. R., Thomas, R., & Dawe, H. R. (2014). Meckel-Gruber syndrome and the role of primary cilia in kidney, skeleton, and central nervous system development. *Organogenesis*, *10*(1), 96-107. <a href="https://doi.org/10.4161/org.27375">https://doi.org/10.4161/org.27375</a>
- Barrera, N. P., Shaifta, Y., McFadzean, I., Ward, J. P. T., Henderson, R. M., & Edwardson, J. M. (2007). AFM imaging reveals the tetrameric structure of the TRPC1 channel. *Biochemical and Biophysical Research Communications*, *358*(4), 1086-1090. <a href="https://doi.org/10.1016/j.bbrc.2007.05.039">https://doi.org/https://doi.org/10.1016/j.bbrc.2007.05.039</a>
- Beales, P., & Jackson, P. K. (2012). Cilia the prodigal organelle. *Cilia*, 1(1), 1. <a href="https://doi.org/10.1186/2046-2530-1-1">https://doi.org/10.1186/2046-2530-1-1</a>
- Bennett, H. W., Gustavsson, A. K., Bayas, C. A., Petrov, P. N., Mooney, N., Moerner, W. E., & Jackson, P. K. (2020). Novel fibrillar structure in the inversin compartment of primary cilia revealed by 3D single-molecule superresolution microscopy. *Mol Biol Cell*, *31*(7), 619-639. <a href="https://doi.org/10.1091/mbc.E19-09-0499">https://doi.org/10.1091/mbc.E19-09-0499</a>

- Berbari, N. F., Johnson, A. D., Lewis, J. S., Askwith, C. C., & Mykytyn, K. (2008). Identification of ciliary localization sequences within the third intracellular loop of G protein-coupled receptors. *Mol Biol Cell*, *19*(4), 1540-1547. https://doi.org/10.1091/mbc.e07-09-0942
- Berbari, N. F., O'Connor, A. K., Haycraft, C. J., & Yoder, B. K. (2009). The Primary Cilium as a Complex Signaling Center. *Current Biology*, 19(13), R526-R535. https://doi.org/https://doi.org/10.1016/j.cub.2009.05.025
- Bergmann, C., Guay-Woodford, L. M., Harris, P. C., Horie, S., Peters, D. J. M., & Torres, V. E. (2018). Polycystic kidney disease. *Nat Rev Dis Primers*, *4*(1), 50. https://doi.org/10.1038/s41572-018-0047-y
- Bertiaux, E., Mallet, A., Fort, C., Blisnick, T., Bonnefoy, S., Jung, J., Lemos, M., Marco, S., Vaughan, S., Trépout, S., Tinevez, J. Y., & Bastin, P. (2018). Bidirectional intraflagellar transport is restricted to two sets of microtubule doublets in the trypanosome flagellum. *J Cell Biol*, 217(12), 4284-4297. https://doi.org/10.1083/jcb.201805030
- Besschetnova, T. Y., Kolpakova-Hart, E., Guan, Y., Zhou, J., Olsen, B. R., & Shah, J. V. (2010). Identification of Signaling Pathways Regulating Primary Cilium Length and Flow-Mediated Adaptation. *Current Biology*, *20*(2), 182-187. https://doi.org/https://doi.org/10.1016/j.cub.2009.11.072
- Bezares-Calderón, L. A., Berger, J., & Jékely, G. (2020). Diversity of cilia-based mechanosensory systems and their functions in marine animal behaviour. *Philos Trans R Soc Lond B Biol Sci*, 375(1792), 20190376. https://doi.org/10.1098/rstb.2019.0376
- Bhogaraju, S., Engel, B. D., & Lorentzen, E. (2013). Intraflagellar transport complex structure and cargo interactions. *Cilia*, *2*(1), 10. https://doi.org/10.1186/2046-2530-2-10
- Blackman, L. M., Arikawa, M., Yamada, S., Suzaki, T., & Hardham, A. R. (2011). Identification of a Mastigoneme Protein from Phytophthora nicotianae. *Protist*, *162*(1), 100-114. https://doi.org/https://doi.org/10.1016/j.protis.2010.01.005
- Bloodgood, R. A. (2010). Sensory reception is an attribute of both primary cilia and motile cilia. *Journal of Cell Science*, *123*(4), 505-509. <a href="https://doi.org/10.1242/jcs.066308">https://doi.org/10.1242/jcs.066308</a>
- Boucher, C., & Sandford, R. (2004). Autosomal dominant polycystic kidney disease (ADPKD, MIM 173900, PKD1 and PKD2 genes, protein products known as polycystin-1 and polycystin-2). *Eur J Hum Genet*, *12*(5), 347-354. https://doi.org/10.1038/sj.ejhg.5201162
- Bouck, G. B. (1969). EXTRACELLULAR MICROTUBULES: The Origin, Structure, and Attachment of Flagellar Hairs in Fucus and Ascophyllum Antherozoids. *Journal of Cell Biology*, 40(2), 446-460. https://doi.org/10.1083/jcb.40.2.446
- Bouck, G. B. (1971). THE STRUCTURE, ORIGIN, ISOLATION, AND COMPOSITION OF THE TUBULAR MASTIGONEMES OF THE OCHROMONAS FLAGELLUM. *The Journal of Cell Biology*, *50*, 362 384.
- Brazelton, W. J., Amundsen, C. D., Silflow, C. D., & Lefebvre, P. A. (2001). The bld1 mutation identifies the Chlamydomonas osm-6 homolog as a gene required for flagellar assembly. *Curr Biol*, *11*(20), 1591-1594. <a href="https://doi.org/10.1016/s0960-9822(01)00485-7">https://doi.org/10.1016/s0960-9822(01)00485-7</a>
- Brennen, C. (1976). Locomotion of flagellates with mastigonemes. *J Mechanochem Cell Motil*, 3(3), 207-217.

- Breslow, D. K., & Holland, A. J. (2019). Mechanism and Regulation of Centriole and Cilium Biogenesis. *Annu Rev Biochem*, 88, 691-724. <a href="https://doi.org/10.1146/annurev-biochem-013118-111153">https://doi.org/10.1146/annurev-biochem-013118-111153</a>
- Brooker, B. E. (1965). Mastigonemes in a bodonid flagellate. *Experimental Cell Research*, 37(2), 300-305. https://doi.org/https://doi.org/10.1016/0014-4827(65)90178-3
- Bustamante-Marin, X. M., & Ostrowski, L. E. (2017). Cilia and Mucociliary Clearance. *Cold Spring Harb Perspect Biol*, 9(4). https://doi.org/10.1101/cshperspect.a028241
- Cao, E., Liao, M., Cheng, Y., & Julius, D. (2013). TRPV1 structures in distinct conformations reveal activation mechanisms. *Nature*, *504*(7478), 113-118. <a href="https://doi.org/10.1038/nature12823">https://doi.org/10.1038/nature12823</a>
- Cassioli, C., & Baldari, C. T. (2019). A Ciliary View of the Immunological Synapse. *Cells*, 8(8), 789. <a href="https://www.mdpi.com/2073-4409/8/8/789">https://www.mdpi.com/2073-4409/8/8/789</a>
- Choi, S. S. A., Chan, H. H., Chan, C. M., Wang, X., Webb, S. E., Leung, K. W., Tsim, K. W. K., & Miller, A. L. (2022). Neuromasts and Olfactory Organs of Zebrafish Larvae Represent Possible Sites of SARS-CoV-2 Pseudovirus Host Cell Entry. *J Virol*, 96(24), e0141822. <a href="https://doi.org/10.1128/jvi.01418-22">https://doi.org/10.1128/jvi.01418-22</a>
- Christensen, S. T., Morthorst, S. K., Mogensen, J. B., & Pedersen, L. B. (2017). Primary Cilia and Coordination of Receptor Tyrosine Kinase (RTK) and Transforming Growth Factor  $\beta$  (TGF- $\beta$ ) Signaling. *Cold Spring Harb Perspect Biol*, 9(6). https://doi.org/10.1101/cshperspect.a028167
- Claude-Taupin, A., Dupont, N., & Codogno, P. (2022). Autophagy and the primary cilium in cell metabolism: What's upstream? *Front Cell Dev Biol*, *10*, 1046248. <a href="https://doi.org/10.3389/fcell.2022.1046248">https://doi.org/10.3389/fcell.2022.1046248</a>
- Cole, D. G., Diener, D. R., Himelblau, A. L., Beech, P. L., Fuster, J. C., & Rosenbaum, J. L. (1998). Chlamydomonas kinesin-II-dependent intraflagellar transport (IFT): IFT particles contain proteins required for ciliary assembly in Caenorhabditis elegans sensory neurons. *J Cell Biol*, 141(4), 993-1008. https://doi.org/10.1083/jcb.141.4.993
- Corbit, K. C., Shyer, A. E., Dowdle, W. E., Gaulden, J., Singla, V., Chen, M. H., Chuang, P. T., & Reiter, J. F. (2008). Kif3a constrains beta-catenin-dependent Wnt signalling through dual ciliary and non-ciliary mechanisms. *Nat Cell Biol*, *10*(1), 70-76. https://doi.org/10.1038/ncb1670
- Corey, D. P., García-Añoveros, J., Holt, J. R., Kwan, K. Y., Lin, S. Y., Vollrath, M. A., Amalfitano, A., Cheung, E. L., Derfler, B. H., Duggan, A., Géléoc, G. S., Gray, P. A., Hoffman, M. P., Rehm, H. L., Tamasauskas, D., & Zhang, D. S. (2004). TRPA1 is a candidate for the mechanosensitive transduction channel of vertebrate hair cells. *Nature*, *432*(7018), 723-730. <a href="https://doi.org/10.1038/nature03066">https://doi.org/10.1038/nature03066</a>
- Craft, J. M., Harris, J. A., Hyman, S., Kner, P., & Lechtreck, K. F. (2015). Tubulin transport by IFT is upregulated during ciliary growth by a cilium-autonomous mechanism. *J Cell Biol*, 208(2), 223-237. <a href="https://doi.org/10.1083/jcb.201409036">https://doi.org/10.1083/jcb.201409036</a>
- Das, P., Mekonnen, B., Alkhofash, R., Ingle, A., Workman, E. B., Feather, A., Liu, P., & Lechtreck, K. F. (2023). Small Interactor of PKD2 (SIP), a novel PKD2-related single-pass transmembrane protein, is required for proteolytic processing and ciliary import of Chlamydomonas PKD2. *bioRxiv*. <a href="https://doi.org/10.1101/2023.06.13.544839">https://doi.org/10.1101/2023.06.13.544839</a>
- Dougherty, G. W., Loges, N. T., Klinkenbusch, J. A., Olbrich, H., Pennekamp, P., Menchen, T., Raidt, J., Wallmeier, J., Werner, C., Westermann, C., Ruckert, C., Mirra, V., Hjeij, R., Memari, Y., Durbin, R., Kolb-Kokocinski, A., Praveen, K., Kashef, M. A., Kashef, S.,

- Eghtedari, F., Häffner, K., Valmari, P., Baktai, G., Aviram, M., Bentur, L., Amirav, I., Davis, E. E., Katsanis, N., Brueckner, M., Shaposhnykov, A., Pigino, G., Dworniczak, B., & Omran, H. (2016). DNAH11 Localization in the Proximal Region of Respiratory Cilia Defines Distinct Outer Dynein Arm Complexes. *Am J Respir Cell Mol Biol*, *55*(2), 213-224. <a href="https://doi.org/10.1165/rcmb.2015-03530C">https://doi.org/10.1165/rcmb.2015-03530C</a>
- Drummond, I. A. (2011). Polycystins, focal adhesions and extracellular matrix interactions. *Biochim Biophys Acta*, *1812*(10), 1322-1326. https://doi.org/10.1016/j.bbadis.2011.03.003
- Du Toit, A. (2014). An ion channel for cilia. *Nature Reviews Molecular Cell Biology*, *15*(2), 78-78. <a href="https://doi.org/10.1038/nrm3736">https://doi.org/10.1038/nrm3736</a>
- Dutcher, S. K. (2020). Asymmetries in the cilia of Chlamydomonas. *Philos Trans R Soc Lond B Biol Sci*, 375(1792), 20190153. <a href="https://doi.org/10.1098/rstb.2019.0153">https://doi.org/10.1098/rstb.2019.0153</a>
- Dutcher, S. K., & O'Toole, E. T. (2016). The basal bodies of Chlamydomonas reinhardtii. *Cilia*, 5, 18. https://doi.org/10.1186/s13630-016-0039-z
- Edwards, B. F. L., Wheeler, R. J., Barker, A. R., Moreira-Leite, F. F., Gull, K., & Sunter, J. D. (2018). Direction of flagellum beat propagation is controlled by proximal/distal outer dynein arm asymmetry. *Proceedings of the National Academy of Sciences*, 115(31), E7341-E7350. <a href="https://doi.org/doi:10.1073/pnas.1805827115">https://doi.org/doi:10.1073/pnas.1805827115</a>
- Emmer, B. T., Maric, D., & Engman, D. M. (2010). Molecular mechanisms of protein and lipid targeting to ciliary membranes. *J Cell Sci*, 123(Pt 4), 529-536. https://doi.org/10.1242/jcs.062968
- Endres, R. G., & Wingreen, N. S. (2009). Maximum Likelihood and the Single Receptor. *Physical Review Letters*, *103*(15), 158101. https://doi.org/10.1103/PhysRevLett.103.158101
- Esarte Palomero, O., Larmore, M., & DeCaen, P. G. (2023). Polycystin Channel Complexes. *Annu Rev Physiol, 85*, 425-448. <a href="https://doi.org/10.1146/annurev-physiol-031522-084334">https://doi.org/10.1146/annurev-physiol-031522-084334</a>
- Fisch, C., & Dupuis-Williams, P. (2011). Ultrastructure of cilia and flagella back to the future! *Biology of the Cell*, 103(6), 249-270. https://doi.org/https://doi.org/10.1042/BC20100139
- Fischer, E. (1894). Einfluss der Configuration auf die Wirkung der Enzyme. *Berichte der deutschen chemischen Gesellschaft*, *27*(3), 2985-2993. https://doi.org/https://doi.org/10.1002/cber.18940270364
- Follit, J. A., Li, L., Vucica, Y., & Pazour, G. J. (2010). The cytoplasmic tail of fibrocystin contains a ciliary targeting sequence. *J Cell Biol*, 188(1), 21-28. https://doi.org/10.1083/jcb.200910096
- Garcia, G., 3rd, Raleigh, D. R., & Reiter, J. F. (2018). How the Ciliary Membrane Is Organized Inside-Out to Communicate Outside-In. *Curr Biol*, 28(8), R421-r434. https://doi.org/10.1016/j.cub.2018.03.010
- Giamarchi, A., Feng, S., Rodat-Despoix, L., Xu, Y., Bubenshchikova, E., Newby, L. J., Hao, J., Gaudioso, C., Crest, M., Lupas, A. N., Honoré, E., Williamson, M. P., Obara, T., Ong, A. C., & Delmas, P. (2010). A polycystin-2 (TRPP2) dimerization domain essential for the function of heteromeric polycystin complexes. *Embo j*, *29*(7), 1176-1191. https://doi.org/10.1038/emboi.2010.18

- Gonçalves, J., & Pelletier, L. (2017). The Ciliary Transition Zone: Finding the Pieces and Assembling the Gate. *Mol Cells*, 40(4), 243-253. https://doi.org/10.14348/molcells.2017.0054
- Gopalakrishnan, J., Feistel, K., Friedrich, B. M., Grapin-Botton, A., Jurisch-Yaksi, N., Mass, E., Mick, D. U., Müller, R. U., May-Simera, H., Schermer, B., Schmidts, M., Walentek, P., & Wachten, D. (2023). Emerging principles of primary cilia dynamics in controlling tissue organization and function. *Embo j*, *42*(21), e113891. https://doi.org/10.15252/embj.2023113891
- Grieben, M., Pike, A. C., Shintre, C. A., Venturi, E., El-Ajouz, S., Tessitore, A., Shrestha, L., Mukhopadhyay, S., Mahajan, P., Chalk, R., Burgess-Brown, N. A., Sitsapesan, R., Huiskonen, J. T., & Carpenter, E. P. (2017). Structure of the polycystic kidney disease TRP channel Polycystin-2 (PC2). *Nat Struct Mol Biol*, *24*(2), 114-122. <a href="https://doi.org/10.1038/nsmb.3343">https://doi.org/10.1038/nsmb.3343</a>
- Guemez-Gamboa, A., Coufal, Nicole G., & Gleeson, Joseph G. (2014). Primary Cilia in the Developing and Mature Brain. *Neuron*, *82*(3), 511-521. https://doi.org/10.1016/j.neuron.2014.04.024
- Ha, K., Nobuhara, M., Wang, Q., Walker, R. V., Qian, F., Schartner, C., Cao, E., & Delling, M. (2020). The heteromeric PC-1/PC-2 polycystin complex is activated by the PC-1 Nterminus. *Elife*, 9. <a href="https://doi.org/10.7554/eLife.60684">https://doi.org/10.7554/eLife.60684</a>
- Hardy, E., & Tsiokas, L. (2020). Polycystins as components of large multiprotein complexes of polycystin interactors. *Cell Signal*, *72*, 109640. https://doi.org/10.1016/j.cellsig.2020.109640
- Haycraft, C. J., Schafer, J. C., Zhang, Q., Taulman, P. D., & Yoder, B. K. (2003). Identification of CHE-13, a novel intraflagellar transport protein required for cilia formation. *Exp Cell Res*, 284(2), 251-263. https://doi.org/10.1016/s0014-4827(02)00089-7
- Hellmich, U. A., & Gaudet, R. (2014). Structural biology of TRP channels. *Handb Exp Pharmacol*, 223, 963-990. https://doi.org/10.1007/978-3-319-05161-1\_10
- Hickey, D., Vilfan, A., & Golestanian, R. (2021). Ciliary chemosensitivity is enhanced by cilium geometry and motility. *eLife*, *10*. <a href="https://doi.org/10.7554/eLife.66322">https://doi.org/10.7554/eLife.66322</a>
- Holwill, M. E., & Peters, P. D. (1974). Dynamics of the hispid flagellum of Ochromonas danica. The role of mastigonemes. *J Cell Biol*, *62*(2), 322-328. https://doi.org/10.1083/jcb.62.2.322
- Hong, J. J., Kim, K. E., Park, S. Y., Bok, J., Seo, J. T., & Moon, S. J. (2021). Differential Roles of Tubby Family Proteins in Ciliary Formation and Trafficking. *Molecules and Cells*, 44(8), 591-601. <a href="https://doi.org/https://doi.org/10.14348/molcells.2021.0082">https://doi.org/https://doi.org/10.14348/molcells.2021.0082</a>
- Hsiao, Y.-C., Tuz, K., & Ferland, R. J. (2012). Trafficking in and to the primary cilium. *Cilia*, *1*(1), 4. <a href="https://doi.org/10.1186/2046-2530-1-4">https://doi.org/10.1186/2046-2530-1-4</a>
- Hu, J., & Harris, P. C. (2020). Regulation of polycystin expression, maturation and trafficking. *Cell Signal*, *72*, 109630. <a href="https://doi.org/10.1016/j.cellsig.2020.109630">https://doi.org/10.1016/j.cellsig.2020.109630</a>
- Hwang, J., Yanagisawa, H., Davis, K. C., Hunter, E. L., Fox, L. A., Jimenez, A. R., Goodwin, R. E., Gordon, S. A., Stuart, C. D. E., Bower, R., Porter, M. E., Dutcher, S. K., Sale, W. S., Lechtreck, K. F., & Alford, L. M. (2024). Assembly of FAP93 at the proximal axoneme in Chlamydomonas cilia. *Cytoskeleton (Hoboken)*, *81*(11), 539-555. https://doi.org/10.1002/cm.21818
- Ishikawa, H., & Marshall, W. F. (2017). Intraflagellar Transport and Ciliary Dynamics. *Cold Spring Harb Perspect Biol*, 9(3). https://doi.org/10.1101/cshperspect.a021998

- Ishikawa, T. (2017). Axoneme Structure from Motile Cilia. *Cold Spring Harb Perspect Biol*, 9(1). https://doi.org/10.1101/cshperspect.a028076
- Jahn, T. L., & Bovee, E. C. (1965). Mechanisms of Movement in Taxonomy of Sarcodina. I. As a Basis for a New Major Dichotomy into Two Classes, Autotractea and Hydraulea. *The American Midland Naturalist*, 73(1), 30-40. <a href="https://doi.org/10.2307/2423319">https://doi.org/10.2307/2423319</a>
- Jara-Oseguera , A. s., Llorente , I., Rosenbaum , T., & Islas , L. n. D. (2008). Properties of the Inner Pore Region of TRPV1 Channels Revealed by Block with Quaternary Ammoniums. *Journal of General Physiology*, *132*(5), 547-562. https://doi.org/10.1085/jgp.200810051
- Jing, J., Wu, Z., Wang, J., Luo, G., Lin, H., Fan, Y., & Zhou, C. (2023). Hedgehog signaling in tissue homeostasis, cancers and targeted therapies. *Signal Transduction and Targeted Therapy*, 8(1), 315. https://doi.org/10.1038/s41392-023-01559-5
- Jordan, M. A., Diener, D. R., Stepanek, L., & Pigino, G. (2018). The cryo-EM structure of intraflagellar transport trains reveals how dynein is inactivated to ensure unidirectional anterograde movement in cilia. *Nat Cell Biol*, *20*(11), 1250-1255. <a href="https://doi.org/10.1038/s41556-018-0213-1">https://doi.org/10.1038/s41556-018-0213-1</a>
- Kamennaya, N. A., Kennaway, G., Sleigh, M. A., & Zubkov, M. V. (2022). Notable predominant morphology of the smallest most abundant protozoa of the open ocean revealed by electron microscopy. *Journal of Plankton Research*, *44*(4), 542-558. <a href="https://doi.org/10.1093/plankt/fbac031">https://doi.org/10.1093/plankt/fbac031</a>
- Kedei, N., Szabo, T., Lile, J. D., Treanor, J. J., Olah, Z., Iadarola, M. J., & Blumberg, P. M. (2001). Analysis of the Native Quaternary Structure of Vanilloid Receptor 1\*210. *Journal of Biological Chemistry*, 276(30), 28613-28619. https://doi.org/https://doi.org/10.1074/jbc.M103272200
- Kilburn, C., & Winey, M. (2008). Basal bodies. *Current Biology*, *18*(2), R56-R57. https://doi.org/10.1016/j.cub.2007.10.057
- Kim, J., Hsia, E. Y., Brigui, A., Plessis, A., Beachy, P. A., & Zheng, X. (2015). The role of ciliary trafficking in Hedgehog receptor signaling. *Sci Signal*, 8(379), ra55. https://doi.org/10.1126/scisignal.aaa5622
- Kim, S., Nie, H., Nesin, V., Tran, U., Outeda, P., Bai, C. X., Keeling, J., Maskey, D., Watnick, T., Wessely, O., & Tsiokas, L. (2016). The polycystin complex mediates Wnt/Ca(2+) signalling. *Nat Cell Biol*, *18*(7), 752-764. <a href="https://doi.org/10.1038/ncb3363">https://doi.org/10.1038/ncb3363</a>
- Kobori, T., Smith, G. D., Sandford, R., & Edwardson, J. M. (2009). The transient receptor potential channels TRPP2 and TRPC1 form a heterotetramer with a 2:2 stoichiometry and an alternating subunit arrangement. *J Biol Chem*, 284(51), 35507-35513. <a href="https://doi.org/10.1074/jbc.M109.060228">https://doi.org/10.1074/jbc.M109.060228</a>
- Koefoed, K., Veland, I. R., Pedersen, L. B., Larsen, L. A., & Christensen, S. T. (2014). Cilia and coordination of signaling networks during heart development. *Organogenesis*, *10*(1), 108-125. <a href="https://doi.org/10.4161/org.27483">https://doi.org/10.4161/org.27483</a>
- Komiya, Y., & Habas, R. (2008). Wnt signal transduction pathways. Organogenesis, 4(2), 68-75. https://doi.org/10.4161/org.4.2.5851
- Kozminski, K. G., Johnson, K. A., Forscher, P., & Rosenbaum, J. L. (1993). A motility in the eukaryotic flagellum unrelated to flagellar beating. *Proc Natl Acad Sci U S A*, 90(12), 5519-5523. https://doi.org/10.1073/pnas.90.12.5519

- Kuek, L. E., & Lee, R. J. (2020). First contact: the role of respiratory cilia in host-pathogen interactions in the airways. *Am J Physiol Lung Cell Mol Physiol*, *319*(4), L603-l619. <a href="https://doi.org/10.1152/ajplung.00283.2020">https://doi.org/10.1152/ajplung.00283.2020</a>
- Lechtreck, K.-F., Johnson, E. C., Sakai, T., Cochran, D., Ballif, B. A., Rush, J., Pazour, G. J., Ikebe, M., & Witman, G. B. (2009). The Chlamydomonas reinhardtii BBSome is an IFT cargo required for export of specific signaling proteins from flagella. *Journal of Cell Biology*, 187(7), 1117-1132. <a href="https://doi.org/10.1083/jcb.200909183">https://doi.org/10.1083/jcb.200909183</a>
- Lechtreck, K. F. (2015). IFT-Cargo Interactions and Protein Transport in Cilia. *Trends Biochem Sci*, 40(12), 765-778. <a href="https://doi.org/10.1016/j.tibs.2015.09.003">https://doi.org/10.1016/j.tibs.2015.09.003</a>
- Lechtreck, K. F., Van De Weghe, J. C., Harris, J. A., & Liu, P. (2017). Protein transport in growing and steady-state cilia. *Traffic*, *18*(5), 277-286. https://doi.org/10.1111/tra.12474
- Legal, T., Parra, M., Tong, M., Black, C. S., Joachimiak, E., Valente-Paterno, M., Lechtreck, K., Gaertig, J., & Bui, K. H. (2023). CEP104/FAP256 and associated cap complex maintain stability of the ciliary tip. *Journal of Cell Biology*, 222(11). <a href="https://doi.org/10.1083/jcb.202301129">https://doi.org/10.1083/jcb.202301129</a>
- Li, M., Jiang, J., & Yue, L. (2006). Functional Characterization of Homo- and Heteromeric Channel Kinases TRPM6 and TRPM7. *Journal of General Physiology*, *127*(5), 525-537. https://doi.org/10.1085/jgp.200609502
- Lindemann, C. B., & Lesich, K. A. (2021). The many modes of flagellar and ciliary beating: Insights from a physical analysis. *Cytoskeleton (Hoboken)*, *78*(2), 36-51. https://doi.org/10.1002/cm.21656
- Liu, J., Xiao, Q., Xiao, J., Niu, C., Li, Y., Zhang, X., Zhou, Z., Shu, G., & Yin, G. (2022). Wnt/β-catenin signalling: function, biological mechanisms, and therapeutic opportunities. Signal Transduction and Targeted Therapy, 7(1), 3. <a href="https://doi.org/10.1038/s41392-021-00762-6">https://doi.org/10.1038/s41392-021-00762-6</a>
- Liu, P., Liu, Y., & Zhou, J. (2023). Ciliary mechanosensation roles of polycystins and mastigonemes. *Journal of Cell Science*, 136(3). https://doi.org/10.1242/jcs.260565
- Liu, P., Lou, X., Wingfield, J. L., Lin, J., Nicastro, D., & Lechtreck, K. (2020). Chlamydomonas PKD2 organizes mastigonemes, hair-like glycoprotein polymers on cilia. *J Cell Biol*, 219(6). <a href="https://doi.org/10.1083/jcb.202001122">https://doi.org/10.1083/jcb.202001122</a>
- Louka, P., Vasudevan, K. K., Guha, M., Joachimiak, E., Wloga, D., Tomasi, R. F.-X., Baroud, C. N., Dupuis-Williams, P., Galati, D. F., Pearson, C. G., Rice, L. M., Moresco, J. J., Yates, J. R., III, Jiang, Y.-Y., Lechtreck, K., Dentler, W., & Gaertig, J. (2018). Proteins that control the geometry of microtubules at the ends of cilia. *Journal of Cell Biology*, *217*(12), 4298-4313. <a href="https://doi.org/10.1083/jcb.201804141">https://doi.org/10.1083/jcb.201804141</a>
- Malone, A. M., Anderson, C. T., Tummala, P., Kwon, R. Y., Johnston, T. R., Stearns, T., & Jacobs, C. R. (2007). Primary cilia mediate mechanosensing in bone cells by a calcium-independent mechanism. *Proc Natl Acad Sci U S A*, *104*(33), 13325-13330. https://doi.org/10.1073/pnas.0700636104
- Maruyama, Y., Ogura, T., Mio, K., Kiyonaka, S., Kato, K., Mori, Y., & Sato, C. (2007). Three-dimensional Reconstruction Using Transmission Electron Microscopy Reveals a Swollen, Bell-shaped Structure of Transient Receptor Potential Melastatin Type 2 Cation Channel\*. *Journal of Biological Chemistry*, 282(51), 36961-36970. <a href="https://doi.org/10.1074/jbc.M705694200">https://doi.org/10.1074/jbc.M705694200</a>

- Masyuk, A. I., Masyuk, T. V., & LaRusso, N. F. (2008). Cholangiocyte primary cilia in liver health and disease. *Dev Dyn*, *237*(8), 2007-2012. https://doi.org/10.1002/dvdy.21530
- Mesland, D. A. M. (1976). Mating in Chlamydomonas eugametos. *Archives of Microbiology*, 109(1), 31-35. <a href="https://doi.org/10.1007/BF00425109">https://doi.org/10.1007/BF00425109</a>
- Mill, P., Christensen, S. T., & Pedersen, L. B. (2023). Primary cilia as dynamic and diverse signalling hubs in development and disease. *Nat Rev Genet*, *24*(7), 421-441. https://doi.org/10.1038/s41576-023-00587-9
- Mio, K., Ogura, T., Kiyonaka, S., Hiroaki, Y., Tanimura, Y., Fujiyoshi, Y., Mori, Y., & Sato, C. (2007). The TRPC3 Channel Has a Large Internal Chamber Surrounded by Signal Sensing Antennas. *Journal of Molecular Biology*, *367*(2), 373-383. <a href="https://doi.org/10.1016/j.jmb.2006.12.043">https://doi.org/https://doi.org/10.1016/j.jmb.2006.12.043</a>
- Mizuno, N., Taschner, M., Engel, B. D., & Lorentzen, E. (2012). Structural studies of ciliary components. *J Mol Biol*, 422(2), 163-180. https://doi.org/10.1016/j.jmb.2012.05.040
- Morris, R. L., & Scholey, J. M. (1997). Heterotrimeric kinesin-II is required for the assembly of motile 9+2 ciliary axonemes on sea urchin embryos. *J Cell Biol*, *138*(5), 1009-1022. <a href="https://doi.org/10.1083/jcb.138.5.1009">https://doi.org/10.1083/jcb.138.5.1009</a>
- Morthorst, S. K., Christensen, S. T., & Pedersen, L. B. (2018). Regulation of ciliary membrane protein trafficking and signalling by kinesin motor proteins. *The FEBS Journal*, 285(24), 4535-4564. https://doi.org/https://doi.org/10.1111/febs.14583
- Murdoch, J. N., & Copp, A. J. (2010). The relationship between sonic Hedgehog signaling, cilia, and neural tube defects. *Birth Defects Res A Clin Mol Teratol*, 88(8), 633-652. <a href="https://doi.org/10.1002/bdra.20686">https://doi.org/10.1002/bdra.20686</a>
- Mykytyn, K., & Askwith, C. (2017). G-Protein-Coupled Receptor Signaling in Cilia. *Cold Spring Harb Perspect Biol*, 9(9). https://doi.org/10.1101/cshperspect.a028183
- Nachury, M. V., & Mick, D. U. (2019). Establishing and regulating the composition of cilia for signal transduction. *Nat Rev Mol Cell Biol*, *20*(7), 389-405. https://doi.org/10.1038/s41580-019-0116-4
- Namdeo, S., Khaderi, S. N., den Toonder, J. M. J., & Onck, P. R. (2011). Swimming direction reversal of flagella through ciliary motion of mastigonemes a). *Biomicrofluidics*, *5*(3). <a href="https://doi.org/10.1063/1.3608240">https://doi.org/10.1063/1.3608240</a>
- Niida, Y., Togi, S., & Ura, H. (2021). Molecular Bases of Human Malformation Syndromes Involving the SHH Pathway: GLIA/R Balance and Cardinal Phenotypes. *Int J Mol Sci*, 22(23). <a href="https://doi.org/10.3390/ijms222313060">https://doi.org/10.3390/ijms222313060</a>
- Nilius, B., Owsianik, G., & Voets, T. (2008). Transient receptor potential channels meet phosphoinositides. *The EMBO Journal*, *27*(21), 2809-2816-2816. https://doi.org/https://doi.org/10.1038/emboj.2008.217
- Oda, T., Yanagisawa, H., & Kikkawa, M. (2015). Detailed structural and biochemical characterization of the nexin-dynein regulatory complex. *Mol Biol Cell*, *26*(2), 294-304. https://doi.org/10.1091/mbc.E14-09-1367
- Olbrich, H., Cremers, C., Loges, Niki T., Werner, C., Nielsen, Kim G., Marthin, June K., Philipsen, M., Wallmeier, J., Pennekamp, P., Menchen, T., Edelbusch, C., Dougherty, Gerard W., Schwartz, O., Thiele, H., Altmüller, J., Rommelmann, F., & Omran, H. (2015). Loss-of-Function GAS8 Mutations Cause Primary Ciliary Dyskinesia and Disrupt the

- Nexin-Dynein Regulatory Complex. *The American Journal of Human Genetics*, 97(4), 546-554. <a href="https://doi.org/https://doi.org/10.1016/j.ajhg.2015.08.012">https://doi.org/https://doi.org/10.1016/j.ajhg.2015.08.012</a>
- Ong, A. C. M., & Harris, P. C. (2005). Molecular pathogenesis of ADPKD: The polycystin complex gets complex. *Kidney International*, *67*(4), 1234-1247. https://doi.org/10.1111/j.1523-1755.2005.00201.x
- Orts-Del'Immagine, A., Cantaut-Belarif, Y., Thouvenin, O., Roussel, J., Baskaran, A., Langui, D., Koëth, F., Bivas, P., Lejeune, F. X., Bardet, P. L., & Wyart, C. (2020). Sensory Neurons Contacting the Cerebrospinal Fluid Require the Reissner Fiber to Detect Spinal Curvature In Vivo. *Curr Biol*, *30*(5), 827-839.e824. <a href="https://doi.org/10.1016/j.cub.2019.12.071">https://doi.org/10.1016/j.cub.2019.12.071</a>
- Oshima, D., Yoshida, M., Saga, K., Ito, N., Tsuji, M., Isu, A., Watanabe, N., Wakabayashi, K.-i., & Yoshimura, K. (2023). Mechanoresponses mediated by the TRP11 channel in cilia of Chlamydomonas reinhardtii. *iScience*, *26*(10), 107926. <a href="https://doi.org/10.1016/j.isci.2023.107926">https://doi.org/10.1016/j.isci.2023.107926</a>
- Padovano, V., Mistry, K., Merrick, D., Gresko, N., & Caplan, M. J. (2020). A cut above (and below): Protein cleavage in the regulation of polycystin trafficking and signaling. *Cell Signal*, 72, 109634. https://doi.org/10.1016/j.cellsig.2020.109634
- Pala, R., Alomari, N., & Nauli, S. M. (2017). Primary Cilium-Dependent Signaling Mechanisms. *Int J Mol Sci*, 18(11). https://doi.org/10.3390/ijms18112272
- Paolocci, E., & Zaccolo, M. (2023). Compartmentalised cAMP signalling in the primary cilium. *Front Physiol*, *14*, 1187134. <a href="https://doi.org/10.3389/fphys.2023.1187134">https://doi.org/10.3389/fphys.2023.1187134</a>
- Park, K., & Leroux, M. R. (2022). Composition, organization and mechanisms of the transition zone, a gate for the cilium. *EMBO Rep*, 23(12), e55420. https://doi.org/10.15252/embr.202255420
- Pazour, G. J., Dickert, B. L., Vucica, Y., Seeley, E. S., Rosenbaum, J. L., Witman, G. B., & Cole, D. G. (2000). Chlamydomonas IFT88 and its mouse homologue, polycystic kidney disease gene tg737, are required for assembly of cilia and flagella. *J Cell Biol*, 151(3), 709-718. <a href="https://doi.org/10.1083/jcb.151.3.709">https://doi.org/10.1083/jcb.151.3.709</a>
- Pennick, N. C., & Clarke, K. J. (1972). Paraphysomonas Butcheri sp. nov. a marine, colourless, scale-bearing member of the Chrysophyceae. *British Phycological Journal*, 7(1), 45-48. <a href="https://doi.org/10.1080/00071617200650051">https://doi.org/10.1080/00071617200650051</a>
- Piperno, G., & Mead, K. (1997). Transport of a novel complex in the cytoplasmic matrix of <i>Chlamydomonas&#x2009;</i>flagella. *Proceedings of the National Academy of Sciences*, 94(9), 4457-4462. <a href="https://doi.org/doi:10.1073/pnas.94.9.4457">https://doi.org/doi:10.1073/pnas.94.9.4457</a>
- Qian, F., Germino, F. J., Cai, Y., Zhang, X., Somlo, S., & Germino, G. G. (1997). PKD1 interacts with PKD2 through a probable coiled-coil domain. *Nat Genet*, *16*(2), 179-183. <a href="https://doi.org/10.1038/ng0697-179">https://doi.org/10.1038/ng0697-179</a>
- R. Ferreira, R., Fukui, H., Chow, R., Vilfan, A., & Vermot, J. (2019). The cilium as a force sensor–myth versus reality. *Journal of Cell Science*, *132*(14). https://doi.org/10.1242/jcs.213496
- Reiter, J. F., Blacque, O. E., & Leroux, M. R. (2012). The base of the cilium: roles for transition fibres and the transition zone in ciliary formation, maintenance and compartmentalization. *EMBO reports*, *13*(7), 608-618. https://doi.org/https://doi.org/10.1038/embor.2012.73

- Reiter, J. F., & Leroux, M. R. (2017). Genes and molecular pathways underpinning ciliopathies. *Nat Rev Mol Cell Biol*, *18*(9), 533-547. https://doi.org/10.1038/nrm.2017.60
- Resnick, A., & Hopfer, U. (2007). Force-response considerations in ciliary mechanosensation. *Biophys J*, 93(4), 1380-1390. https://doi.org/10.1529/biophysj.107.105007
- Rogowski, J. A., Staiger, D., Patrick, T., Horbar, J., Kenny, M., & Lake, E. T. (2013). Nurse staffing and NICU infection rates. *JAMA Pediatr*, *167*(5), 444-450. https://doi.org/10.1001/jamapediatrics.2013.18
- Rosenfeld, C. S. (2019). Male reproductive tract cilia beat to a different drummer. *Proc Natl Acad Sci U S A*, 116(9), 3361-3363. <a href="https://doi.org/10.1073/pnas.1900112116">https://doi.org/10.1073/pnas.1900112116</a>
- Sang, L., Miller, Julie J., Corbit, Kevin C., Giles, Rachel H., Brauer, Matthew J., Otto, Edgar A., Baye, Lisa M., Wen, X., Scales, Suzie J., Kwong, M., Huntzicker, Erik G., Sfakianos, Mindan K., Sandoval, W., Bazan, J. F., Kulkarni, P., Garcia-Gonzalo, Francesc R., Seol, Allen D., O'Toole, John F., Held, S., Reutter, Heiko M., Lane, William S., Rafiq, Muhammad A., Noor, A., Ansar, M., Devi, Akella Radha R., Sheffield, Val C., Slusarski, Diane C., Vincent, John B., Doherty, Daniel A., Hildebrandt, F., Reiter, Jeremy F., & Jackson, Peter K. (2011). Mapping the NPHP-JBTS-MKS Protein Network Reveals Ciliopathy Disease Genes and Pathways. *Cell*, 145(4), 513-528. https://doi.org/10.1016/j.cell.2011.04.019
- Saternos, H., Ley, S., & AbouAlaiwi, W. (2020). Primary Cilia and Calcium Signaling Interactions. *Int J Mol Sci*, *21*(19). https://doi.org/10.3390/ijms21197109
- Satir, P. (2017). CILIA: before and after. *Cilia*, *6*, 1. <a href="https://doi.org/10.1186/s13630-017-0046-8">https://doi.org/10.1186/s13630-017-0046-8</a>
- Schou, K. B., Pedersen, L. B., & Christensen, S. T. (2015). Ins and outs of GPCR signaling in primary cilia. *EMBO reports*, *16*(9), 1099-1113-1113. https://doi.org/https://doi.org/10.15252/embr.201540530
- Ségaliny, A. I., Tellez-Gabriel, M., Heymann, M. F., & Heymann, D. (2015). Receptor tyrosine kinases: Characterisation, mechanism of action and therapeutic interests for bone cancers. *J Bone Oncol*, 4(1), 1-12. <a href="https://doi.org/10.1016/j.jbo.2015.01.001">https://doi.org/10.1016/j.jbo.2015.01.001</a>
- Shen, P. S., Yang, X., DeCaen, P. G., Liu, X., Bulkley, D., Clapham, D. E., & Cao, E. (2016). The Structure of the Polycystic Kidney Disease Channel PKD2 in Lipid Nanodiscs. *Cell*, 167(3), 763-773.e711. <a href="https://doi.org/10.1016/j.cell.2016.09.048">https://doi.org/10.1016/j.cell.2016.09.048</a>
- Sherpa, R. T., Mohieldin, A. M., Pala, R., Wachten, D., Ostrom, R. S., & Nauli, S. M. (2019). Sensory primary cilium is a responsive cAMP microdomain in renal epithelia. *Scientific Reports*, 9(1), 6523. https://doi.org/10.1038/s41598-019-43002-2
- Shin, J. B., Adams, D., Paukert, M., Siba, M., Sidi, S., Levin, M., Gillespie, P. G., & Gründer, S. (2005). Xenopus TRPN1 (NOMPC) localizes to microtubule-based cilia in epithelial cells, including inner-ear hair cells. *Proc Natl Acad Sci U S A*, 102(35), 12572-12577. <a href="https://doi.org/10.1073/pnas.0502403102">https://doi.org/10.1073/pnas.0502403102</a>
- Siemens, J., Zhou, S., Piskorowski, R., Nikai, T., Lumpkin, E. A., Basbaum, A. I., King, D., & Julius, D. (2006). Spider toxins activate the capsaicin receptor to produce inflammatory pain. *Nature*, 444(7116), 208-212. https://doi.org/10.1038/nature05285

- Soares, H., Carmona, B., Nolasco, S., Viseu Melo, L., & Gonçalves, J. (2019). Cilia Distal Domain: Diversity in Evolutionarily Conserved Structures. *Cells*, 8(2). <a href="https://doi.org/10.3390/cells8020160">https://doi.org/10.3390/cells8020160</a>
- Spencer, W. J., Lewis, T. R., Pearring, J. N., & Arshavsky, V. Y. (2020). Photoreceptor Discs: Built Like Ectosomes. *Trends Cell Biol*, *30*(11), 904-915. https://doi.org/10.1016/j.tcb.2020.08.005
- Stepanek, L., & Pigino, G. (2016). Microtubule doublets are double-track railways for intraflagellar transport trains. *Science*, *352*(6286), 721-724. https://doi.org/10.1126/science.aaf4594
- Su, Q., Hu, F., Ge, X., Lei, J., Yu, S., Wang, T., Zhou, Q., Mei, C., & Shi, Y. (2018). Structure of the human PKD1-PKD2 complex. *Science*, *361*(6406). https://doi.org/10.1126/science.aat9819
- Sun, S., Fisher, R. L., Bowser, S. S., Pentecost, B. T., & Sui, H. (2019). Three-dimensional architecture of epithelial primary cilia. *Proc Natl Acad Sci U S A, 116*(19), 9370-9379. https://doi.org/10.1073/pnas.1821064116
- Sun, X.-h., Zhu, Y.-y., Wang, L., Liu, H.-l., Ling, Y., Li, Z.-l., & Sun, L.-b. (2017). The Catsper channel and its roles in male fertility: a systematic review. *Reproductive Biology and Endocrinology*, *15*(1), 65. <a href="https://doi.org/10.1186/s12958-017-0281-2">https://doi.org/10.1186/s12958-017-0281-2</a>
- Szymanska, K., & Johnson, C. A. (2012). The transition zone: an essential functional compartment of cilia. *Cilia*, 1(1), 10. <a href="https://doi.org/10.1186/2046-2530-1-10">https://doi.org/10.1186/2046-2530-1-10</a>
- Teal, T. H., Guillemette, T., Chapman, M., & Margulis, L. (1998). Acronema sippewissettensis Gen. Nov. Sp. Nov., microbial mat bicosoecid (Bicosoecales = Bicosoecida). *Eur J Protistol*, *34*(4), 402-414. <a href="https://doi.org/10.1016/s0932-4739(98)80009-6">https://doi.org/10.1016/s0932-4739(98)80009-6</a>
- Tomuleasa, C., Tigu, A. B., Munteanu, R., Moldovan, C. S., Kegyes, D., Onaciu, A., Gulei, D., Ghiaur, G., Einsele, H., & Croce, C. M. (2024). Therapeutic advances of targeting receptor tyrosine kinases in cancer. *Signal Transduct Target Ther*, *9*(1), 201. <a href="https://doi.org/10.1038/s41392-024-01899-w">https://doi.org/10.1038/s41392-024-01899-w</a>
- Tottori, S., & Nelson, B. J. (2013). Artificial helical microswimmers with mastigoneme-inspired appendages. *Biomicrofluidics*, 7(6), 61101. https://doi.org/10.1063/1.4827915
- Tran, P. V., Sharma, M., Li, X., & Calvet, J. P. (2014). Developmental signaling: does it bridge the gap between cilia dysfunction and renal cystogenesis? *Birth Defects Res C Embryo Today*, *102*(2), 159-173. <a href="https://doi.org/10.1002/bdrc.21065">https://doi.org/10.1002/bdrc.21065</a>
- Tran, T., Roullier-Gall, C., Verdier, F., Martin, A., Schmitt-Kopplin, P., Alexandre, H., Grandvalet, C., & Tourdot-Maréchal, R. (2022). Microbial Interactions in Kombucha through the Lens of Metabolomics. *Metabolites*, *12*(3). <a href="https://doi.org/10.3390/metabo12030235">https://doi.org/10.3390/metabo12030235</a>
- Tsukazaki, T., Chiang, T. A., Davison, A. F., Attisano, L., & Wrana, J. L. (1998). SARA, a FYVE Domain Protein that Recruits Smad2 to the TGFβ Receptor. *Cell*, 95(6), 779-791. <a href="https://doi.org/10.1016/S0092-8674(00)81701-8">https://doi.org/10.1016/S0092-8674(00)81701-8</a>
- van de Graaf, S. F. J., Hoenderop, J. G. J., & Bindels, R. J. M. (2006). Regulation of TRPV5 and TRPV6 by associated proteins. *American Journal of Physiology-Renal Physiology*, 290(6), F1295-F1302. <a href="https://doi.org/10.1152/ajprenal.00443.2005">https://doi.org/10.1152/ajprenal.00443.2005</a>
- Wan, K. Y., & Jékely, G. (2020). On the unity and diversity of cilia. *Philos Trans R Soc Lond B Biol Sci*, 375(1792), 20190148. <a href="https://doi.org/10.1098/rstb.2019.0148">https://doi.org/10.1098/rstb.2019.0148</a>

- Wang, L., Wen, X., Wang, Z., Lin, Z., Li, C., Zhou, H., Yu, H., Li, Y., Cheng, Y., Chen, Y., Lou, G., Pan, J., & Cao, M. (2022). Ciliary transition zone proteins coordinate ciliary protein composition and ectosome shedding. *Nature Communications*, *13*(1), 3997. <a href="https://doi.org/10.1038/s41467-022-31751-0">https://doi.org/10.1038/s41467-022-31751-0</a>
- Wang, X., Li, G.-H., Zou, C.-G., Ji, X.-L., Liu, T., Zhao, P.-J., Liang, L.-M., Xu, J.-P., An, Z.-Q., Zheng, X., Qin, Y.-K., Tian, M.-Q., Xu, Y.-Y., Ma, Y.-C., Yu, Z.-F., Huang, X.-W., Liu, S.-Q., Niu, X.-M., Yang, J.-K., Huang, Y., & Zhang, K.-Q. (2014). Bacteria can mobilize nematodetrapping fungi to kill nematodes. *Nature Communications*, *5*(1), 5776. <a href="https://doi.org/10.1038/ncomms6776">https://doi.org/10.1038/ncomms6776</a>
- Warburton-Pitt, S. R., Silva, M., Nguyen, K. C., Hall, D. H., & Barr, M. M. (2014). The nphp-2 and arl-13 genetic modules interact to regulate ciliogenesis and ciliary microtubule patterning in C. elegans. *PLoS Genet*, *10*(12), e1004866. https://doi.org/10.1371/journal.pgen.1004866
- Wei, D., Quaranta, G., Aubin-Tam, M.-E., & Tam, D. S. W. (2024). The younger flagellum sets the beat for Chlamydomonas reinhardtii. *eLife*, *13*, e86102. <a href="https://doi.org/10.7554/eLife.86102">https://doi.org/10.7554/eLife.86102</a>
- Wingfield, J. L., & Lechtreck, K. F. (2018). Chlamydomonas Basal Bodies as Flagella Organizing Centers. *Cells*, 7(7). <a href="https://doi.org/10.3390/cells7070079">https://doi.org/10.3390/cells7070079</a>
- Winokurow, N., & Schumacher, S. (2019). A role for polycystin-1 and polycystin-2 in neural progenitor cell differentiation. *Cell Mol Life Sci*, 76(14), 2851-2869. https://doi.org/10.1007/s00018-019-03072-x
- Witman, G. B., Carlson, K., Berliner, J., & Rosenbaum, J. L. (1972). Chlamydomonas flagella. I. Isolation and electrophoretic analysis of microtubules, matrix, membranes, and mastigonemes. *J Cell Biol*, *54*(3), 507-539. <a href="https://doi.org/10.1083/jcb.54.3.507">https://doi.org/10.1083/jcb.54.3.507</a>
- Wu, M., Wu, S., Chen, W., & Li, Y.-P. (2024). The roles and regulatory mechanisms of TGF- $\beta$  and BMP signaling in bone and cartilage development, homeostasis and disease. *Cell Research*, 34(2), 101-123. <a href="https://doi.org/10.1038/s41422-023-00918-9">https://doi.org/10.1038/s41422-023-00918-9</a>
- Xiao, Z. S., & Quarles, L. D. (2010). Role of the polycytin-primary cilia complex in bone development and mechanosensing. *Ann N Y Acad Sci*, 1192(1), 410-421. https://doi.org/10.1111/j.1749-6632.2009.05239.x
- Yagi, T., Uematsu, K., Liu, Z., & Kamiya, R. (2009). Identification of dyneins that localize exclusively to the proximal portion of Chlamydomonas flagella. *Journal of Cell Science*, 122(9), 1306-1314. <a href="https://doi.org/10.1242/jcs.045096">https://doi.org/10.1242/jcs.045096</a>
- Yamamoto, R., Hwang, J., Ishikawa, T., Kon, T., & Sale, W. S. (2021). Composition and function of ciliary inner-dynein-arm subunits studied in Chlamydomonas reinhardtii. *Cytoskeleton (Hoboken)*, 78(3), 77-96. https://doi.org/10.1002/cm.21662
- Yang, D., Zhou, Q., Labroska, V., Qin, S., Darbalaei, S., Wu, Y., Yuliantie, E., Xie, L., Tao, H., Cheng, J., Liu, Q., Zhao, S., Shui, W., Jiang, Y., & Wang, M.-W. (2021). G protein-coupled receptors: structure- and function-based drug discovery. *Signal Transduction and Targeted Therapy*, 6(1), 7. <a href="https://doi.org/10.1038/s41392-020-00435-w">https://doi.org/10.1038/s41392-020-00435-w</a>
- Yang, S.-H., Wang, D., Chen, C., Xu, C.-L., & Xie, H. (2020). Evaluation of Stratiolaelaps scimitus (Acari: Laelapidae) for controlling the root-knot nematode, Meloidogyne incognita (Tylenchida: Heteroderidae). *Scientific Reports*, 10(1), 5645. <a href="https://doi.org/10.1038/s41598-020-62643-2">https://doi.org/10.1038/s41598-020-62643-2</a>

- Yang, Y., & Mlodzik, M. (2015). Wnt-Frizzled/planar cell polarity signaling: cellular orientation by facing the wind (Wnt). *Annu Rev Cell Dev Biol*, *31*, 623-646. <a href="https://doi.org/10.1146/annurev-cellbio-100814-125315">https://doi.org/10.1146/annurev-cellbio-100814-125315</a>
- Ye, F., Nager, A. R., & Nachury, M. V. (2018). BBSome trains remove activated GPCRs from cilia by enabling passage through the transition zone. *J Cell Biol*, *217*(5), 1847-1868. <a href="https://doi.org/10.1083/jcb.201709041">https://doi.org/10.1083/jcb.201709041</a>
- Yoder, B. K. (2007). Role of primary cilia in the pathogenesis of polycystic kidney disease. *J Am Soc Nephrol*, *18*(5), 1381-1388. <a href="https://doi.org/10.1681/asn.2006111215">https://doi.org/10.1681/asn.2006111215</a>
- Yoshiba, S., Shiratori, H., Kuo, I. Y., Kawasumi, A., Shinohara, K., Nonaka, S., Asai, Y., Sasaki, G., Belo, J. A., Sasaki, H., Nakai, J., Dworniczak, B., Ehrlich, B. E., Pennekamp, P., & Hamada, H. (2012). Cilia at the node of mouse embryos sense fluid flow for left-right determination via Pkd2. *Science*, *338*(6104), 226-231. https://doi.org/10.1126/science.1222538
- Yu, F. H., & Catterall, W. A. (2004). The VGL-Chanome: A Protein Superfamily Specialized for Electrical Signaling and Ionic Homeostasis. *Science's STKE*, 2004(253), re15. https://doi.org/doi:10.1126/stke.2532004re15
- Yu, Y., Ulbrich, M. H., Li, M.-H., Buraei, Z., Chen, X.-Z., Ong, A. C. M., Tong, L., Isacoff, E. Y., & Yang, J. (2009). Structural and molecular basis of the assembly of the TRPP2/PKD1 complex. *Proceedings of the National Academy of Sciences*, *106*(28), 11558-11563. <a href="https://doi.org/doi:10.1073/pnas.0903684106">https://doi.org/doi:10.1073/pnas.0903684106</a>
- Yuan, S., & Sun, Z. (2013). Expanding horizons: ciliary proteins reach beyond cilia. *Annu Rev Genet*, 47, 353-376. <a href="https://doi.org/10.1146/annurev-genet-111212-133243">https://doi.org/10.1146/annurev-genet-111212-133243</a>
- Yuan, X., & Yang, S. (2016). Primary Cilia and Intraflagellar Transport Proteins in Bone and Cartilage. *J Dent Res*, 95(12), 1341-1349. https://doi.org/10.1177/0022034516652383
- Yue, S., Tang, L.-Y., Tang, Y., Tang, Y., Shen, Q.-H., Ding, J., Chen, Y., Zhang, Z., Yu, T.-T., Zhang, Y. E., & Cheng, S. Y. (2014). Requirement of Smurf-mediated endocytosis of Patched1 in sonic hedgehog signal reception. *eLife*, *3*, e02555. https://doi.org/10.7554/eLife.02555
- Zaghloul, N. A., & Katsanis, N. (2009). Mechanistic insights into Bardet-Biedl syndrome, a model ciliopathy. *J Clin Invest*, 119(3), 428-437. <a href="https://doi.org/10.1172/jci37041">https://doi.org/10.1172/jci37041</a>
- Zhang, F., Xiao, X., Li, Y., Wu, H., Deng, X., Jiang, Y., Zhang, W., Wang, J., Ma, X., & Zhao, Y. (2021). Therapeutic Opportunities of GPBAR1 in Cholestatic Diseases. *Front Pharmacol*, *12*, 805269. <a href="https://doi.org/10.3389/fphar.2021.805269">https://doi.org/10.3389/fphar.2021.805269</a>
- Zhang, M., Ma, Y., Ye, X., Zhang, N., Pan, L., & Wang, B. (2023). TRP (transient receptor potential) ion channel family: structures, biological functions and therapeutic interventions for diseases. *Signal Transduct Target Ther*, 8(1), 261. https://doi.org/10.1038/s41392-023-01464-x
- Zheng, J. (2013). Molecular mechanism of TRP channels. *Compr Physiol*, *3*(1), 221-242. https://doi.org/10.1002/cphy.c120001
- Zhong, B. H., & Dong, M. (2024). The implication of ciliary signaling pathways for epithelial-mesenchymal transition. *Mol Cell Biochem*, 479(6), 1535-1543. https://doi.org/10.1007/s11010-023-04817-w

# **CHAPTER 2**

The PKD2-related protein Small Interactor of PKD2 (SIP) promotes assembly and ciliary entry of the Chlamydomonas PKD2<sup>1</sup>

<sup>&</sup>lt;sup>1</sup> Das, P., Mekonnen, B., Alkhofash, R., Ingle, A., Workman, B., Feather, A., Zhang, G., Chasen, N., Liw, P., Lechtreck, K., The PKD2-related protein Small Interactor of PKD2 (SIP) promotes assembly and ciliary entryof the Chlamydomonas PKD2. J Cell Sci (2024) 137 (1): jcs261497. Reprinted here with permission of the publisher, The Company of Biologists.

### 2.1Abstract

In *Chlamydomonas*, the channel PKD2 is primarily present in the distal region of cilia, where it is attached to the axoneme and mastigonemes, extracellular polymers of MST1. In a smaller, proximal ciliary region, PKD2 is more mobile and lacks mastigonemes. Here, we show that the PKD2 regions are established early during ciliogenesis and increase proportionally in length as cilia elongate. Zygotic rescue of PKD2-deficient cilia was incomplete with PKD2 restored predominately in the proximal region, suggesting that axonemal binding of PKD2 requires *de novo* assembly of cilia. We identified Small Interactor of PKD2 (SIP), a PKD2-related, single-pass transmembrane protein, as part of the PKD2-mastigoneme complex. In *sip* mutants, stability and proteolytic processing of PKD2 in the cell body were reduced and PKD2-mastigoneme complexes were absent from the cilia. Like the *pkd2* and *mst1* mutants, *sip* swam with reduced velocity. Cilia of the *pkd2* mutant beat with an increase frequency but were less efficient in moving the cells, suggesting a structural role for the PKD2-SIP-mastigoneme complex in increasing the effective surface of *Chlamydomonas* cilia.

In chimeric zygotes, tagged PKD2 rapidly entered the proximal region of PKD2-deficient cilia whereas assembly of the distal region was hindered, suggesting that axonemal binding of PKD2 requires *de novo* assembly of cilia.

# 2.2 introduction

Cilia and eukaryotic flagella are microtubule-based cell projections with motile and sensory functions. The latter involves channels and receptors in the ciliary membrane, which covers the ciliary axoneme and is continuous with the plasma membrane. Rather than being homogenous in

composition, the ciliary membrane often contains sub-compartments, in which specific membrane proteins are concentrated. In the auditory cilia of *Drosophila* chordotonal neurons, for example, the TRP channel NompC is localized in parts of the distal zone whereas voltagegated TRPV channels are present in the proximal zone. (Wangchu Xiang et al., 2022). Also in Drosophila, the PKD2 orthologue AMO is located near the tip of sperm cilia (Kottgen et al., 2011; Watnick et al., 2003). Similarly, the olfactory cyclic nucleotide-gated channel subunit 1 (OcNC1) is concentrated in the distal segments of rat olfactory cilia (Matsuzaki et al., 1999). The salt-sensing receptor guanylate cyclase GCY-22 also resides in the distal region of C. elegans primary cilia of ASER neurons (van der Burght et al., 2020). In the latter, the localization of GCY-22 requires motor-driven intraflagellar transport (IFT), a protein shuttle dedicated to the assembly and maintenance of cilia, to continuously capture the receptor along the length of cilia and return it to the tip by anterograde IFT. Thus, proteins can be confined to certain ciliary regions dynamically by active transport. However, other membrane protein patterns are more static likely involving anchoring of membrane proteins to underlying axonemal structures. Indeed, NompC attaches via its 29 ankyrin repeats to the underlying microtubules, forming a spring-like connection, which contributes to mechanical gating of the channel (Zhang et al., 2015). In addition to patterns along the proximo-distal axis, some membrane proteins assume additional levels of order around the circumference of cilia. An example is the multiprotein channel complex CatSper, which forms four intricately patterned rows, the race stripes, along the principal piece of mammalian sperm flagella (Chung et al., 2014; Zhao et al., 2022). The observations raise numerous questions including how such membrane proteins are targeted to their specific positions within cilia, how the length of the specialized membrane subdomains is determined and how these regions scale with respect to the overall length of cilia.

Another open question is what role such membrane protein patterns play in the variety of motile and sensory functions exhibited in cilia across species and cell types.

To start addressing these questions, we analyzed the distribution of the TRP channel PKD2 in *Chlamydomonas*, a tractable system for the genetic, biochemical, microscopic and functional analysis of cilia (Dutcher, 1995; Lechtreck, 2016; Pazour et al., 2005; Silflow & Lefebvre, 2001). In mammals, PKD1 and PKD2 form a 1:3 complex and the proteins are present on cilia in the kidney and the embryonic node (Pennekamp et al., 2002; Su et al., 2018). Mutations in either protein cause autosomal dominant polycystic kidney disease and PKD2 participates in the determination of the left-right body axis, likely by sensing the flow generated by the motile monocilia in the center of the node (Wu & Somlo, 2000). PKD2 is preferentially located on the dorsal side of non-motile nodal cilia, facing the flow-generating center of the murine embryonic node (Katoh et al., 2023). This localization supports the idea that a specific position within cilia or orientation with respect to the flow could contribute to PKD2 function. In C. elegans, the polycystin homologues LOV-1/PC1 and PKD-2/PC2 are expressed specifically in male-specific sensory neurons; both proteins localize to primary cilia, and are required for male mating behavior (Barr & Sternberg, 1999; Walsh et al., 2022). PKD2 is also present in non-metazoans, which typically lack PKD1 homologues, raising questions about the composition and function of PKD2 channel complexes in those species. In fission yeast, a PKD2-like protein, which possesses nine transmembrane helices, is located in the plasma membrane, contributing to cellular calcium homeostasis. It has been proposed that this protein is responsible for sensing membrane tension during cytokinesis (Poddar et al., 2022). In *Chlamydomonas*, PKD2 is cleaved within the large extracellular loop between transmembrane helix 1 and 2 via a currently unknown mechanism (Huang et al., 2007). Cleavage occurs in the cell body and the two PKD2

fragments enter cilia, remaining associated to each other (Huang et al., 2007; Liu et al., 2020). Within cilia, PKD2 attaches, directly or indirectly, to the axonemal doublet microtubules (DMTs) 4 and 8 and is required for anchoring the mastigonemes, thread-like extracellular polymers of the glycoprotein MST1, to the ciliary surface (Liu et al., 2023; Liu et al., 2020). The ultrastructure of MST1 was recently solved and is dominated by immunoglobulin-like and Sushi domains, structural elements observed in may extracellular proteins (Wang et al., 2023). On the cilia, the mastigoneme rows are oriented perpendicular to the plane of the ciliary beat, generating a fanlike structure (Nakamura et al., 1996; Witman et al., 1972). This arrangement should increase the effective surface of the cilium, affecting the cell's swimming velocity (Liu et al., 2020; Nakamura et al., 1996). However, the phenotype of PKD2- and MST1-deficient cells is subtle and the swimming velocity of mastigoneme-deficient cells has been analyzed repeatedly with conflicting outcomes (Amador et al., 2020; Liu et al., 2020; Nakamura et al., 1996; Wang et al., 2023). In addition to the stationary PKD2-mastigoneme complexes in the distal region of Chlamydomonas cilia, PKD2 without attached mastigonemes is present in a separate proximal region of cilia; here, PKD2 is more mobile, moving by slow diffusion (Liu et al., 2020). This raises the question how cells sort and assemble PKD2 into two distinct ciliary domains.

Here, we analyzed how the distribution of PKD2 in *Chlamydomonas* is established during both ciliary assembly and the repair of PKD2-deficient full-length cilia, and how this distribution is linked to ciliary length. Further, we identified Small Interactor of PKD2 (SIP), a novel single-pass transmembrane protein, related to the amino-terminal portion of PKD2. Cilia of the *sip* mutant largely lack PKD2-mastigoneme complexes and swim with reduced velocity. In the *sip* mutant, the stability and proteolytic processing of PKD2 in the cell body were strongly

reduced, suggesting a role for SIP in PKD2 processing, a potential prerequisite for its entry into cilia.

### Results

# 2.3 The two PKD2 regions are established early during cilia regeneration

In full-length *Chlamydomonas* cilia, PKD2 is organized into two distinct regions: a ~2.7 μm long region occupying the proximal part of the cilia, in which PKD2 fused at its C-terminus to mNeonGreen (PKD2-NG) moves by slow diffusion and lacks mastigonemes, and the distal region of ~6 μm length, in which PKD2 forms two more-or-less irregular rows anchoring the mastigonemes to the ciliary surface (Fig. 1A, B, Table 1) (Liu et al., 2020). The PKD2-NG rows are not always clearly discernable in our micrographs since their distance of ~200 nm is near the limit of resolution of standard light microscopy (DeCaen et al., 2013). The proximal and distal PKD2-NG regions are typically (>90% of cilia) separated by a more or less conspicuous gap of ~1 µm length lacking PKD2 but for the occasional particle passing through by IFT or diffusion (Figs. 1C). Further, PKD2-NG was present in a punctate pool in the apical region of the cells (Fig. S1A d, e). To study how the PKD2 regions develop during cilia formation, pkd2 PKD2-NG cells were de-ciliated by a pH shock and analyzed at various time points during cilia regeneration using in vivo total internal reflection fluorescence microscopy (TIRFM). The distribution of PKD2-NG in a proximal and distal region with a gap separating the two was apparent in most of the short regenerating cilia that were analyzed; in a subset of cells, PKD2-NG was absent or sparse within the proximal region of short regenerating cilia (Fig. 1D).

In *Chlamydomonas*, PKD2 is a confirmed cargo of IFT but IFT of PKD2 was not observed in *C. elegans*(Huang et al., 2007; Liu et al., 2020; Qin et al., 2005). *In vivo* imaging showed low

IFT frequencies of *Chlamydomonas* PKD2-NG in both full-length (i.e., cilia of cells not treated by a pH shock) and regenerating cilia, (0.81 events/min vs 0.35 events/min, respectively; Fig 1E, F) ((Huang et al., 2007; Liu et al., 2020). PKD2-NG was, however, more abundant in full-length cilia, which could result in more frequent transports via IFT. Since IFT of PKD2-NG is not upregulated during ciliary regeneration (as it has been described for many axonemal proteins (Lechtreck, 2022) this may suggest that the majority of PKD2-NG enters the ciliary compartment through an IFT-independent process.

# 2.4 Efficient assembly of PKD2-NG into the distal region requires de novo assembly of cilia To determine if PKD2 can be added in the correct pattern to fully assembled *pkd2* mutant cilia, we mated *pkd2* and *pkd2* PKD2-NG gametes (Fig. 2). After cell fusion, PKD2-NG present in the shared cytoplasm of the zygotes, is available for incorporation into the *pkd2*-derived cilia, which initially lack PKD2 (Fig. 2A). In zygotes analyzed ~1h after mixing of the gametes, PKD2-NG had entered the proximal ~1/3 region of the *pkd2*-derived cilia but only a very few particles were present in the distal region (Fig. 2 B and C). An incomplete rescue of the *pkd2*-derived cilia was also observed in zygotes analyzed 2 or 3 hours after mixing of the gametes with PKD2-NG largely restricted to the proximal region in those cilia; the distribution of PKD2-NG in the *pkd2 PKD2-NG*-derived cilia remained apparently unaltered (Fig. 2 B and C). Such incompletely rescued zygotes accounted for 88% of the zygotes summarized from all three time points with the remaining 12% of zygotes having overall weak or no detectable PKD2-NG signal in the cilia (n = 44 zygotes analyzed). The latter can be attributed to low PKD2-NG expression in a subset of cells, as is frequently observed with transgenes in clonal cultures of *Chlamydomonas*.

To test if the lack of PKD2 assembly into the distal region is a zygote-specific feature, we deciliated zygotes using a pH shock and allowed them to regenerate all four cilia (Fig. 2A, D, E). In 77% of the 39 zygotes analyzed, the cilia displayed the normal compartmentalization of PKD2-NG with a 1:2 length ratio between the proximal and distal region (Fig. 2D, E). The remaining zygotes either largely lacked PKD2-NG or, more frequently, possessed two incompletely rescued and two normal cilia; the latter zygotes were likely derived from gametes present in the mating mixture at the time of the pH shock and only fusing after deciliation and cilia regeneration (not shown).

We also mated *pkd2 PKD2-NG* and wild-type gametes to visualize the exchange of untagged PKD2 in the wild type-derived cilia with PKD2-NG. As described above, PKD2-NG quickly entered the proximal 1/3 region of the two wild-types derived cilia in 91% of zygotes analyzed but was largely excluded from the distal region of those cilia. These data indicate that PKD2-NG assembly into full-length zygotic cilia is largely limited to the proximal mobile region, in which PKD2 is more dynamic and is exchanged with PKD2 in the cell body. The data suggest that anchoring of PKD2 complexes to the axoneme occurs preferentially during ciliary assembly.

# We hypothesized that the complex arrangement of PKD2 observed in *Chlamydomonas* cilia likely involves additional proteins. To identify additional components of the ciliary PKD2-MST1 complex, we immunopurified PKD2-NG from detergent extracts of *pkd2 PKD2-NG* and *mst1-1 pkd2 PKD2-NG* cilia using an anti-NG nanobody trap (Fig. S2A). The latter strain was chosen because the lack of MST1 reduces the presence of PKD2-NG in the distal cilia region

2.5 Identification of Small Interactor of PKD2 (SIP) as a novel PKD2-associated protein

(Fig. S2B) (Liu et al., 2020). Therefore, proteins specifically interacting with PKD2 in the distal region could be also reduced in mst1-1 in comparison to the pkd2 PKD2-NG rescue strain. The wild-type strain g1 was used as a control. Silver staining identified several bands in the eluates of the PKD2-NG expressing strains that were absent in the control eluates (Fig. S2A). A prominent band of ~250 kD was present in the pkd2 PKD2-NG eluate but not in that of the mst1-1 pkd2 PKD2-NG and control strains and likely represents MST1. The analysis was carried out in several biological replicates (four for the pkd2 PKD2-NG and three for the mst1-1 pkd2 PKD2-NG and the control strain, respectively) and the eluates were subjected to mass spectrometry (Table S1). Certain abundant (e.g., tubulin) and sticky proteins (e.g., FMG-1) were detected in all 10 samples; PKD2 was detected in the seven experimental samples but not in the controls. As expected, MST1 was only present in the samples from the pkd2 PKD2-NG rescue strain. An additional 27 proteins were identified in most of the pkd2 PKD2-NG and/or mst1-1 pkd2 PKD2-NG samples (Table S1). While only present in the experimental samples, we noticed that this list also encompassed proteins that we repeatedly detected in GFP and NG pulldowns in unrelated experiments (e.g., ODA5-associated adenylate kinase and enolase) and proteins, such as chlorophyll-binding proteins, which are cell body contaminants.

To triage, we obtained known or putative mutants in genes encoding proteins specific for the experimental samples and processed them for whole mount EM (Table S1). Of the six strains analyzed, only strain LMJ.RY0402.143879 from the *Chlamydomonas* CLiP mutant collection lacked mastigonemes (Fig. 3A). The absence of mastigonemes was confirmed by immunofluorescence staining with monoclonal anti-MST1 (Nakamura et al., 1996), which further revealed that the pool of MST1/mastigonemes observed in the apical region of control cells, is dispersed in LMJ.RY0402.143879 cells, as previously described for the *pkd2* mutant

(Fig. S3A) (Liu et al., 2020; Nakamura et al., 1996). This strain carries an insertion on chromosome 11 in the second intron of CHLRE 11g475150, which encodes the uncharacterized protein A8JFQ9 CHLRE (Fig. S2C). The protein is predicted to consist of 361 residues and possesses a single transmembrane domain. It is annotated as "Similar to PKD2" in the Phytozome database (https://phytozome-next.jgi.doe.gov/) because it shares similarity with the N-terminal region of Chlamydomonas PKD2, including a stretch of 30 residues with 80% identity (Figs. S4B, C and 4B depicted in mangenta). Alphafold2 predicts remarkably similar structures for A8JFQ9 CHLRE and the N-terminal region of *Chlamydomonas* PKD2, encompassing the first transmembrane helix and parts of the extracellular top domain (Fig. 3B). In NCBI Blastp searches of Chlamydomonas proteins, PKD2 and A8JFQ9 CHLRE identified each other as reciprocal second-best hits (E value 7e-30). For reasons of simplicity, we will refer to A8JFQ9 CHLRE as Small Interactor of PKD2 (SIP). SIP was the only protein enriched in the pulldowns of the pkd2 PKD2-NG strain compared to the mst1-1 sample (Table S1). The SIP gene is present in the genomes of various green alga (i.e., Chlorophyta) including Chlamydomodales with MST1-based mastigonemes such as *Volvox carteri* as well as species without MST1, such as *Trebuxia sp.* and *Micromonas sp.*, and species that apparently lack the ability to form cilia (e.g., Scenedesmus sp.). Outside of green algae, homologues of Chlamydomonas SIP were not detected (Table S2).

A polyclonal antibody raised against recombinant SIP identified a band of ~36 kD in western blots of isolated control cilia, which is close to the predicted molecular weight of SIP of 39,718 (Figs. 4C, S4D). The immunoreactive band was absent in cilia from strain LMJ.RY0402.143879, revealing that these mutant lacks SIP; we therefore refer to this strain as sip (Figs. 4C, D, S4B). PKD2 and MST1 were largely absent from sip mutant cilia (Fig. 3C).

For rescue, we expressed untagged SIP in the *sip* mutant; the presence of both the transgenic cDNA-based and the insertional mutant alleles was confirmed by PCR (Fig. S2D and E). Western blotting showed that expression of SIP restored PKD2 and MST1 levels in cilia, and whole mount EM showed the presence of mastigonemes on *sip SIP* cilia (Fig. 3A, C). Of note, during the course of this study, the *sip* mutant occasionally regained the ability to express some SIP (Figs. 3D). While not further analyzed here, it is likely that cells occasionally acquired the ability to splice out the large intron generated by the insertion of the selectable marker cassette into intron 2 (Fig. S2C). Cilia of control and *sip* mutants equally reacted with anti-SIP in immunofluorescence assays, suggesting that this antibody is not suitable for immunocytochemistry. We also failed to express tagged SIP in *Chlamydomonas*; therefore, the localization of SIP within cilia remains unknown. However, we note PKD2 and SIP cofractionated during Triton X-114 phase partitioning of isolated cilia and were present mostly in the soluble matrix fraction with a minor portion remaining attached to the axonemes (Fig. S3E).

To further analyze the interdependence between PKD2, SIP and mastigonemes, cilia were isolated from control cells and the corresponding mutants and then compared by Western blotting using antibodies directed against PKD2, SIP, and MST1 (Fig. 3D). In our hands, monoclonal anti-MST1 failed to detect MST1 in western blots and we raised a novel polyclonal antibody against ~173-residue fragment of MST1 encoded by exon 14 (i.e., residue 1307 – 1480); this polyclonal anti-MST1 identified MST1 in Western blot experiments but was not suitable for immunofluorescence approaches (Fig. S3F). As expected, all three proteins were detected in control cilia with PKD2 running as two bands, the larger N-terminal fragment and the smaller C-terminal fragment, as previously reported (Fig. 3C, D) (Huang et al., 2007; Liu et al., 2020). In the *pkd2* mutant, MST1 and SIP were not detected, indicating that PKD2 holds a central role in

the complex and is required for the ciliary presence of MST1 and SIP (Fig. 3D). In *mst1-1* cilia, PKD2 and SIP were present but significantly reduced (Fig. 3D). PKD2 and MST1 were strongly reduced (Fig. 3D) or undetectable (Fig. 3C) in *sip* mutant cilia, revealing that SIP is required for the presence of PKD2-mastigoneme complexes in cilia.

To analyze the behavior of residual PKD2 in *sip* cilia, we expressed PKD2-NG in the *sip* mutant and a control strain, which both also expressed the endogenous PKD2 (Fig. S3G). As expected from the biochemical analysis of cilia (Fig. 3C, D), PKD2-NG was severely reduced (~10% of cells analyzed) or not detected (~90%) in *sip* cilia (Fig. 4A). Residual PKD2-NG was mostly stationary. Further, an organized pool of PKD2-NG with the protein present near the basal bodies and along the microtubular cytoskeleton seen in control cells, was not observed in *sip PKD2-NG* cells (Fig. S1A and B).

The near absence of PKD2 from *sip* mutant cilia raised the possibility that PKD2 is trapped in the cell body of these mutants. In immunoblots loaded with control whole cell samples, anti-PKD2 recognized full-length PKD2 (~230 kD) and the two proteolytic fragments of 90 and 140 kD, corresponding to the C- and N-terminal fragments of PKD2 (Huang et al., 2007; Liu et al., 2020) (Figs. 3C, D, 5B, C). In *sip* cells, the overall amount of PKD2 was reduced and, interestingly, residual PKD2 was mostly uncleaved whereas the proteolytic fragments were essentially undetectable (Figs. 4B, C). Expression of SIP in *sip* was able to rescue normal levels of both PKD2 and the PKD2 fragments (Fig. 4C). Huang et al. (2007) observed proteolytic cleavage of PKD2 in the cilia-deficient *Chlamydomonas* mutants *bld1* and *bld2*, indicating that cleavage occurs in the cell body and that only the two fragments enter the cilia (Huang et al., 2007). We conclude that SIP is required for the stability and proteolytic processing of PKD2 in

the cell body, the latter being a likely prerequisite for the entry of PKD2 into *Chlamydomonas* cilia.

# 2.6 The PKD2-mastigoneme complex increases the efficiency of the ciliary beat

The swimming velocity of the *sip* mutant was reduced by roughly 20%, similar to that of the pkd2 and mst1-1 mutants (Fig. 5 A, B, D). Expression of transgenic SIP in the sip mutant rescued the motility phenotype. Here, we also analyzed mst1-2 (aka mstg, which is CLiP strain LMJ.RY0402.136134; Table S3), a strain that lacks mastigonemes and was previously shown to swim with normal velocity (Amador et al., 2020). In our hands, when applying our semiautomated analysis of swimming trajectories, mst1-2 instead swam with reduced velocity (Fig. 5B, S5). To further analyze how PKD2 and its associated proteins MST1 and SIP promote fast swimming of *Chlamydomonas*, high speed video recordings were analyzed by visual examination and kymography (Fig. 5C). The beat frequency of the pkd2 mutant cilia was slightly elevated but we observed that the beat efficiency (i.e., the distances a cell moves during each beat cycle) was greatly reduced compared to those of control and pkd2 PKD2-NG rescue cells, providing a likely explanation for the reduced swimming velocity of the pkd2 mutant (Fig. 5 E, F). This observation supports a role of the PKD2-mastigoneme complex in increasing the effective surface of the cilia, allowing for faster swimming. This concept could also explain the somewhat increased beat frequency of pkd2 mutant cilia in comparison to the wild-type and rescue strains, as the absence of mastigonemes will likely reduce the resistance experienced by the beating cilia (Fig. 5E).

### 2.7 Discussion

Here, we analyzed the assembly of PKD2 in *Chlamydomonas* cilia, building on our previous observation that PKD2-NG is subcompartmentalized along the proximo-distal axis of cilia.

Using *Chlamydomonas*, we addressed three questions: 1) How do the PKD2 regions develop and adjust in response to changing parameters such as cilia length? 2) How does the lack of PKD2 affect ciliary motility? 3) Does the formation of PKD2 patterns involve additional proteins?

*Is the proximal PKD2 region a ciliary sorting compartment?* 

In *Chlamydomonas* cilia, two populations of PKD2-NG can be distinguished: PKD2-NG of the distal region is immobile, has a low turnover and binds mastigonemes whereas PKD2-NG in the proximal region lacks mastigonemes, is more mobile and quickly exchanges with PKD2 in the cell body. The proximal region neighbors the transition zone and all ciliary PKD2, with and without astigonemes, will pass into this region when entering cilia. The complex tripartite mastigonemes of the heterokont *Ochromonas* are present in secretory in vesicles with their base already anchored to the vesicular membrane and remaining membrane-anchored during secretion near the ciliary base (Bouck, 1971). In *Chlamydomonas*, loss of PKD2 (or SIP) affects the accumulation of MST1 near the ciliary base, suggesting that all three proteins moves as a complex to secretion sites near the cell apex (Liu et al., 2020). Mastigonemes were not observed in the proximal region of cilia, including within short regrowing cilia, suggesting that after entering the cilium, mastigonemes-PKD2 complexes quickly pass into the distal region (Liu et al., 2020). In contrast, mastigoneme-deficient PKD2-NG complexes in the *mst1-1* mutant are largely contained within the proximal region rather than dispersing along the cilia. Thus, the

proximal ciliary region could function as sorting compartment permitting PKD2-mastigoneme complexes to quickly pass into the distal cilium for anchoring while retaining mastigonemesdeficient PKD2. This leaves open the question after the mechanism by which the margins of the PKD2 regions are defined, particularly the distal border of the proximal region. One possibility is the presence of weaker transient binding sites for PKD2-NG in the proximal region and more stable, PKD2-mastigoneme specific docking sites on DMTs 4 and 8 in the distal region; the gap could be explained by an intercalated region without PKD2 binding sites. Alternatively, the distal border of the proximal region could contain a gate, fencing in PKD2 without mastigonemes, while still permitting PKD2-mastigoneme complexes to pass into the distal cilium. While the transition zone is the main ciliary gate (Garcia-Gonzalo & Reiter, 2012), additional diffusion barriers within the ciliary membrane cannot be excluded. Indeed, Lee et al. reported partitioning of the ciliary membrane along the length of cilia into actin-dependent corals, transiently confining diffusing G-protein coupled receptors (Lee et al., 2018). Further, the ciliary dilation of chordotonal neuron cilia in *Drosophila* defines or maintains the border between the proximal and distal zone (W. Xiang et al., 2022) and, in sperm flagella, the septinbased annulus forms a diffusion barrier between the midpiece and principal piece (Kwitny et al., 2010).

The presence of a distinct PKD2-NG region in the proximal cilium of *Chlamydomonas* is only one of several known structural, biochemical and functional specializations of this region. Ciliary bending is initiated in the proximal region, which possesses a special subset of inner dynein arms of unknown function (Yagi et al., 2009) and a bridge between DMTs 1 and 2. Also, the dynein assembly factor ODA10 is specific for the proximal ~3-4 µm of cilia (Dean & Mitchell, 2015) and the kinases FA2 and LF5 are restricted to the very proximal end of the

ciliary shaft, just above the transition zone (Mahjoub et al., 2002; Tam et al., 2013). Similarly, primary cilia often possess a peri-axonemal "inversin compartment" in the proximal region, which is critical for proper ciliary signaling during left-right asymmetry determination and in kidney development (Bennett et al., 2020; Mochizuki et al., 1998; Shiba et al., 2009). Our data suggests that the proximal region of cilia might be a sorting compartment, ensuring that only fully assembled PKD2-SIP-MST1 complexes enter the more distal cilium whereas mastigonemes-deficient PKD2 complexes are retained.

The length of PKD2 regions is adjusted in a ciliary length-dependent manner

The plus-ends of the axonemal microtubules point toward the ciliary tip and axonemes grow by addition of tubulin to the distal plus-end, with other axonemal substructures added briefly after (Euteneuer & McIntosh, 1981; Hoog et al., 2014; Lechtreck et al., 2013; Rosenbaum & Child, 1967; Witman, 1975). In a simple model, proteins specific for the proximal region of full-length cilia are delivered and assembled early during cilia formation, whereas those specific for more distal regions will follow later. However, our data reveal that the PKD2 regions are not established sequentially as cilia grow. Rather, the two PKD2 regions develop early during ciliogenesis and proportionally adjust in length as cilia elongate. This implies that PKD2 is redistributed, e.g., the proximal border of the distal region must be moved distally as cilia grow, a process that likely involves changes in the underlying axoneme to generate or eliminate PKD2 binding sites. During the assembly of *Drosophila* auditory cilia, dynein motor complexes are initially not confined to their proximal target zone, and ectopic complexes initially observed in the distal zone, are later removed (W. Xiang et al., 2022). Also, the OcNC1 channel subunit, initially present in the proximal segment of assembling rat olfactory cilia, is later moved to its

final position in the distal segment (Matsuzaki et al., 1999). Cilia maturation seemingly involves the trimming and rearranging of proteins incorporated during earlier stages of assembly. For *Chlamydomonas* PKD2, such dynamics also occur when cilia shorten, since proportionality of the PKD2-NG regions is essentially maintained in shortened cilia. This indicates that ciliary resorption is not a simple breakdown from the tip but, at least with respect to Chlamydomonas PKD2, involves reorganization and rescaling.

Efficient axonemal docking of PKD2 requires de novo assembly of cilia

In the distal region of cilia, PKD2-mastigoneme complexes are anchored to just two of the nine doublets, suggesting that only these two doublets provide accessible docking sites for the complex (Liu et al., 2020). Similarly, ODA10 is targeted with high precision to the proximal region of DMT 1 (Dean & Mitchell, 2015). Furthermore, numerous structural specializations typical for one or a subset of the nine DMTs, e.g., the B-tubule beaks, DMT 1-to-2 bridge, absence of ODAs from DTM 1 etc., have been identified in Chlamydomonas cilia, indicating the presence of biochemical differences between the different doublets (Bui et al., 2012; Dutcher, 2020; Hoops & Witman, 1983). The DMTs are continuous with the basal body triplets, each of which possess unique features with respect to their association to basal apparatus fibers and ciliary roots, centrin fibers within the triplet cylinder, and their position within the cell and with respect to the mother basal bodies during their genesis (Geimer & Melkonian, 2004; Holmes & Dutcher, 1989; Wingfield & Lechtreck, 2018). Likely, distinct features of the triplet microtubules determine individual characteristics hardwired into the axonemal DMTs. PKD2-NG docking into the distal region of fully assembled cilia is a rather slow process. Perhaps, the docking sites on the DMTs 4 and 8 are obscured or absent in such full-length zygotic cilia and

efficient axonemal anchoring of PKD2 into two rows requires *de novo* assembly of cilia. Currently, it is unknown whether PKD2 interacts directly with the DMTs or indirectly via a linker protein. A putative linker protein that co-assembles with PKD2 or the intracellular regions of PKD2 could integrate into the microtubules during elongation whereas appending PKD2 or its linker to fully formed DMTs could be difficult. Alternative mechanisms to explain targeting of PKD2 to specific DMTs, such as transport along and delivery to specific DMTs, appear less likely.

The PKD2-SIP-mastigoneme complex increases the efficiency of the ciliary beat

Previously, we showed that the *pkd2* and *mst1-1* mutants swim with moderately (minus ~20%) reduced velocity (Liu et al., 2020). Similarly, Nakamura et al. (1996) observed a 20-30% reduction of the swimming velocity combined with a slight (~10%) increase in beat frequency after mastigonemes were removed from control cilia by treatment with a monoclonal antibody against MST1 (Nakamura et al., 1996). In a recent study by Wang and colleagues, only a slight reduction in swimming velocity was reported for mst1-1; the mutant, however, swam slower than controls at high viscosity and displayed reduced gravitaxis (Wang et al., 2023). Swimming velocity was unaffected in *mst1-2*, another CLiP strain lacking mastigonemes (Amador et al., 2020; Wang et al., 2023). In *Chlamydomonas*, swimming velocity varies greatly depending on culture conditions, cell density, time of the day, assay conditions such as light and temperature etc. and a standardized approach to determine swimming speed is missing. Here, we developed a simple plugin for Fiji/ImageJ to extract swimming velocities from long-exposure micrographs, allowing us to analyze a large number of cells. Using this tool, we determined that the *pkd2*, *sip* and both *mst1* mutants all swam with reduced velocity. A common feature of all four mutants

(i.e., pkd2, sip, mst1-1 and -2) is the absence of mastigonemes from cilia. These  $\sim 800$ -nm long hairs project from both sides of the cilium oriented approximately perpendicular to the plane of ciliary beating. Assuming that the mastigonemes are sufficiently stiff to somewhat project laterally from cilia rather than being dragged behind, they would increase the surface of the beating cilium. This would improve the efficiency of the ciliary beat, allowing cells to travel a larger distance during each beat cycle compared to cells without mastigonemes. High-speed video revealed that pkd2 cells traveled less than control cells during each ciliary beat cycle while the bending motion was similar and the beat frequency was slightly (~8%) increased. The latter is similar to observation on control cells after experimental removal of the mastigonemes (Nakamura et al., 1996). Compared to controls, the beat frequency was also higher for mst1-2 but the difference was not significant (Amador et al., 2020). These data support a parsimonious model for the function of Chlamydomonas PKD2, in which its prime role is to anchor the mastigonemes to the ciliary surface, forming a fan-like superstructure, which increases the ciliary surface, beat efficiency and swimming velocity. However, this concept generates a conundrum because the overall domain structure and sequence of Chlamydomonas and mammalian PKD2 is well conserved (Huang et al., 2007). We consider it therefore likely that *Chlamydomonas* PKD2 is a functional channel, as it has been demonstrated for mammalian PKD2, which appears to be gated by both mechanical means (i.e., nodal flow) and a PKD1-derived ligand (Cao et al., 2015; Ha et al., 2020; Katoh et al., 2023). Further, Chlamydomonas PKD2 is associated to both an extracellular and an intracellular component, i.e., the mastigonemes, and the axoneme, a design observed for various mechanically gated channels, which use deformation of the associated structures to regulate opening (Ferreira et al., 2019; Sun et al., 2019). But for the reduced swimming velocity, which, we argue, results from the lack of mastigonemes rather than a failure

of PKD2's assumed channel functions, we did not notice additional phenotypical defects of the *Chlamydomonas pkd2* mutant. In detail, *pkd2* appeared normal during phototaxis, photoshock, mating and gliding motility. This does not exclude a role of PKD2-based ion currents in *Chlamydomonas* cilia during behaviors that are difficult to recognize and assay. As PKD2 is reduced in *mst1* cilia and *pkd2* cilia lack mastigonemes, assigning individual role to each protein is difficult. Loss-of-function and gain-of-function PKD2 mutants, which still bind mastigonemes and the axoneme, could allow for a better assessment of the putative channel function of *Chlamydomonas* PKD2.

SIP promotes proteolytic processing and ciliary entry of PKD2

To identify proteins required for ciliary targeting and patterning of PKD2, we isolated PKD2 complexes from ciliary detergent extracts and identified the single-pass transmembrane protein SIP as an interactor of *Chlamydomonas* PKD2. Mammalian PKD2 interacts with the triple-pass transmembrane protein TMEM33 in the ER and the 11-transmembrane domain protein PKD1 in cilia; single-pass interactors of PKD2 were not identified (Arhatte et al., 2019; Wu & Somlo, 2000). Single-pass transmembrane proteins, however, are part of the ciliary CatSper channel complex in mammalian sperm flagellar. This complex contains at least three single-pass transmembrane proteins (e.g., CatSper  $\gamma$ , CatSper  $\delta$ , CatSper  $\zeta$ ), which are required for proper trafficking, assembly and/or function of the complex in the principal piece of sperm flagella (Chung et al., 2017; Singh & Rajender, 2015). Further, sodium channels encompass single-pass beta subunits, which regulate channel gating, localization, and anchoring to the cytoskeleton (Isom, 2001). Interestingly, SIP is highly reminiscent of the N-terminal region of Chlamydomonas PKD2, giving it the appearance of a PKD2 fragment. In detail, SIP

corresponds to the non-pore forming transmembrane helix 1 and parts of the extracellular top domain of PKD2. Our data indicate that Chlamydomonas SIP is required for the processing of PKD2 in the cell body, before traveling together with PKD2 into cilia. In *Chlamydomonas*, PKD2 is cleaved within its large extracellular domain between helix 1 and 2 and only the two resulting fragments, which remain associated, enter cilia (Huang et al., 2007; Liu et al., 2020). In *sip* mutants, the overall amount of PKD2 is reduced, the amount of its fragments was severely diminished and its apical accumulation was not apparent. We propose that proteolytic processing of PKD2 is a prerequisite for its entry into cilia and that SIP is somehow participates in PKD2 processing, e.g., by contributing to the assemble of a cleavable PKD2 complex, ensuring its proper localization, or generating a site on the complex to recruit a protease (Fig. S3G). In mammals and C. elegans, polycystin1/PKD1, the binding partner of PKD2 in these organisms, undergoes cleavage at the G-Protein-Coupled Receptor Proteolysis Site motif in the extracellular domain; proteolytic processing of PKD1 is involved in its localization to the cell surface and, in C. elegans, relevant for its localization to cilia (Chapin et al., 2010; Walsh et al., 2022). To summarize, our data suggest a mutual codependency of PKD2, SIP and MST1/mastigonemes for entry into Chlamydomonas cilia.

The presence of SIP-encoding genes is limited to the genomes of various green algae including those with *Chlamydomonas*-like mastigonemes but also other species that lack mastigonemes/MST1 and even cilia. This suggests that SIP is a green algal PKD2 interacting protein rather than being specifically required for the binding of PKD2 to mastigonemes and DMTs. Axonemal docking of PKD2, however, might involve a component, which is tightly associated with DTMs 4 and 8 and therefore not released by detergent treatment as used here to

identify SIP. Future work using proximity labeling techniques; i.e., via expression of PKD2- or SIP-biotin ligase fusions, might provide a strategy to shed light on axonemal docking of PKD2.

#### 2.8 Materials and Methods

Strains, culture conditions and genotyping

Chlamydomonas strains used in this study are enlisted in Table S3. The wild-type strain CC-620, and the mutant strains *lf4* (CC-4534) and *fla10* (CC-1919), and the rescue strain *pkd2 PKD2-NG* (CC-5899) are available from the Chlamydomonas Resource Center. The original *pkd2* mutant (LMJ.RY0402.204581), and the *sip* (LMJ.RY0402.143879) and *mst1-1* (LMJ.RY0402.052413) and *mst1-2* (LMJ.RY0402.136134) strains were obtained from the *Chlamydomonas* Library Project (<a href="https://www.chlamylibrary.org/allMutants">https://www.chlamylibrary.org/allMutants</a>) (Li et al., 2019). mutant CC-5235 and g1 (Pazour et al., 1995) were used as wild-type controls. The *mst1-1 pkd2 PKD2-NG*, *lf4 pkd2 PKD2-GFP*, *fla10 pkd2 PKD2-GFP* were generated by mating. The *pkd2 PKD2-GFP* was previously described (Liu et al., 2020). Here, we used a *pkd2* mutant that was outcrossed twice with g1. Cells were grown in modified minimal (M) medium (<a href="https://www.chlamycollection.org/methods/media-recipes/minimal-or-m-medium-and-derivatives-sager-granick/">https://www.chlamycollection.org/methods/media-recipes/minimal-or-m-medium-and-derivatives-sager-granick/</a>) and maintained at 22°C with a light/dark cycle of 14:10 h; large cultures used for cilia isolation were aerated with air enriched with 0.5% CO<sub>2</sub>.

#### Transgenic strain generation

To rescue the *sip* mutant, cDNA of *SIP* gene was amplified from using primers 1 and 2 (Table S4) and *Chlamydomonas* cDNA as a template and inserted into the pGenD. To provide antibiotic resistance, the hygromycin cassette was amplified using primer 3 and 4 (Table S4) inserted into the pGenD-SIP plasmid. The resulting pGenD-SIP+Hyg plasmid was linearized using XbaI and transformed in the *sip* mutant by electroporation (Invitrogen Neon<sup>TM</sup> Transfection system).

Transformants were selected on TAP plates containing  $20\mu g/ml$  hygromycin (Bio Basic). Clones expressing SIP protein were identified using whole mount EM based on the restoration of mastigonemes on the ciliary surface, which was observed in one out of more than 60 transgenic clones analyzed. The presence of SIP, PKD2 and MST1 in cilia was confirmed by western blot analysis and the *sip SIP* genotype was confirmed using PCR using Primers 5 and 6 (Table S4) to track the *sip* insertional allele and primers 7 and 2 to track the transgene; primers 8 and 9 were used to amplify a part of the  $g\beta$  gene to verify DNA quality (Zamora et al., 2004).

#### Ciliary regeneration

Vegetative cells or zygotes in M medium were deciliated by a pH-shock (pH 4.2 for 30 s), transferred to fresh M medium (M-N for zygotes), and allowed to regrow cilia under constant light with agitation. Samples were analyzed at various time point during cilia regeneration by TIRFM.

#### Mating experiments

To generate gametes, 100 ml of vegetative cells were grown for 4-5 days to a cell density of  $2\times10^6$  cells/ml. The evening prior to the mating experiment, cells were transferred to 15 ml M-N medium and aerated overnight under constant light. In the morning, cells were transferred to 2 ml of 1/5 M-N supplemented with 10 mM HEPES and incubated for an additional 30 minutes, followed by mixing of gametes of opposite mating type. For TIRFM, the cell suspension was mounted for in vivo imaging at various time points after mixing of the gametes. The distribution of PKD2-NG in cilia was scored by visual examination. To obtain progeny, the cells suspension

was incubated in light without agitation for 4-6 hours, plated onto dry mating pates (TAP medium with 4% agar or 1.8% phytogel; <a href="https://www.chlamycollection.org/methods/media-recipes/tap-and-tris-minimal/">https://www.chlamycollection.org/methods/media-recipes/tap-and-tris-minimal/</a>), incubated overnight in light, air-dried, and stored for >10 days in the dark. Plates were transferred to -20°C for 2 days, thawed, dried, and incubated in constant light for several days. Colonies were streaked for single cell and progeny with the desired traits was identified using TIRFM, geno- and phenotyping, PCR and western blotting.

#### Isolation of cilia

To isolate cilia, cells were washed and concentrated in 10mM HEPES (pH 7.4), resuspended in 10 ml of HEPES-Magnesium-Sucrose (HMS; 10 mM HEPES, pH 7.4, 5 mM MgSO<sub>4</sub>) and immediately deciliated by adding 2.5 ml of dibucaine-HCl (25 mM in H<sub>2</sub>O; Sigma-Aldrich) and vigorous pipetting (Craige et al., 2013). After addition of 20 ml of 0.7 mM EGTA in HMS, the cell bodies were removed by centrifugation (1,150 g, 3 min, 4°C; Sorvall Legend XTR, Thermo Fisher Scientific). Ten, the supernatant was underlaid with a sucrose cushion (10 ML of 25% sucrose in HMS) and the remaining cell bodies were removed by centrifugation  $(1,700 \times g, 4^{\circ}C,$ 10 min). Cilia in the upper phase were sedimented by centrifugation (27,000 × g, 4°C, 20 min; Beckman Coulter, Avanti JXN-26), resuspended in HEPES -Magnesium-EGTA-Potassium (HMEK; 30 mM HEPES, 5 mM MgSO<sub>4</sub>, 0.5 mM EGTA, and 25 mM KCl) supplemented with 1% protease inhibitor cocktail (PI, Sigma-Aldrich, P9599), and lyzed for 20 minutes on ice with Triton X-100 or, if phase partitioning was planned, Triton X-114 (each 1% final concentration). The axonemes were separated from the membrane+matrix fraction centrifugation  $(27,000 \times g,$ 4°C, 15 minutes). For phase partitioning, the supernatant was incubated at 30°C for 5 minutes; phase separation is evident by the cloudy appearance of the solution. The micelles were

harvested by centrifuged  $(1,700 \times g; 22 \,^{\circ}C; 5 \,^{\circ}minutes)$  leading to an upper aqueous phase (matrix fraction) and a detergent phase (membrane fraction). Proteins in the detergent phase were further purified by methanol-chloroform precipitation.

#### *Immunoprecipitation*

Cilia isolated from *pkd2 PKD2-NG*, *mst1-1 pkd2 PKD2-NG* and an untransformed control strain were resuspended in HMEK supplemented with 100 mM NaCl (final concentration) and protease inhibitor cocktail and lysed by addition of 1% NP-40 (final concentration). The axonemes were removed by centrifugation (27,000 g, 4°C, 15 min) and the supernatant was incubated with anti-NG nanobody agarose beads (Allele Biotechnology) for 1 hour at 4°C using a rotisserie. The loaded beads were washed twice with HMEK containing 150mM NaCl and bound proteins were eluted using 200 mM glycine, pH 2.5. The eluate, input, and flow-through were analyzed using silver-stained gels (Silver Stain Plus Kit, Bio-Rad Laboratories) and the eluate was subjected to mass spectrometry using an Orbitrap Elite system at the Proteomics and Mass Spectrometry Core Facility at the University of Georgia.

#### Antibodies and Western blotting

Anti-SIP and anti-MST1 antibodies were generated as follows: The coding region of *SIP* was amplified by PCR from *Chlamydomonas* cDNA using primers 2 and 10 (Table S4) and cloned into the EcoRI site in the pMAL-cRI vector (downstream of the Maltose Binding Protein/MBP sequence). Similarly, a ~500-bp long stretch encoded by exon 15 exon of *MST1* was amplified by PCR from a *Chlamydomonas* genomic DNA using primers 11 and 12 (Table S4) and inserted into the EcoR1 site of pMAL-cRI. The MBP-fusions of SIP and the MST1 fragment were

expressed in *E. coli* and purified using amylose resin according to the instructions of the manufacturer (New England Biolabs). Polyclonal antisera in rabbits were produced by Pocono Rabbit Farm and Laboratory and the anti-SIP antibody was affinity-purified using SIP protein immobilized on PVDF membrane.

Whole cell samples, isolated cilia or ciliary fractions were incubated for 5 minutes at 95°C in Laemmli SDS sample buffer, separated by SDS-PAGE using Bio-Rad TGX precast gels, and transferred to PVDF membrane. Membranes were blocked in TBS supplemented with 0.05 Tween20, 3% Bovine Serum Albumin and 3% fish gelatin followed by standard imunostaining protocols, i.e., incubation in the diluted primary antibodies for overnight at 4°C with agitation (primary anti-bodies used in this study are listed in Table S4) and incubation in diluted secondary antibodies (i.e., anti-mouse, 1:3000 and anti-rabbit IgG, 1:4000 conjugated to horseradish peroxidase; Invitrogen 31432/AB\_228302 and 31460/AB\_228341, respectively) for ~60 minutes at room temperature. For visualization, membranes were incubated in chemiluminescence substrate (SuperSignal West Pico PLUS or Atto; Thermo Fisher Scientific) and the images were captured using a Bio-Rad ChemiDoc MP imaging system and the Image Lab software.

Whole mount negative stain electron microscopy

For whole mount EM, a formvar/carbon-coated 100 mesh electron microscope grid (FCF100-Cu-50, Electron Microscopy Sciences) was place on a drop of concentrated cells ( $\sim 2 \times 10^7$  cells/ml in water) on parafilm for 3 minutes. After removing excess cells using filter paper, the grid was put on a drop of 2% uranyl acetate in water for 1 to 2 minutes. Finally, the grid was washed with distilled water. Images were collected using a JEOL JEM1011 electron microscope. CC-620 was used as a positive control to screen for sip SIP rescue strains.

Swimming velocity and high-speed video

To measure the swimming velocity, cells were resuspended in fresh M medium, placed in a chambered plastic slide (14-377-259; Fisherbrand), and observed using an inverted light microscope (TMS; Nikon). Images were recorded using a MU500 camera (Amscope) and the associated Topview software at a fixed exposure time of 1 second. The length of the swimming trajectories (such as those shown in Fig. 6A) were analyzed using a newly developed "LengthAnalysisTool" plugin for ImageJ (National Institutes of Health); the plugin is described at https://github.com/Abha99/Length-Analysis-Tool. In brief, high-contrast long-exposure images obtained using non-phototactic red light were converted to 8-bit and analyzed using the plugin, resulting in an image, in which the recognized trajectories are outlined and numbered and a pop-up table with the measurements including the end-to-end distance representing the linear velocity of the cells and the contour length of the path representing the actual velocity; the latter was used here (Fig. S4). The annotated image and the table were examined and false tracks were deleted. Excel was used for statistical analysis and bar graphs and violin plots were prepared using GraphPad Prism.

#### *In vivo TIRF imaging*

Samples for *in vivo* imaging were prepared as follows: at room temperature, 10 μl of cells were placed inside of a ring of petroleum jelly onto a 24x60 mm No. 1.5 coverslip and allowed to settle for ~1-3 min. Then, a 22x22 mm No. 1.5 coverslip with 5 μl of immobilization buffer (10mM HEPES, 5mM EGTA, pH 7.4) was inverted onto the larger cover glass to form a sealed observation chamber; the immobilization buffer was omitted for the gliding and secretion assay. For TIRF imaging, we used a Nikon Eclipse Ti-U inverted light microscope equipped with a

60x/1.49 NA objective lens and a 40 mW 488 nm diode laser (Spectraphysics) (Lechtreck, 2013). Images were recorded at 10 fps using the iXon X3 DU897 EMCCD camera (Andor) and the Elements software package (Nikon). Still images mostly represent 10 frame walking averages. ImageJ (National Institutes of Health) and the KymoResliceWide plug-in were used to analyze the recordings and generate kymograms. Kymograms, individual frames, and videos were cropped and adjusted for brightness and contrast in ImageJ and Photoshop CC 2018 (Adobe); Illustrator CC 2018 (Adobe) was used to assemble the figures.

For drug treatments, cells were resuspended in M medium with 20 mM mM LiCl or 20 mM NaPPi, pH 6.9; the experiments were repeated twice or more.

High-speed video analysis

For high-speed video analysis at 1000 fps, we used an inverted Eclipse Ti2 microscope (NIKON) equipped with a long distance DIC condenser and a 40x 0.95 Planapo objective. Images were recorded using an EoSens 3CL camera (Mikrotron) and an CORE2 DVR Express rapid storage device (IO Industries). Cells were concentrated and placed in an observation chamber. Recordings were exported in AVI format and analyzed using ImageJ.

Structure Predictions

The publicly available Google ColabFold project

(https://www.ncbi.nlm.nih.gov/pmc/articles/PMC9184281/) was used to generate structure

predictions with Alphafold 2 (<a href="https://www.nature.com/articles/s41586-021-03819-2">https://www.nature.com/articles/s41586-021-03819-2</a>). Structure figures were generated using Pymol software.

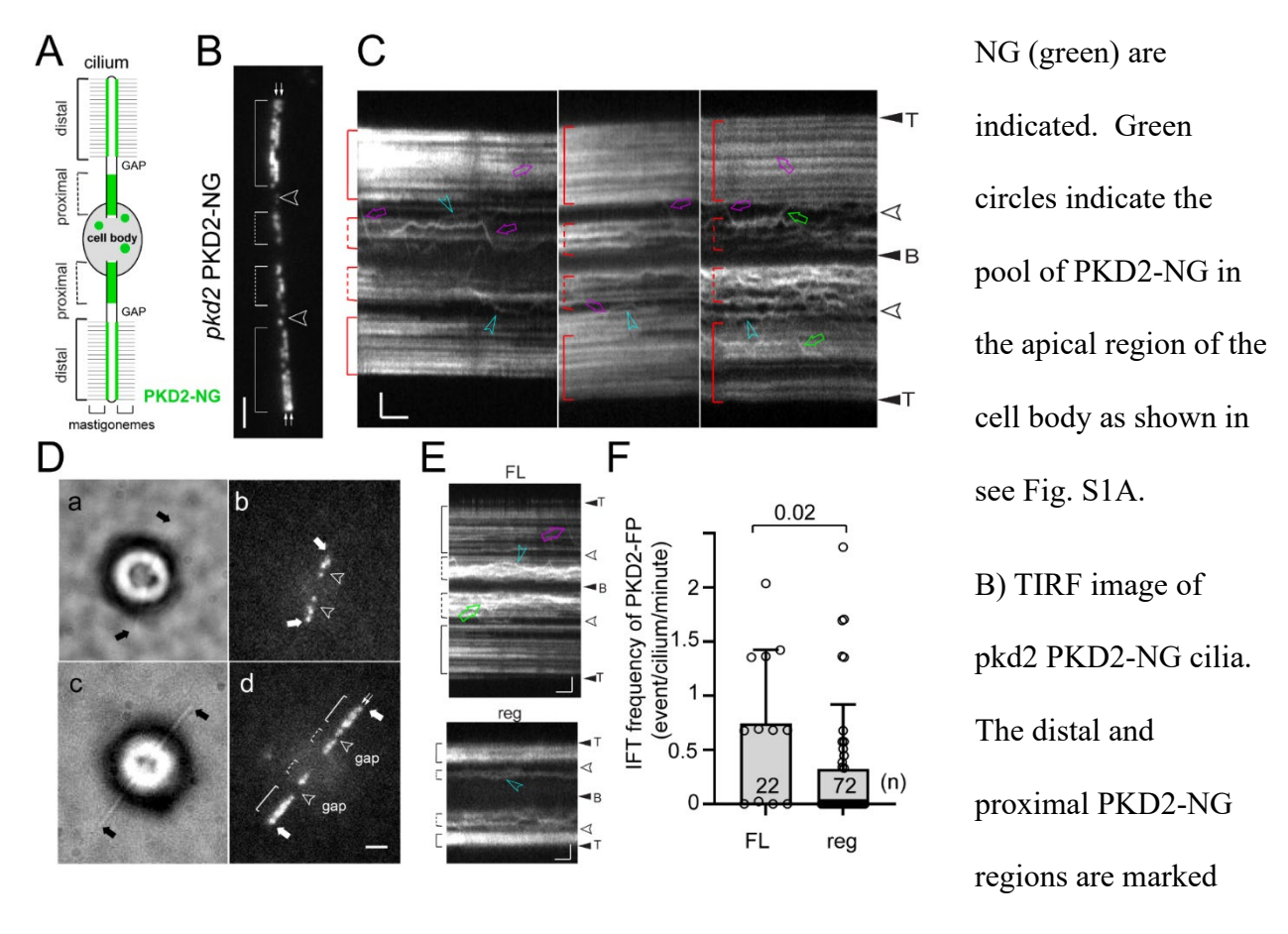
#### 2.9 Acknowledgements

B.M. and E.B.W. received CURO Research Assistantships for undergraduate researchers from the University of Georgia. We acknowledge expert services by the UGA Proteomics and Mass Spectrometry Core, which is supported by the National Institutes of Health (grant S10RR028859). This study was supported by a grant by the National Institutes of Health (R01GM139856 to K.L.). The content is solely the responsibility of the authors and does not necessarily represent the official views of the National Institutes of Health.

#### 2.10 Figure with legends

Figure 2.1) PKD2 regions develop early during ciliogenesis

A) Schematic representation of an adhered Chlamydomonas cell. The mastigonemes and PKD2-



with brackets. Open arrowheads indicate the gap regions. Small arrows indicate the rows of PKD2-NG. Bar =  $2\mu m$ .

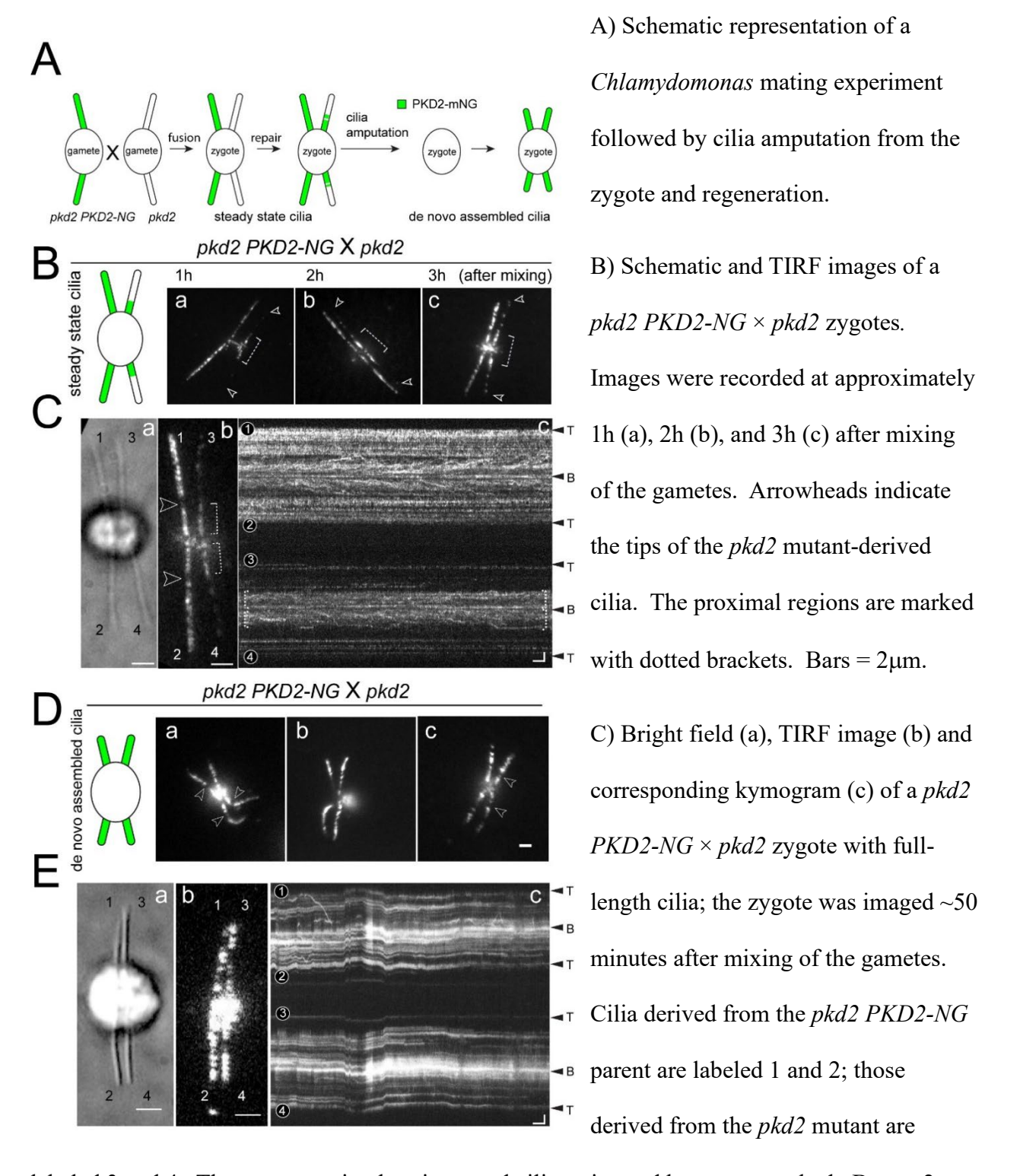
- C) Kymograms of full length pkd2 PKD2-NG cilia. The ciliary tips (T), bases (B), the distal and proximal regions, and gaps are marked. Magenta arrow, retrograde IFT; green arrow, anterograde IFT; blue arrowheads, apparent diffusion of PKD2-NG. Bars = 2s and 2 $\mu$ m.
- D) Bright field (a, c) and TIRF (b, d) images of *pkd2 PKD2–mNG* cells regenerating cilia.

  Arrowheads indicate the gap and single arrows indicate the ciliary tips. The distal and proximal

PKD2-NG regions and the intercalated gap are marked with brackets and arrowheads. Small double arrows in a indicate the two rows of PKD2-NG. Bars =  $2\mu m$ .

- E) Kymograms of full length (FL) and regenerating (reg) *pkd2* PKD2-NG cilia. The ciliary tips (T), bases (B), the distal and proximal regions, and gaps are marked. Magenta arrow, retrograde IFT; green arrow, anterograde IFT; blue arrowheads, apparent diffusion of PKD2-NG. Bars = 2s and 2μm.
- F) Combined anterograde and retrograde IFT frequency of PKD2-NG in full length (FL) and regenerating (reg) *pkd2 PKD2-NG* cilia. Error bars show the standard deviation; the number of cilia analyzed (n) and the result of a 2-tailed t-test are indicated.

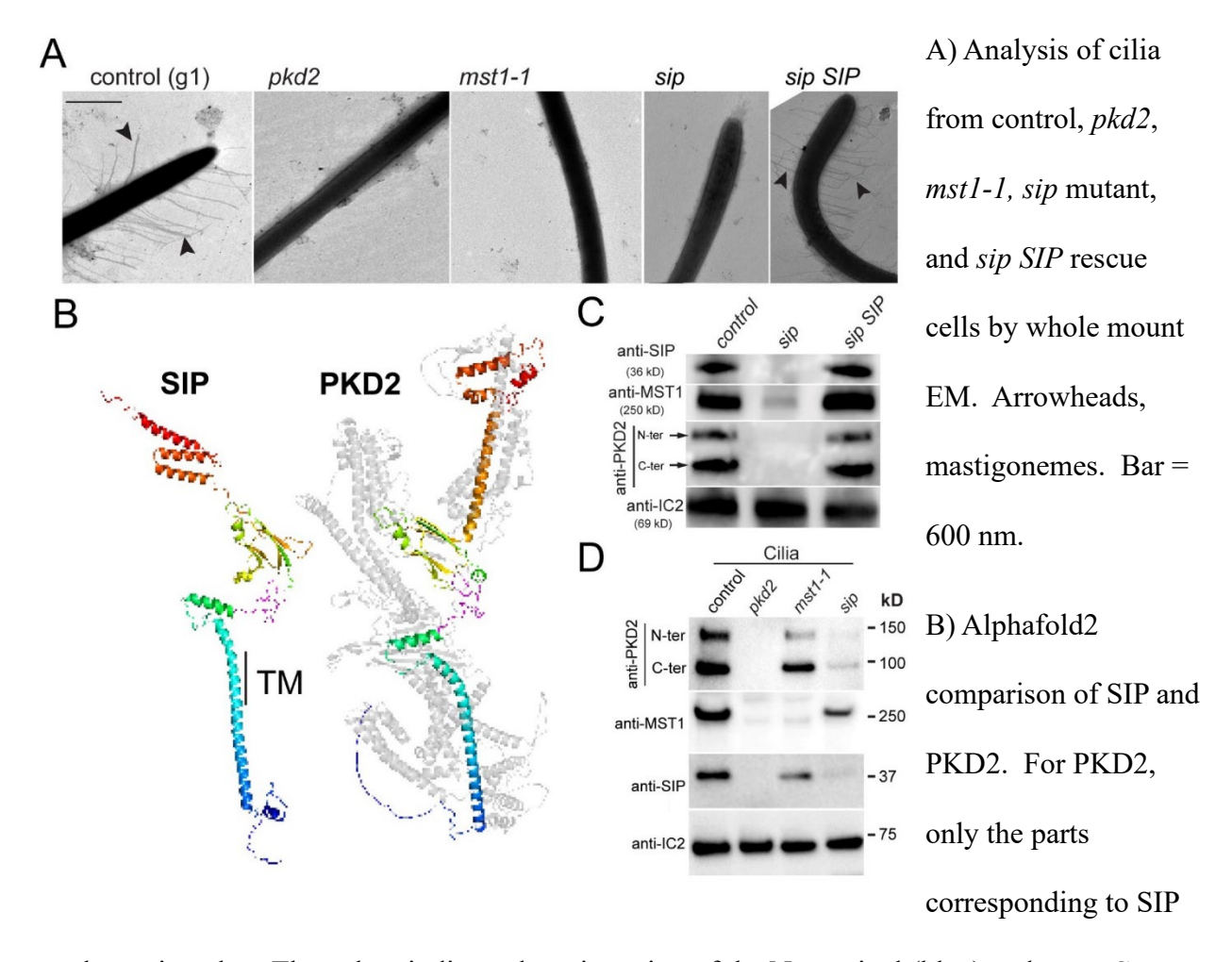
Figure 2.2) Assembly of PKD2 into the distal region of pkd2 cilia requires de novo cilia



labeled 3 and 4. The gaps, proximal regions, and ciliary tips and bases are marked. Bars =  $2\mu m$  (a and b) and  $2\mu m$  2s (c).

- D) Schematic and TIRF images of *pkd2 PKD2-NG* × *pkd2* zygotes at ~60 minutes after deciliation of the cells in the mating mixture by a pH shock. Bars =  $2\mu$ m.
- E) Bright field (a), TIRF image (b) and corresponding kymogram (c) of a *pkd2 PKD2-NG* × pkd2 zygote recorded at ~40 minutes after the pH shock. The cilia are labeled 1 to 4; the ciliary tips and bases are marked. Bars =  $2\mu$ m (a and b) and  $2\mu$ m 2s (c).

Figure 2.3) Ciliary presence of the PKD2-mastigoneme complex requires small interactor of PKD2 (SIP)



are shown in color. The colors indicate the orientation of the N-terminal (blue) and more C-terminal (red) regions. A 30bp fold that is remarkably well conserved between SIP and PKD2 is in magenta (See Fig. S3C). TM, position of the transmembrane domain of SIP.

C) Western blot analysis of cilia isolated from control, the *sip* mutant and the *sip SIP* rescue strain. The membrane was probed with anti-SIP, anti-MST1, anti-PKD2 and, as a control for equal loading, anti-IC2, a subunit of the outer dynein arms. Ciliary PKD2 runs as two bands of 100 kD (representing the C-terminal fragment) and 130 kD (representing the N-terminal fragment).

D) Western blot analysis of isolated cilia from control and the *pkd2*, *mst1-1* and *sip* mutant cells probed with anti-PKD2, anti-MST1, anti-SIP and anti-IC2. Note traces of SIP present in the *sip* mutant, indicating that some expression of the protein was restored.

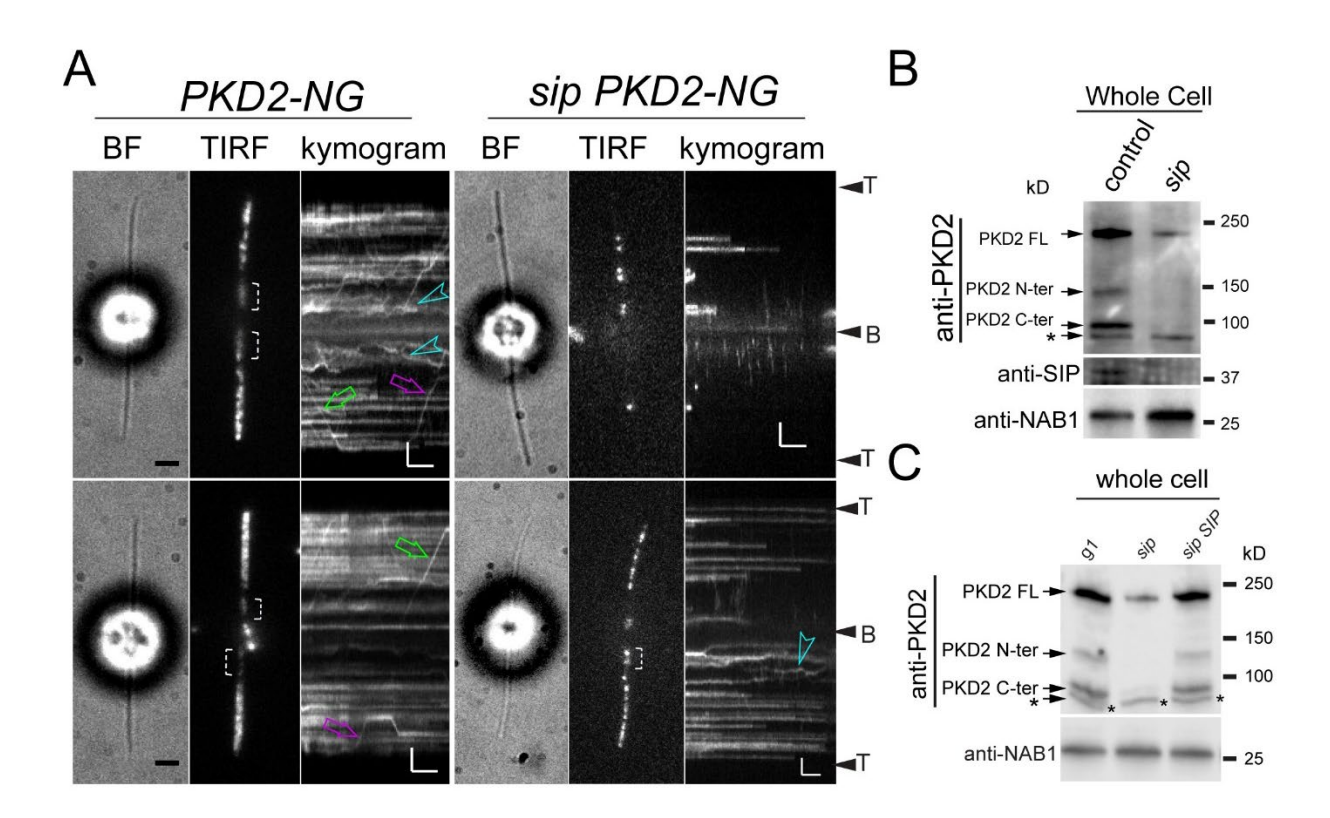


Figure 2.4) SIP is required for proteolytic cleavage of PKD2

- A) Bright field (BF) and TIRF images and the corresponding kymograms of *PKD2-NG* and *sip PKD2-NG* cells. Discernable proximal PKD2 regions are marked by brackets; green and magenta arrows indicate anterograde and retrograde IFT; blue arrowhead marks mobile PKD2-NG. The ciliary tips (T) and bases (B) are indicated. Bars (= 2 μm 2s.
- B) Western blot analysis of whole cell samples of the control and *sip* strain with anti-PKD2, anti-SIP and NAB1, a nuclear protein that serves as a loading control for whole cell samples. Note the reduction of full-length PKD2 (FL) and near absence of the N- and C-terminal fragments of PKD2 in the *sip* mutant.
- C) Western blot of whole cell samples of control (g1), the *sip* mutant, and the *sip SIP* rescue strain probed with anti-PKD2 and anti-NAB1, as a loading control. Full-length PKD2 and the

fragments are indicated. Note near absence of PKD2 fragments in *sip* mutant strains. \*, cross-reacting unspecific bands.

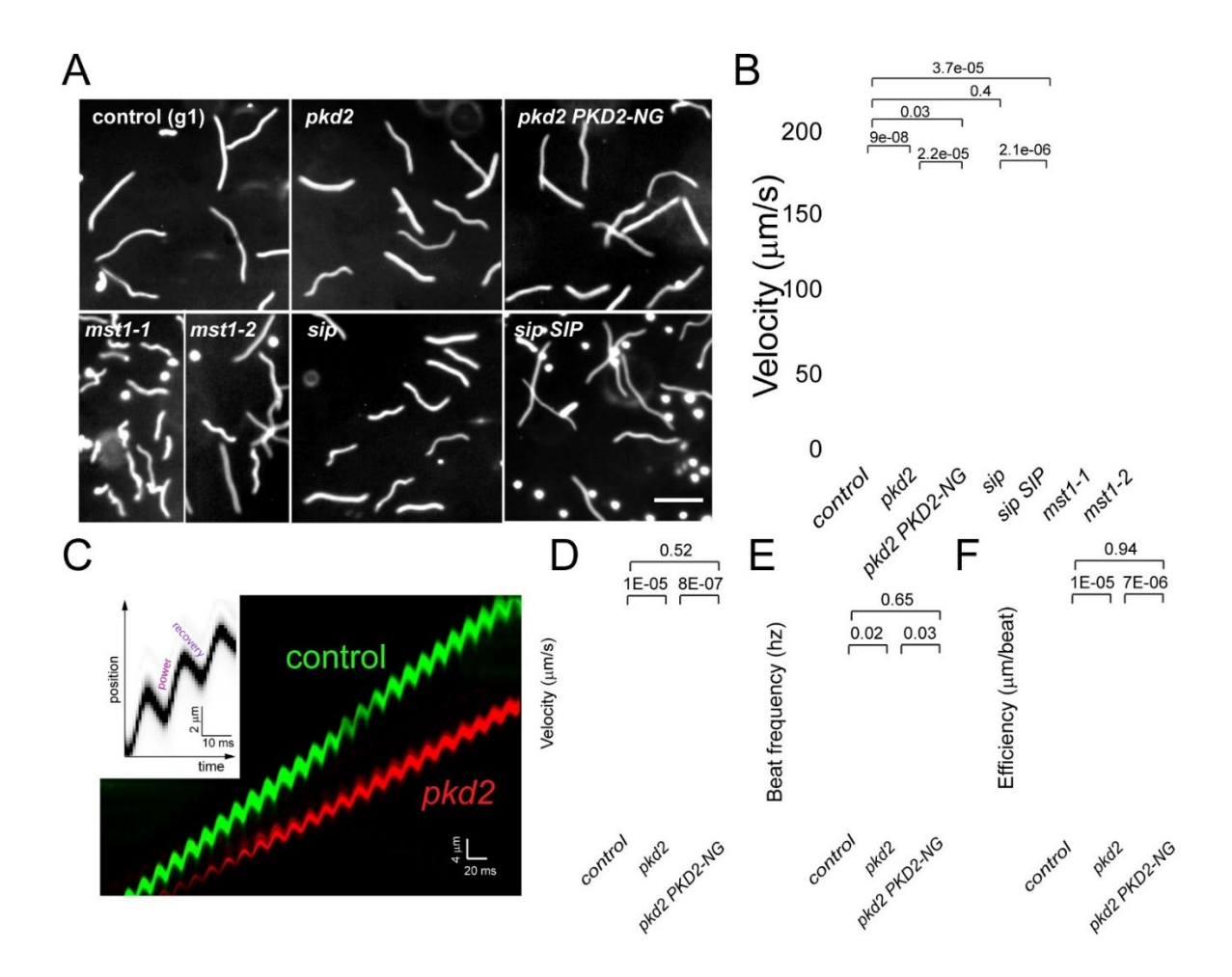


Figure 2.5) Loss of PKD2-mastigoneme complexes reduces the efficiency of the ciliary beat

- A) Micrographs obtained by 1-s exposure showing the swimming paths of control, the pkd2, mst1-1, mst1-2, and sip1 mutants, and the pkd2 PKD2-NG and the sip SIP rescue strains. Bar =  $100\mu m$ .
- B) Bar graph showing the swimming velocity of various strains as determined by the "LengthAnalysisTool" (see Materials and Methods). The standard deviations, individual data points and results of 2-tailed t-tests are indicated.

- C) Overlay kymogram based on high-speed recordings of a control (g1; green) and a *pkd2* mutant (red) cell. The insert marks the power and recovery stroke in a kymogram. Note that both cells have a similar beat frequency but the *pkd2* cell moves with reduced velocity.
- D) Violin plots of the velocity (a), ciliary beat frequency (b) and beat efficiency (c) of control, *pkd2* and *pkd2 PKD2-NG* cells. The results of 2-tailed t-tests are indicated. Shown are the data from one of two experiments with similar outcomes, each involving 20 or more cells per strain.

## 2.11 Tables

Table 2.1: List of strains used in this study.

Name	Genoytpe	Reference
CC-620 (Wild-type)	Nit, nit2,mt <sup>+</sup>	Chlamydomonas Genetics Centre
gl (wild-type)	nit1, agg1, mt <sup>+</sup>	
$pkd2$ (progeny selected from $pkd2^{\text{CLiP}}$ backcrossed twice with $g1$ )	cw15, pkd2, mt <sup>-</sup>	
lf4 (CC-4543)		
pkd2 PKD2-mNG	pkd2, mt <sup>-</sup>	This study
PKD2-GFP	$mt^+$	
lf4 pkd2 PKD2-GFP		This study
mini <sup>CLiP</sup>	cw15, mini, mt	This study
mini MINI	mt <sup>-</sup>	This study
mst1 (LMJ.RY0402.052413)	cw15, mst1, mt <sup>-</sup>	(Liu et al., 2020)
mst1 pkd2 PKD2-mNG	mst1, pkd2	(Liu et al., 2020)

Table 2.2) List of primers.

Primer number	Primer name	Sequence (5' to 3')
1	SIP anti	5'CGCGAATTCATGGCAGAACAACACCCGAG3'
2	SIP anti	5'CGCGAATTCTTACACCGCCGCGGTTCCC3'
3	CLONING	5'CGCCATATGGCAGAACAACACCCGAG3'
4	GENO MINI	5'CGCGGATCCATGGCAGAACGTGAGTCGCCT3'
5	JONI	5'TGTCGCTGAAAGTGGAGGTC3'
6	MSTf ANTI	5'CGCGAATTCGTGTCAACTTCTGGCGCTAC3'
7	MSTr ANTI	5'CGCGAATTCTCACTGGCACGCAGTGGCACC3'
8	g-beta f1	5'CAAGCTGAAGAACAACCTGGTG3'
9	g-beta r1	5'CTTGCTGGTGATGTTGAACTCG3'
10	hyg hind	5'CGCAAGCTTGTTTCTTGCGCTATGACACTTG3'
11	hyg	5'CGCAAGCTTCGCTTCAAATA3'

Table 2.3) list of anti-bodies

Name	Host	Dilution WB	Dilution IF	Reference
Anti-PKD2	rb	1:2000		(Huang et al.,2007)
Anti-SIP	rb	1:2000		This study
Anti-MST1	rb	1:2000		This study
Anti-MST1	mo		1:200	(Nakamura et al., 1996)
Anti-IC2	mo	1:1000		(King and Witman, 1990)
Anti-CAH6	rb	1:500		(Yu et al.,2020)
Anti-IFT139	mo	1:100		(Cole et al., 1998)

.

#### 2.12 Supplementary Results:

### Figure S1

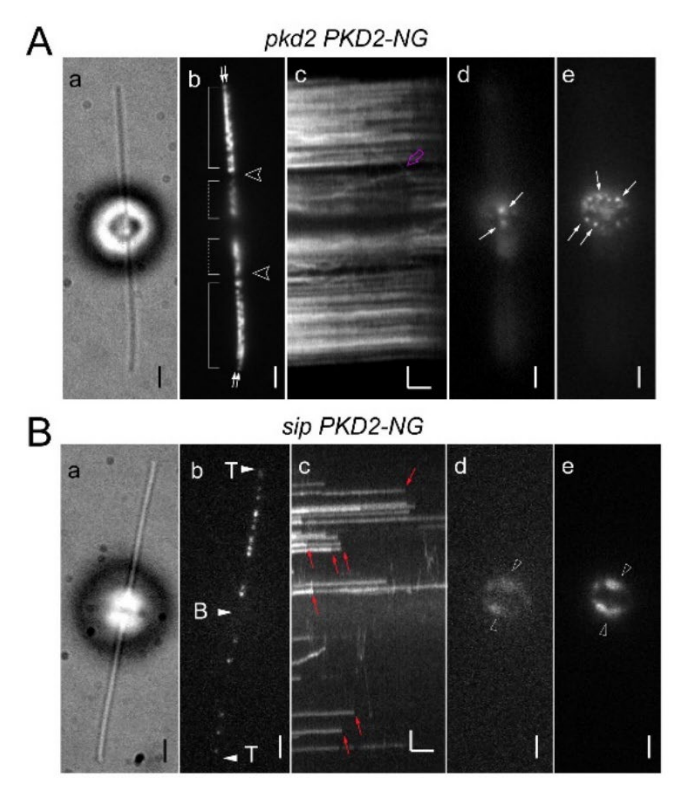


Fig. S1. The PKD2-NG cell body pool

A) Bright field (a), TIRF images (b, d, e) and corresponding kymogram (c) of a pkd2 PKD2-NG cell. Shown are different focal planes of the same cell, showing the adhered cilia (b), the basal body level (d) and an optical section through the cell apex (e). Arrow in c, PKD2-NG particle move through the gap. White arrows in d and e, PKD2-NG punctae in the cell body. Note dotted distribution of PKD2-NG in the

latter indicative for an association with the sub-membranous microtubule cage of the cell body. Bars =  $2s\ 2\mu m$ .

B) Bright field (a), TIRF images (b, d, e) and corresponding kymogram (c) of a sip PKD2-NG cell. Shown are different focal planes of the same cell, showing the adhered cilia (b), the basal body level (d) and an optical section through the cell apex (e). Red arrows in c, bleaching events of PKD2-NG. Some particles bleached in a single step while others bleached in two steps, indicating two PKD2-NG particles. White arrowheads in d and e, autofluorescence of the plastid. Bars = 2s 2µm

## Figure S2

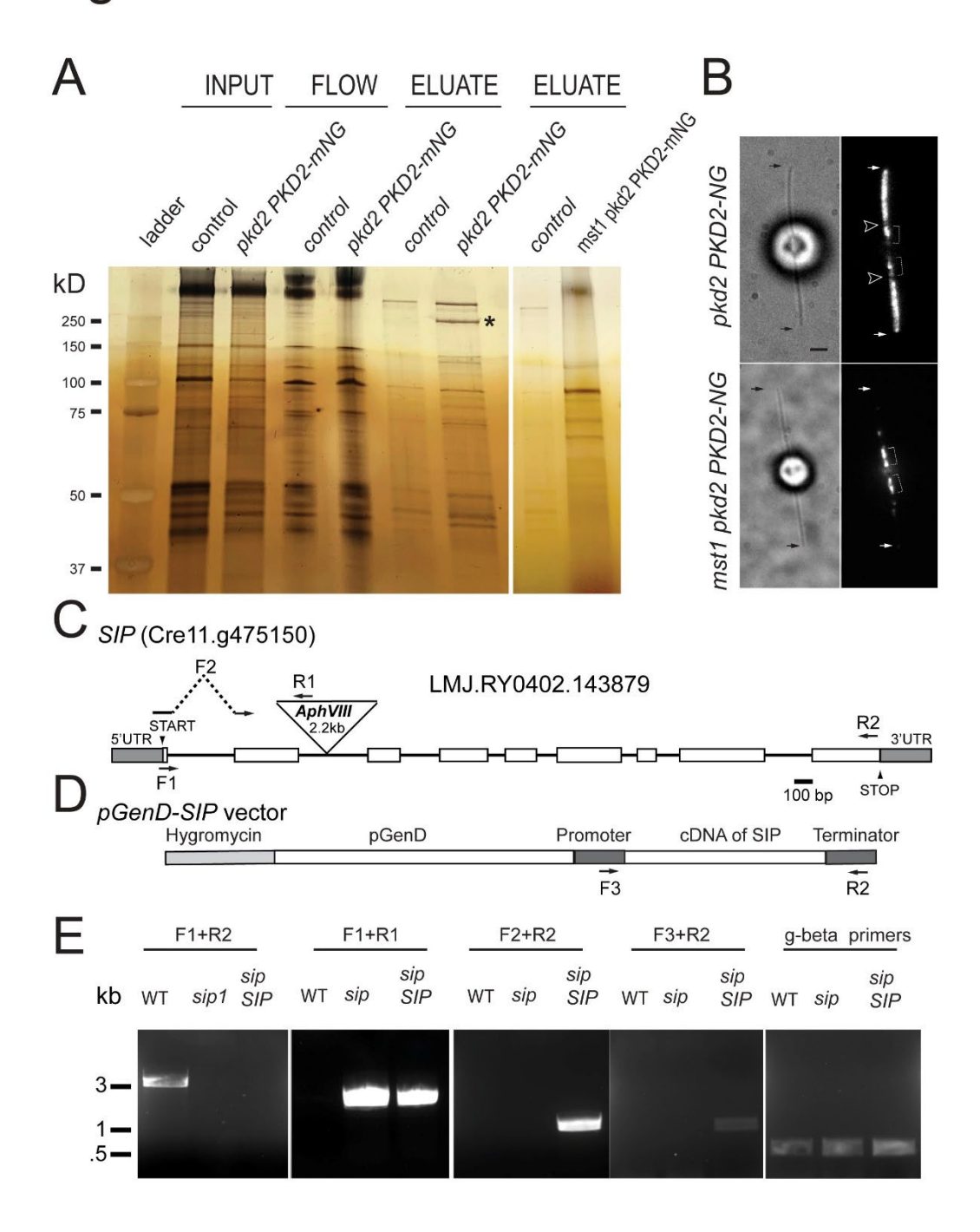


*Fig. S2. Identification of SIP as a PKD2 interacting protein* A) Silver-stained gel analyzing the PKD2-NG pull-down assays from control (expressing endogenous PKD2), pkd2 PKD2-NG (null in endogenous PKD2 and expressing PKD2-NG) and mst1-1 pkd2 PKD2-NG (no mastigonemes

or PKD2; expressing PKD2-NG). The lanes are showing the ciliary detergent extract (INPUT), flow through (FLOW), and eluates from the antiNG-nanobody sepharose trap. \*, putative MST1 band.

- B) Bright field and TIRF images of pkd2 PKD2-NG and mst1-1 pkd2 PKD2-NG cells. The ciliary tips (small arrows) and the gaps (arrowheads) are marked. Bar =  $2\mu$ m.
- C) Genomic map of the SIP/Cre11.g475150 gene. The positions of the AphVIII insertion in the CLiP mutant and of the primers used to track the insertion (as shown in panel E) are indicated.
- D) Schematic presentation of the cDNA-based construct used to rescue the sip mutant. The positions of the primers used to track the transgene are indicated.
- E) Agarose gels of PCR reactions used to genotype control, sip mutant and sip SIP rescue cells.

# Figure S3

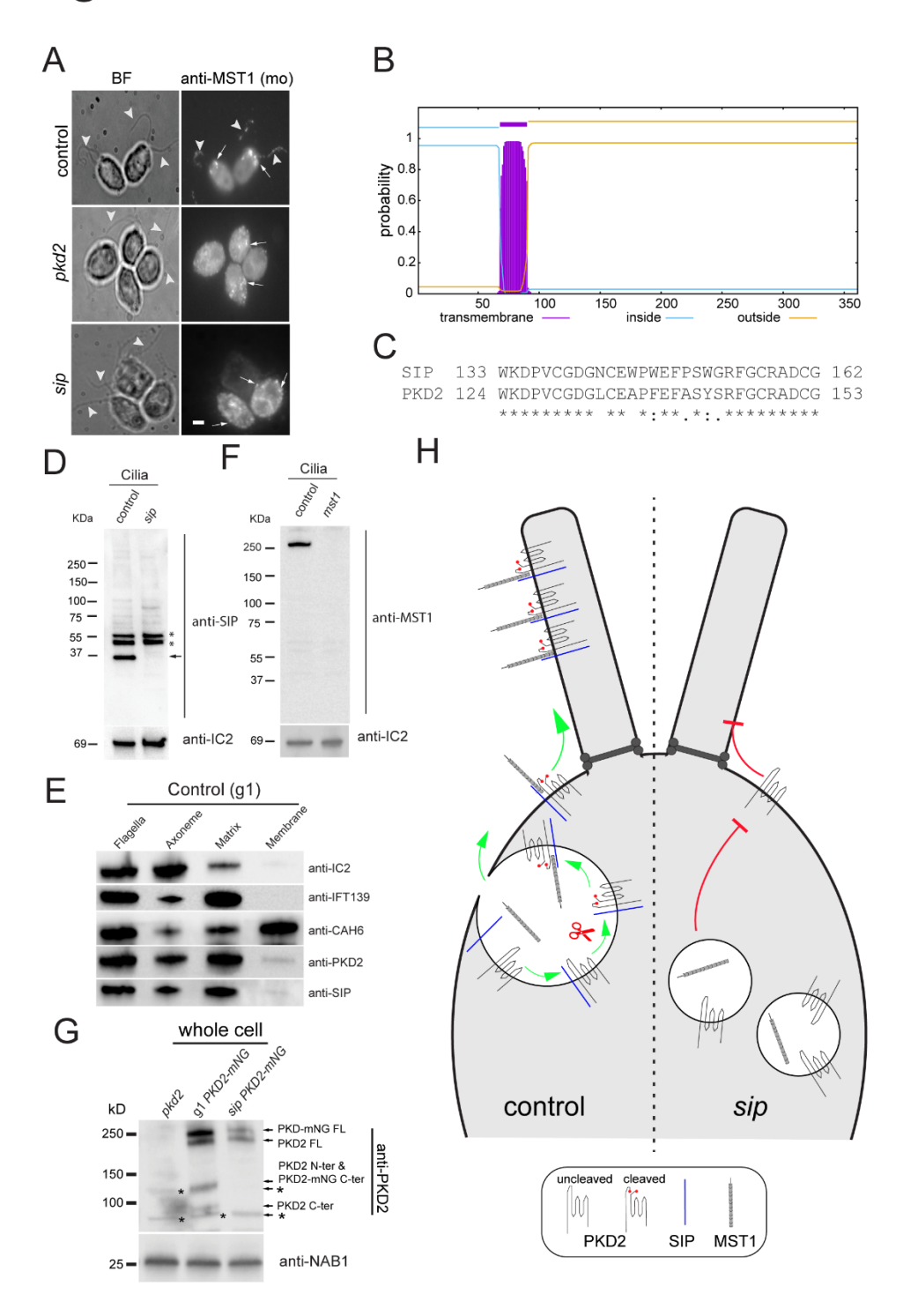


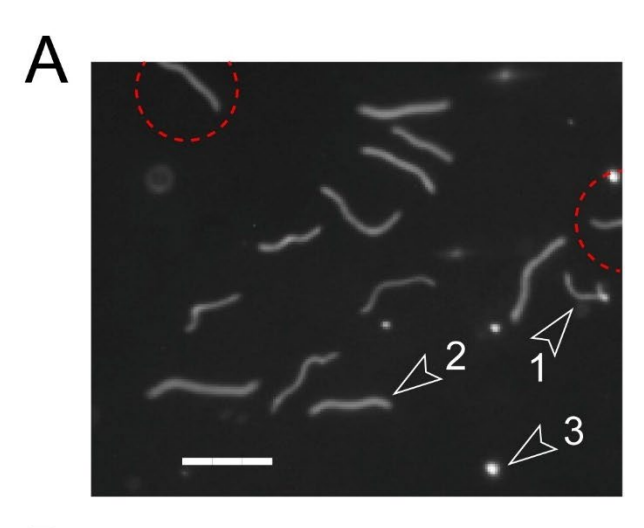
*Fig. S3. Antibodies to SIP and MST1* A) Immunofluorescence staining of control, pkd2 and sip mutant cells with monoclonal antiMST1 (Nakamura et al., 1996). The pool of MST1 in control

cells and dispersed MST1 spots in pkd2 and sip cells are marked by arrows. Arrowheads, cilia. Bar =  $2\mu m$ .

- B) Prediction of the transmembrane domain of SIP using TMHMM-2.0 at the Technical University of Denmark (https://services.healthtech.dtu.dk/services/TMHMM-2.0/). Purple, blue and orange lines indicate the sole transmembrane domain (residue 69 85), the intra- and the extracellular regions, respectively.
- C) Conserved sequence stretches of Chlamydomonas PKD2 and SIP.
- D) Western blot of cilia isolated from control and the sip mutant and probed with anti-SIP. Arrow, position of SIP; \*, bands cross-reacting with anti-SIP.
- E) Western blot analysis of cilia and ciliary fractions of a wild-type control strain (g1) obtained by Triton X-114 phase partitioning and stained with antibodies to SIP and antibodies to the ODA subunit IC2, the membrane-associated protein CAH6, and the IFT-B protein IFT139, respectively, as markers for the axonemal, membrane (i.e., detergent-soluble phase), and matrix (i.e., aqueous phase) fractions.
- F) Western blot of cilia isolated from control and the mst1-1 mutant probed with polyclonal antiMST1. In D and F, anti-IC2 was used as a loading control.
- G) Western blot of whole cell samples from the strains indicated probed with anti-PKD2 and anti-NAB1, as a loading control. Tagged and endogenous full-length PKD2 and the derived fragments are indicated. Note near absence of PKD2 fragments in sip mutant strains. \*, crossreacting unspecific bands.

H) Hypothetical model depicting assembly and targeting of the PKD2-SIP-mastigoneme complexes to cilia. In control cells, formation of the PKD2-SIP complex permits cleavage of PKD2 and sorting of vesicles to the cell apex. Then, complexes of cleaved PKD2, SIP, and mastigonemes enter the cilia. In sip mutants, PKD2 cleavage and interaction with the mastigonemes fails, MST1 and PKD2-containing vesicles are prevented from accumulating at the cell apex, and uncleaved PKD2 is prevented from entering cilia.

# Figure S4





C

File Edit Font		lit Font	Results		
	ld	Length	Length in pixels	Velocity(µm/s)	
1	1	81.154	87.369	119.259	
2	2	41.881	47.322	64.595	
3	3	44.272	48.018	65.544	
4	4	61.074	66.511	90.787	
5	5	41.304	42.180	57.576	
6	6	59.808	77.259	105.459	
7	7	65.123	69.361	94.677	
8	8	59.540	64.117	87.520	
9	9	54.781	63.670	86.910	
10	10	45.651	48.262	65.878	
11	11	69.971	76.241	104.069	

Fig. S4. Analysis of swimming velocity using the Length Analysis Tool plugin in ImageJ A) Micrograph of mst1 cells obtained by a 1-s exposure. White lines are the trajectories of swimming cells. Bar =  $100\mu m$ . B) Result image of the Length Analysis Tool Fiji plugin. Trajectories in contact with the image border were eliminated (dashed circles). Trajectories appearing branched or crossing each other were not analyzed (arrowhead 1). Occasionally, the ends of trajectories were not correctly recognized by the plugin (arrowhead 2). Nonmoving cells (arrowhead 3) were not considered by the plugin as the trajectory length is below the set threshold. C) Corresponding result table. Length, end-to-end length; Length in pixels, actual length of the path. The velocity data are based on the length-inpixels measurement.

protein	link	M W	pkd2 PKD2-NG (4 repeats)			mst1 pkd2 PKD2-NG (3 repeats)				Ratio of	
			hit s	Coverag e (averag e %)	Total peptide s (averag e #)	Unique peptide s (averag e #)	hit s	Coverag e (%)	Total peptide s (averag e #)	Unique peptides (average #)	covera ge (pkd2 PKD2- NG/mst1 pkd2 PKD2- NG)
PKD2	Cre17.g71530	162 6	4/4	11.8	40.2	19.5	3/3	8.9	45	15	1.33
MST1	Cre16.g65060	198 7	4/4	6.2	23.7	9.7	0/3	0	0	0	-
FAP48	<u>Cre16.g66545</u> <u>0</u>	314 0	2/4	1.4	7.5	4	3/3	5	52.7	15.3	0.28
FAP24*	Cre02.g08105 0	537	3/4	5	5.5	2.7	2/3	6.2	8.3	2.7	0.8
enolase	<u>Cre12.g51320</u> <u>0</u>	477	4/4	8.7	7.2	3.7	3/3	13.6	18	3.3	0.64
IFT172	<u>Cre17.g70390</u> <u>0</u>	175 5	2/4	2.5	9.7	4.2	3/3	7.6	46.3	13.7	0.33
FAP154	<u>Cre08.g36210</u> <u>0</u>	444 1	2/4	0.7	7.2	2.7	3/3	3.4	42	12	0.2
ODA5- associated AK	Cre01.g02975	560	2/4	3.7	4.7	1.2	3/3	14.9	22	4.3	0.25
IFT144	<u>Cre02.g09507</u> 2	132 1	2/4	1.4	4.5	2	3/3	6.3	28.3	8.3	0.22
FAP39	<u>Cre02.g14510</u> 0	930	2/4	2.7	3.5	2	2/3	3.2	12	2.7	0.83
FAP10*	Cre12.g50535 0	100 9	2/4	3.1	5.5	3	3/3	7.2	21.3	6.7	0.43
SIP*	<u>Cre11.g47515</u> <u>0</u>	361	4/4	9.4	6.7	3.5	1/3	4.7	5	1.7	2
EF-2	<u>Cre17.g73725</u> <u>0</u>	845	1/4	1.2	2.5	1	3/3	5	13.7	4	0.23
FAP5	<u>Cre12.g51855</u> <u>0</u>	134 7	1/4	1	2.2	1.5	3/3	5.8	28	8.3	0.18
FAP208*	<u>Cre11.g48200</u> <u>1</u>	137 3	1/4	0.7	2	1	3/3	2.4	10.7	3	0.31
IFT38	<u>Cre17.g72125</u> <u>0</u>	325	1/4	2.2	1.5	0.7	3/3	10.4	10.6	4	0.37
IFT139	<u>Cre06.g26880</u> <u>0</u>	131 1	2/4	1.4	3	2	3/3	3.7	16.3	5.7	0.37
FAP295/PRKG 2*	<u>Cre16.g66320</u> <u>0</u>	718	1/4	1.3	1	0.7	3/3	13.8	53.3	11.3	0.09
Chlorophyll a/b BP	<u>Cre01.g06691</u> <u>7</u>	253	1/4	1.6	1	0.5	1/3	2.5	5.3	0.7	0.63
IFT122	<u>Cre01.g06582</u> <u>2</u>	123 9	1/4	1.4	2.5	1.5	3/3	2.8	14.3	4	0.48
phosphoglycer omutase	<u>Cre06.g27205</u> <u>0</u>	557	1/4	1.4	2	1	2/3	5	11.7	3.3	0.29

IFT70	<u>Cre07.g34220</u> <u>0</u>	647	1/4	0.66	1	0.5	3/3	5.1	12.3	4.3	0.13
actin (IDA5)*	<u>Cre13.g60370</u> <u>0</u>	377	3/4	5.44	4	2	3/3	14.2	22.7	5.6	0.38
FAP148	<u>Cre10.g43460</u> <u>0</u>	173 2	1/4	0.55	1.5	1	1/3	1.8	9.3	3.3	0.29
FAP333 (ARF)	<u>Cre12.g48625</u> <u>0</u>	181	1/4	3.6	1.5	0.5	3/3	17.3	12.3	2.7	0.21
EF-3	Cre04.g22270 0	105 3	2/4	2	3.5	2.25	3/3	3.9	11.7	4.7	0.51
FAP252/BUG1	<u>Cre01.g06582</u> <u>2</u>	352	1/4	1.6	1	0.5	1/3	3	3	1	0.51
psbC	<u>Cre10.g46665</u> <u>0</u>	461	2/4	3.1	2.7	1.2	2/3	5.1	10	2	0.6
FAP19/CGK2	<u>Cre02.g07690</u> <u>0</u>	102 7	1/4	0.5	0.7	0.5	2/3	5.6	22.7	5.7	0.09

Table S1. Mass spectrometry of PKD2-NG immune-isolates. List of proteins identified by mass spectrometry of PKD2-NG complexes pulled-down from the pkd2 PKD2-NG and mst1-1 pkd2 PKD2-NG strains. The protein names, Phytozome accession numbers, hits (peptides identified in x of n experimental samples), coverage, total and unique peptides, and the ratio between the coverage in two experimental strains are indicated. The following proteins were found in all preparations, including those from the untagged control strain: FMG-1, FMG-1b, FAP33, FAP12, beta-tubulin, cobalamin-independent methionine synthase, eukaryotic translation elongation factor 1 alpha 1, putative blue light receptor, alphatubulin, IFT88, S-Adenosyl homocysteine hydrolase, IFT72/74, IFT81, IFT80, IFT57. The \* indicates proteins, for which putative or confirmed mutants were obtained from the Chlamydomonas Resource Center; of these strains, only the sip mutant lacked mastigonemes.

	MINI-PKD2 (361)		MST1 (1	987)	PKD2 (1645)		
species	length	% identity	length	% identity	length	% identity	
		(%		(%coverage)		(%	
		coverage)				coverage)	
Chlamydomonas	368	98.2 (93)	1955	55.8 (89)	1643	94.5 (99)	
incerta							
Gonium	359	85.4 (91)	868	52.8 (34)	1629	76.5 (99)	
pectorale							
Volvox carteri	405	79.3 (91)	835	51.5 (34)	1606	67.3 (95)	
Trebuxia sp. A1-2	478	58.7 (73)	n.d.		1618	48.9 (90)	
Chlorella ohadii *	456	51.2 (66)	n.d.		1721	38.1 (73)	
Scenedesmus sp.	300	48.4 (78)	n.d.		1582	43 (99)	
NREL 46B-D3 *							
Dunaliella salina	360	37.5 (93)	n.d.		1784	47.4 (95)	

**Table S2.** Distribution and Conservation of SIP in green algae. The C. reinhardtii sequences for SIP, PKD2, and MST1 and Uniprot Blast were used search for related sequences of each protein in green algae. In contrast to mammalian PKD2 homologues, green algal PKD2 possess a large insertion in the extracellular loop 1. The UniProt accession numbers, or, if those were not available, the NCBI accession numbers, are shown.

### 2.13 References

- Amador, G. J., Wei, D., Tam, D., & Aubin-Tam, M. E. (2020). Fibrous Flagellar Hairs of Chlamydomonas reinhardtii Do Not Enhance Swimming. *Biophys J*, *118*(12), 2914-2925. <a href="https://doi.org/10.1016/j.bpj.2020.05.003">https://doi.org/10.1016/j.bpj.2020.05.003</a>
- Arhatte, M., Gunaratne, G. S., El Boustany, C., Kuo, I. Y., Moro, C., Duprat, F., Plaisant, M., Duval, H., Li, D., Picard, N., Couvreux, A., Duranton, C., Rubera, I., Pagnotta, S., Lacas-Gervais, S., Ehrlich, B. E., Marchant, J. S., Savage, A. M., van Eeden, F. J. M., Wilkinson, R. N., Demolombe, S., Honore, E., & Patel, A. (2019). TMEM33 regulates intracellular calcium homeostasis in renal tubular epithelial cells. *Nat Commun*, *10*(1), 2024. https://doi.org/10.1038/s41467-019-10045-y
- Barr, M. M., & Sternberg, P. W. (1999). A polycystic kidney-disease gene homologue required for male mating behaviour in C. elegans [Research Support, Non-U.S. Gov't]. *Nature*, 401(6751), 386-389. https://doi.org/10.1038/43913
- Bennett, H. W., Gustavsson, A. K., Bayas, C. A., Petrov, P. N., Mooney, N., Moerner, W. E., & Jackson, P. K. (2020). Novel fibrillar structure in the inversin compartment of primary cilia revealed by 3D single-molecule superresolution microscopy. *Mol Biol Cell*, *31*(7), 619-639. <a href="https://doi.org/10.1091/mbc.E19-09-0499">https://doi.org/10.1091/mbc.E19-09-0499</a>
- Bouck, G. B. (1971). The structure, origin, isolation, and composition of the tubular mastigonemes of the Ochromas flagellum. *J Cell Biol*, *50*(2), 362-384. https://doi.org/10.1083/jcb.50.2.362
- Bui, K. H., Yagi, T., Yamamoto, R., Kamiya, R., & Ishikawa, T. (2012). Polarity and asymmetry in the arrangement of dynein and related structures in the Chlamydomonas axoneme. *J Cell Biol*, 198(5), 913-925. <a href="https://doi.org/10.1083/jcb.201201120">https://doi.org/10.1083/jcb.201201120</a>
- Cao, M., Ning, J., Hernandez-Lara, C. I., Belzile, O., Wang, Q., Dutcher, S. K., Liu, Y., & Snell, W. J. (2015). Uni-directional ciliary membrane protein trafficking by a cytoplasmic retrograde IFT motor and ciliary ectosome shedding. *Elife*, *4*. <a href="https://doi.org/10.7554/eLife.05242">https://doi.org/10.7554/eLife.05242</a>
- Chapin, H. C., Rajendran, V., & Caplan, M. J. (2010). Polycystin-1 surface localization is stimulated by polycystin-2 and cleavage at the G protein-coupled receptor proteolytic site. *Mol Biol Cell*, *21*(24), 4338-4348. <a href="https://doi.org/10.1091/mbc.E10-05-0407">https://doi.org/10.1091/mbc.E10-05-0407</a>
- Chung, J. J., Miki, K., Kim, D., Shim, S. H., Shi, H. F., Hwang, J. Y., Cai, X., Iseri, Y., Zhuang, X., & Clapham, D. E. (2017). CatSperzeta regulates the structural continuity of sperm Ca(2+) signaling domains and is required for normal fertility. *Elife*, 6. <a href="https://doi.org/10.7554/eLife.23082">https://doi.org/10.7554/eLife.23082</a>
- Chung, J. J., Shim, S. H., Everley, R. A., Gygi, S. P., Zhuang, X., & Clapham, D. E. (2014). Structurally distinct Ca(2+) signaling domains of sperm flagella orchestrate tyrosine phosphorylation and motility. *Cell*, 157(4), 808-822. <a href="https://doi.org/10.1016/j.cell.2014.02.056">https://doi.org/10.1016/j.cell.2014.02.056</a>
- Craige, B., Brown, J. M., & Witman, G. B. (2013). Isolation of Chlamydomonas flagella. *Curr Protoc Cell Biol, Chapter 3*, Unit 3 41 41-49. https://doi.org/10.1002/0471143030.cb0341s59
- Dean, A. B., & Mitchell, D. R. (2015). Late steps in cytoplasmic maturation of assembly-competent axonemal outer arm dynein in Chlamydomonas require interaction of

- ODA5 and ODA10 in a complex. *Mol Biol Cell*, *26*(20), 3596-3605. https://doi.org/10.1091/mbc.E15-05-0317
- DeCaen, P. G., Delling, M., Vien, T. N., & Clapham, D. E. (2013). Direct recording and molecular identification of the calcium channel of primary cilia [Research Support, N.I.H., Extramural
- Research Support, Non-U.S. Gov't]. *Nature*, *504*(7479), 315-318. https://doi.org/10.1038/nature12832
- Dutcher, S. K. (1995). Flagellar assembly in two hundred and fifty easy-to-follow steps [Research Support, U.S. Gov't, Non-P.H.S.
- Research Support, U.S. Gov't, P.H.S.
- Review]. *Trends Genet*, *11*(10), 398-404. <a href="http://www.ncbi.nlm.nih.gov/pubmed/7482766">http://www.ncbi.nlm.nih.gov/pubmed/7482766</a>
  Dutcher, S. K. (2020). Asymmetries in the cilia of Chlamydomonas. *Philos Trans R Soc Lond B Biol Sci*, 375(1792), 20190153. <a href="https://doi.org/10.1098/rstb.2019.0153">https://doi.org/10.1098/rstb.2019.0153</a>
- Euteneuer, U., & McIntosh, J. R. (1981). Polarity of some motility-related microtubules [Research Support, U.S. Gov't, Non-P.H.S.]. *Proc Natl Acad Sci U S A*, 78(1), 372-376. http://www.ncbi.nlm.nih.gov/pubmed/6941252
- Ferreira, R. R., Fukui, H., Chow, R., Vilfan, A., & Vermot, J. (2019). The cilium as a force sensor-myth versus reality. *J Cell Sci*, 132(14). https://doi.org/10.1242/jcs.213496
- Garcia-Gonzalo, F. R., & Reiter, J. F. (2012). Scoring a backstage pass: mechanisms of ciliogenesis and ciliary access. *J Cell Biol*, 197(6), 697-709. https://doi.org/10.1083/jcb.201111146
- Geimer, S., & Melkonian, M. (2004). The ultrastructure of the Chlamydomonas reinhardtii basal apparatus: identification of an early marker of radial asymmetry inherent in the basal body. *J Cell Sci*, 117(Pt 13), 2663-2674. <a href="https://doi.org/10.1242/jcs.01120">https://doi.org/10.1242/jcs.01120</a>
- Ha, K., Nobuhara, M., Wang, Q., Walker, R. V., Qian, F., Schartner, C., Cao, E., & Delling, M. (2020). The heteromeric PC-1/PC-2 polycystin complex is activated by the PC-1 Nterminus. *Elife*, 9. https://doi.org/10.7554/eLife.60684
- Holmes, J. A., & Dutcher, S. K. (1989). Cellular asymmetry in Chlamydomonas reinhardtii. *J Cell Sci*, 94 ( Pt 2), 273-285. <a href="https://www.ncbi.nlm.nih.gov/pubmed/2621224">https://www.ncbi.nlm.nih.gov/pubmed/2621224</a>
- Hoog, J. L., Lacomble, S., O'Toole, E. T., Hoenger, A., McIntosh, J. R., & Gull, K. (2014). Modes of flagellar assembly in Chlamydomonas reinhardtii and Trypanosoma brucei. *Elife, 3*, e01479. <a href="https://doi.org/10.7554/eLife.01479">https://doi.org/10.7554/eLife.01479</a>
- Hoops, H. J., & Witman, G. B. (1983). Outer doublet heterogeneity reveals structural polarity related to beat direction in Chlamydomonas flagella [Research Support, U.S. Gov't, P.H.S.]. *J Cell Biol*, 97(3), 902-908. <a href="http://www.ncbi.nlm.nih.gov/pubmed/6224802">http://www.ncbi.nlm.nih.gov/pubmed/6224802</a>
- Huang, K., Diener, D. R., Mitchell, A., Pazour, G. J., Witman, G. B., & Rosenbaum, J. L. (2007). Function and dynamics of PKD2 in Chlamydomonas reinhardtii flagella. *J Cell Biol*, 179(3), 501-514. <a href="https://doi.org/10.1083/jcb.200704069">https://doi.org/10.1083/jcb.200704069</a>
- Isom, L. L. (2001). Sodium channel beta subunits: anything but auxiliary. *Neuroscientist*, 7(1), 42-54. <a href="https://doi.org/10.1177/107385840100700108">https://doi.org/10.1177/107385840100700108</a>
- Katoh, T. A., Omori, T., Mizuno, K., Sai, X., Minegishi, K., Ikawa, Y., Nishimura, H., Itabashi, T., Kajikawa, E., Hiver, S., Iwane, A. H., Ishikawa, T., Okada, Y., Nishizaka, T., & Hamada, H. (2023). Immotile cilia mechanically sense the direction of fluid flow for left-right

- determination. *Science*, *379*(6627), 66-71. <a href="https://doi.org/10.1126/science.abq8148">https://doi.org/10.1126/science.abq8148</a>
- Kottgen, M., Hofherr, A., Li, W., Chu, K., Cook, S., Montell, C., & Watnick, T. (2011). Drosophila sperm swim backwards in the female reproductive tract and are activated via TRPP2 ion channels. *PLoS One*, *6*(5), e20031. https://doi.org/10.1371/journal.pone.0020031
- Kwitny, S., Klaus, A. V., & Hunnicutt, G. R. (2010). The annulus of the mouse sperm tail is required to establish a membrane diffusion barrier that is engaged during the late steps of spermiogenesis. *Biol Reprod*, *82*(4), 669-678. <a href="https://doi.org/10.1095/biolreprod.109.079566">https://doi.org/10.1095/biolreprod.109.079566</a>
- Lechtreck, K.-F., Gould, T. J., & Witman, G. B. (2013). Flagellar central pair assembly in Chlamydomonas reinhardtii. *Cilia*, *2*, 15-15. <a href="https://doi.org/10.1186/2046-2530-2-15">https://doi.org/10.1186/2046-2530-2-15</a>
- Lechtreck, K. (2022). Cargo adapters expand the transport range of intraflagellar transport. *J Cell Sci*, 135(24). https://doi.org/10.1242/jcs.260408
- Lechtreck, K. F. (2013). In vivo Imaging of IFT in Chlamydomonas Flagella. *Methods Enzymol*, 524, 265-284. https://doi.org/10.1016/B978-0-12-397945-2.00015-9
- Lechtreck, K. F. (2016). Methods for Studying Movement of Molecules Within Cilia. *Methods Mol Biol*, 1454, 83-96. <a href="https://doi.org/10.1007/978-1-4939-3789-9-6">https://doi.org/10.1007/978-1-4939-3789-9-6</a>
- Lee, S., Tan, H. Y., Geneva, II, Kruglov, A., & Calvert, P. D. (2018). Actin filaments partition primary cilia membranes into distinct fluid corrals. *J Cell Biol*, 217(8), 2831-2849. https://doi.org/10.1083/jcb.201711104
- Li, X., Patena, W., Fauser, F., Jinkerson, R. E., Saroussi, S., Meyer, M. T., Ivanova, N., Robertson, J. M., Yue, R., Zhang, R., Vilarrasa-Blasi, J., Wittkopp, T. M., Ramundo, S., Blum, S. R., Goh, A., Laudon, M., Srikumar, T., Lefebvre, P. A., Grossman, A. R., & Jonikas, M. C. (2019). A genome-wide algal mutant library and functional screen identifies genes required for eukaryotic photosynthesis. *Nat Genet*, *51*(4), 627-635. https://doi.org/10.1038/s41588-019-0370-6
- Liu, P., Liu, Y., & Zhou, J. (2023). Ciliary mechanosensation roles of polycystins and mastigonemes. *J Cell Sci*, 136(3). https://doi.org/10.1242/jcs.260565
- Liu, P., Lou, X., Wingfield, J. L., Lin, J., Nicastro, D., & Lechtreck, K. (2020). Chlamydomonas PKD2 organizes mastigonemes, hair-like glycoprotein polymers on cilia. *J Cell Biol*, 219(6). <a href="https://doi.org/10.1083/jcb.202001122">https://doi.org/10.1083/jcb.202001122</a>
- Mahjoub, M. R., Montpetit, B., Zhao, L., Finst, R. J., Goh, B., Kim, A. C., & Quarmby, L. M. (2002). The FA2 gene of Chlamydomonas encodes a NIMA family kinase with roles in cell cycle progression and microtubule severing during deflagellation. *J Cell Sci*, 115(Pt 8), 1759-1768. <a href="https://doi.org/10.1242/jcs.115.8.1759">https://doi.org/10.1242/jcs.115.8.1759</a>
- Matsuzaki, O., Bakin, R. E., Cai, X., Menco, B. P., & Ronnett, G. V. (1999). Localization of the olfactory cyclic nucleotide-gated channel subunit 1 in normal, embryonic and regenerating olfactory epithelium. *Neuroscience*, *94*(1), 131-140. https://doi.org/10.1016/s0306-4522(99)00228-6
- Mochizuki, T., Saijoh, Y., Tsuchiya, K., Shirayoshi, Y., Takai, S., Taya, C., Yonekawa, H., Yamada, K., Nihei, H., Nakatsuji, N., Overbeek, P. A., Hamada, H., & Yokoyama, T. (1998). Cloning of inv, a gene that controls left/right asymmetry and kidney development. *Nature*, *395*(6698), 177-181. https://doi.org/10.1038/26006

- Nakamura, S., Tanaka, G., Maeda, T., Kamiya, R., Matsunaga, T., & Nikaido, O. (1996).

  Assembly and function of Chlamydomonas flagellar mastigonemes as probed with a monoclonal antibody [Research Support, Non-U.S. Gov't]. *J Cell Sci*, 109 (Pt 1), 57-62. <a href="http://www.ncbi.nlm.nih.gov/pubmed/8834790">http://www.ncbi.nlm.nih.gov/pubmed/8834790</a>
- Pazour, G. J., Agrin, N., Leszyk, J., & Witman, G. B. (2005). Proteomic analysis of a eukaryotic cilium [Research Support, N.I.H., Extramural
- Research Support, U.S. Gov't, Non-P.H.S.
- Research Support, U.S. Gov't, P.H.S.]. *J Cell Biol*, *170*(1), 103-113. https://doi.org/10.1083/jcb.200504008
- Pazour, G. J., Sineshchekov, O. A., & Witman, G. B. (1995). Mutational analysis of the phototransduction pathway of Chlamydomonas reinhardtii [Research Support, Non-U.S. Gov't
- Research Support, U.S. Gov't, P.H.S.]. *J Cell Biol*, 131(2), 427-440. http://www.ncbi.nlm.nih.gov/pubmed/7593169
- Pennekamp, P., Karcher, C., Fischer, A., Schweickert, A., Skryabin, B., Horst, J., Blum, M., & Dworniczak, B. (2002). The ion channel polycystin-2 is required for left-right axis determination in mice. *Curr Biol*, *12*(11), 938-943. <a href="https://doi.org/10.1016/s0960-9822(02)00869-2">https://doi.org/10.1016/s0960-9822(02)00869-2</a>
- Poddar, A., Hsu, Y. Y., Zhang, F., Shamma, A., Kreais, Z., Muller, C., Malla, M., Ray, A., Liu, A. P., & Chen, Q. (2022). Membrane stretching activates calcium permeability of a putative channel Pkd2 during fission yeast cytokinesis. *Mol Biol Cell*, *33*(14), ar134. https://doi.org/10.1091/mbc.E22-07-0248
- Qin, H., Burnette, D. T., Bae, Y. K., Forscher, P., Barr, M. M., & Rosenbaum, J. L. (2005). Intraflagellar transport is required for the vectorial movement of TRPV channels in the ciliary membrane [Comparative Study

Research Support, N.I.H., Extramural

Research Support, Non-U.S. Gov't

Research Support, U.S. Gov't, P.H.S.]. *Curr Biol*, *15*(18), 1695-1699. https://doi.org/10.1016/j.cub.2005.08.047

- Rosenbaum, J. L., & Child, F. M. (1967). Flagellar regeneration in protozoan flagellates. *J Cell Biol*, 34(1), 345-364. http://www.ncbi.nlm.nih.gov/pubmed/6033540
- Shiba, D., Yamaoka, Y., Hagiwara, H., Takamatsu, T., Hamada, H., & Yokoyama, T. (2009). Localization of Inv in a distinctive intraciliary compartment requires the C-terminal ninein-homolog-containing region. *J Cell Sci*, 122(Pt 1), 44-54. <a href="https://doi.org/10.1242/jcs.037408">https://doi.org/10.1242/jcs.037408</a>
- Silflow, C. D., & Lefebvre, P. A. (2001). Assembly and motility of eukaryotic cilia and flagella. Lessons from Chlamydomonas reinhardtii [Research Support, Non-U.S. Gov't

Research Support, U.S. Gov't, Non-P.H.S.

Research Support, U.S. Gov't, P.H.S.

- Review]. *Plant Physiol*, 127(4), 1500-1507. http://www.ncbi.nlm.nih.gov/pubmed/11743094
- Singh, A. P., & Rajender, S. (2015). CatSper channel, sperm function and male fertility. *Reprod Biomed Online*, *30*(1), 28-38. <a href="https://doi.org/10.1016/j.rbmo.2014.09.014">https://doi.org/10.1016/j.rbmo.2014.09.014</a>
- Su, Q., Hu, F., Ge, X., Lei, J., Yu, S., Wang, T., Zhou, Q., Mei, C., & Shi, Y. (2018). Structure of the human PKD1-PKD2 complex. *Science*, *361*(6406). https://doi.org/10.1126/science.aat9819
- Sun, L., Gao, Y., He, J., Cui, L., Meissner, J., Verbavatz, J. M., Li, B., Feng, X., & Liang, X. (2019). Ultrastructural organization of NompC in the mechanoreceptive organelle of Drosophila campaniform mechanoreceptors. *Proc Natl Acad Sci U S A*, *116*(15), 7343-7352. https://doi.org/10.1073/pnas.1819371116
- Tam, L. W., Ranum, P. T., & Lefebvre, P. A. (2013). CDKL5 regulates flagellar length and localizes to the base of the flagella in Chlamydomonas. *Mol Biol Cell*, *24*(5), 588-600. <a href="https://doi.org/10.1091/mbc.E12-10-0718">https://doi.org/10.1091/mbc.E12-10-0718</a>
- van der Burght, S. N., Rademakers, S., Johnson, J. L., Li, C., Kremers, G. J., Houtsmuller, A. B., Leroux, M. R., & Jansen, G. (2020). Ciliary Tip Signaling Compartment Is Formed and Maintained by Intraflagellar Transport. *Curr Biol*, *30*(21), 4299-4306 e4295. https://doi.org/10.1016/j.cub.2020.08.032
- Walsh, J. D., Wang, J., DeHart, M., Nikonorova, I. A., Srinivasan, J., & Barr, M. M. (2022). Tracking N- and C-termini of C. elegans polycystin-1 reveals their distinct targeting requirements and functions in cilia and extracellular vesicles. *PLoS Genet*, *18*(12), e1010560. <a href="https://doi.org/10.1371/journal.pgen.1010560">https://doi.org/10.1371/journal.pgen.1010560</a>
- Wang, Y., Yang, J., Hu, F., Yang, Y., Huang, K., & Zhang, K. (2023). Cryo-EM reveals how the mastigoneme assembles and responds to environmental signal changes. *J Cell Biol*, 222(12). https://doi.org/10.1083/jcb.202301066
- Watnick, T. J., Jin, Y., Matunis, E., Kernan, M. J., & Montell, C. (2003). A flagellar polycystin-2 homolog required for male fertility in Drosophila. *Curr Biol*, *13*(24), 2179-2184. <a href="https://doi.org/10.1016/j.cub.2003.12.002">https://doi.org/10.1016/j.cub.2003.12.002</a>
- Wingfield, J. L., & Lechtreck, K. F. (2018). Chlamydomonas Basal Bodies as Flagella Organizing Centers. *Cells*, 7(7). https://doi.org/10.3390/cells7070079
- Witman, G. B. (1975). THE SITE OF IN VIVO ASSEMBLY OF FLAGELLAR MICROTUBULES\*. Annals of the New York Academy of Sciences, 253(1), 178-191. https://doi.org/doi:10.1111/j.1749-6632.1975.tb19199.x
- Witman, G. B., Carlson, K., Berliner, J., & Rosenbaum, J. L. (1972). Chlamydomonas flagella. I. Isolation and electrophoretic analysis of microtubules, matrix, membranes, and mastigonemes. *J Cell Biol*, *54*(3), 507-539. https://doi.org/10.1083/jcb.54.3.507
- Wu, G., & Somlo, S. (2000). Molecular genetics and mechanism of autosomal dominant polycystic kidney disease. *Mol Genet Metab*, 69(1), 1-15. https://doi.org/10.1006/mgme.1999.2943
- Xiang, W., zur Lage, P., Newton, F. G., Qiu, G., & Jarman, A. P. (2022). The dynamics of protein localisation to restricted zones within Drosophila mechanosensory cilia. *Scientific Reports*, *12*(1), 13338. <a href="https://doi.org/10.1038/s41598-022-17189-w">https://doi.org/10.1038/s41598-022-17189-w</a>
- Xiang, W., Zur Lage, P., Newton, F. G., Qiu, G., & Jarman, A. P. (2022). The dynamics of protein localisation to restricted zones within Drosophila mechanosensory cilia. *Sci Rep*, 12(1), 13338. https://doi.org/10.1038/s41598-022-17189-w

- Yagi, T., Uematsu, K., Liu, Z., & Kamiya, R. (2009). Identification of dyneins that localize exclusively to the proximal portion of Chlamydomonas flagella. *J Cell Sci*, 122(Pt 9), 1306-1314. https://doi.org/10.1242/jcs.045096
- Zamora, I., Feldman, J. L., & Marshall, W. F. (2004). PCR-based assay for mating type and diploidy in Chlamydomonas. *Biotechniques*, *37*(4), 534-536. http://www.ncbi.nlm.nih.gov/pubmed/15517961
- Zhang, W., Cheng, L. E., Kittelmann, M., Li, J., Petkovic, M., Cheng, T., Jin, P., Guo, Z., Gopfert, M. C., Jan, L. Y., & Jan, Y. N. (2015). Ankyrin Repeats Convey Force to Gate the NOMPC Mechanotransduction Channel. *Cell*, *162*(6), 1391-1403. https://doi.org/10.1016/j.cell.2015.08.024
- Zhao, Y., Wang, H., Wiesehoefer, C., Shah, N. B., Reetz, E., Hwang, J. Y., Huang, X., Wang, T. E., Lishko, P. V., Davies, K. M., Wennemuth, G., Nicastro, D., & Chung, J. J. (2022). 3D structure and in situ arrangements of CatSper channel in the sperm flagellum. *Nat Commun*, *13*(1), 3439. <a href="https://doi.org/10.1038/s41467-022-31050-8">https://doi.org/10.1038/s41467-022-31050-8</a>

# Chapter 3

Targeting of distinct ciliary PKD2 complexes in Chlamydomonas<sup>2</sup>

<sup>&</sup>lt;sup>2</sup> Das, P., Lechtreck, K.F., to be submitted to Journal of Cell Biology

#### 3.1 Abstract

Chlamydomonas PKD2 is present in two distinct ciliary compartments. In the distal cilium, PKD2 organizes the mastigonemes by partnering SIP, a single trans membrane helix PKD2-like protein, and MST3, which has a large extracellular domain adorned with numerous MST1 glycoproteins. The PKD2-mastigoneme complexes are attached in two rows along the axoneme and promote fast swimming. In the proximal cilium, PKD2 is mobile and lacks mastigonemes. In mst3 knock-outs, PKD2 is lost from the distal region but retained in the proximal region, indicating the presence of an MST3-indepenent PKD2 complex in cilia. Previous structure-based screening in *Chlamydomonas* had identified seven additional PKD2-like proteins, each predicted to possess five transmembrane domains, an extended extracellular N-terminal region, and to partner with SIP to form a PKD2 channel complex. Mass-spec data showed that three of them localize in cilia like MST3. We show that Scavenger (SCV), one of three ciliary PKD2-like 5-TMH proteins in *Chlamydomonas*, localizes to the proximal ciliary segment and that PKD2 is lost specifically from the proximal region in SCV knock-outs. In cilia of mst3 SCV double mutants, residual PKD2 mostly moved by diffusion and IFT along the length of cilia, suggesting the presence of either an additional MST3 and SCV -independent PKD2 complex or homotetramers of PKD2. In conclusion, *Chlamydomonas* cilia possess at least two biochemically distinct PKD2 complexes, which are sorted to specific sub ciliary regions.

### 3.2 Introduction

Cilia are microtubule-based organelles protuberating from the surface of many cells. The ciliary membrane, although continuous with the cell membrane, is distinct from the cell body plasma membrane due to presence of different kinds of transmembrane proteins (TMPs). The TMPs

localize to specific positions within the ciliary membrane, leading to the formation of patterns. In *Drosophila* auditory cilia, for example, the TRPN (NompC) is located in the distal segment whereas TRPV (Inactive) and TRP channel protein Nanchung (NAN) dominate the proximal ciliary segment (Xiang et al., 2022). Also in *Drosophila*, the PKD2 orthologue AMO is located near the tip of sperm cilia (Kottgen et al., 2011; Watnick et al., 2003). Some membrane proteins establish an additional circumferential pattern around cilia. For example, the multiprotein channel complex CatSper forms four intricately patterned rows, referred to as the race stripes, along the principal piece of mammalian sperm flagella (Chung et al., 2014; Zhao et al., 2022). In the primary cilia of left-right organizer, PKD2 localizes on the dorsal side of cilia sensing the fluid flow and generating asymmetric Ca<sup>2+</sup> response (Delling et al., 2016). How channels and other transmembrane proteins are sorted into specific subciliary regions and how such arrangements contribute to ciliary function remains incompletely understood.

Along with forming unique pattern, TRP proteins also assemble into tetrameric cation channel complexes (Cohen & Moiseenkova-Bell, 2014). Additional in-vitro structural and functional diversification of the TRP channels is achieved by the formation of heterotetrameric complexes (Smith et al., 2002; Strübing et al., 2001). TRPC1 and TRPP2 form heteromeric channels at a 2:2 stoichiometry and exhibit a receptor-operated channel property (Bai et al., 2008; Chen et al., 2020; Du et al., 2014; Tsiokas et al., 1999). TRPV4 and TRPP2 assemble into a heteromeric channel complex (Köttgen et al., 2008). More combinations include TRPC1/TRPC6/ TRPV4 and TRPA1/TRPV1 heteromers(Alessandri-Haber et al., 2009; Salas et al., 2009). TRPA1 and TRPM8 form homo-tetramers (Samanta et al., 2018). Mammalian PKD2 partners with PKD1 in kidney epithelial cilia and PKD1L1 in nodal cilia. In these complexes, the channel pore is blocked by residues contributed by the PKD1 subunits and it is unclear whether

PKD1/PKD1L1 complexes possess a (gated) channel function. PKD2 alone forms an active homo-tetrameric channel, when expressed heterologously but it is unclear whether a PKD2 homo-tetramer possesses a physiologically relevant role as well role in cilia.

In Chlamydomonas, PKD2 forms two rows in the distal region of cilia, and PKD2 complexes are sorted into specific ciliary sub compartments i.e., the proximal and distal cilium, indicating the presence of heterologous PKD2 complexes in Chlamydomonas cilia. In detail, PKD2 in the distal region forms a stable connection with axoneme and anchors mastigonemes into two rows on the 4<sup>th</sup> and 8<sup>th</sup> DMT. Mastigoneme is a thread-like extracellular polymers majorly consisting of glycoprotein MST1 and is unique to the distal cilia of *Chlamydomonas* (Liu et al., 2023; Liu et al., 2020). They are approximately 600-700 nm in length; in comparison cilia have a diameter of approximately 200 nm. The ultrastructure of MST1 is dominated by immunoglobulin-like and Sushi domains, structural elements observed in many extracellular proteins (Wang et al., 2023). On the cilia, the mastigoneme rows are oriented perpendicular to the plane of the ciliary beat. Together, PKD2 and the mastigonemes, form a fan-like structure and loss of PKD2 or mastigonemes could explain the reduced swimming velocity of the corresponding mutants (Nakamura et al., 1996; Witman et al., 1972). Unlike distal zone, proximal PKD2 is not anchored stably to axoneme but more mobile, switching between anchored and diffusing states. Apart from the mobile and the stationary complex, a small fraction of PKD2 is also observed to move by IFT. This raises the question of how PKD2 is sorted into specific ciliary sub-compartments within the ciliary membrane. We reasoned that PKD2 will use distinct interacting partners, that direct the complexes to specific subciliary regions. Recently, we used immunoprecipitation of PKD2-mNG from ciliary detergent extracts to identify Small Interactor of PKD2 (SIP), as a novel interactor of PKD2 (Das et al. 2023). SIP is a single-pass

transmembrane protein, related to the amino-terminal portion of PKD2 i.e., the TMH1 and extracellular TOP domain of PKD2. Cilia of the sip mutant lack or largely lack both the PKD2 as well as mastigonemes and swim with reduced velocity. In *Chlamydomonas*, two proteolytic fragments of PKD2 (i.e., N and C-ter of 130 and 100 KDa in MW) are present in cilia whereas the cell body contains full-length PKD2 and the two fragments, suggesting that the proteolysis happens in cell body. In the sip mutant, the stability and proteolytic processing of PKD2 in the cell body were strongly reduced, suggesting a role for SIP in PKD2 processing, a potential prerequisite for its entry into cilia. However, sip mutant cilia lack PKD2 almost entirely, indicating that SIP has a general role in establishing PKD2 complexes in cilia rather than being required for the proximal or distal PKD2 region. To identify additional components of PKD2 in Chlamydomonas cilia, we fused miniTurbo (miniT) to PKD2 and explored the PKD2 interactome using biotin-avidin pull-downs followed by mass spectrometry. Proximity labelling of proteins via TurboID has been already been shown in *Chlamydomonas (Dentler, 2013)* Proximity labeling identified MST3 as a novel distal PKD2 interactor. During the course of this study, MST3 was identified independently by cryo-EM of isolated mastigonemes (Dai et al., 2024; Huang et al., 2024). The extended N-terminal extracellular region of MST3 forms a central filament, running along the length of the mastigonemes and binding extracellular MST1 via numerous proline-rich repeats. The C-terminal region of MST3 possesses 5 predicted TMHs (TMH1-5) related to PKD2. MST3, however, lacks a region corresponding to the TMH1 and parts of the top domain of PKD2. We proposed that MST3 forms a complex with SIP to achieve a PKD2-like structure (Dai et al. 2024). Here we show that endogenously tagged MST3 localizes to the distal ciliary region, as expected. Further, MST1 and mastigonemes are absent from mst3 cilia and mst1 cilia largely lack MST3, indicating mutual dependency (Dai et al., 2024).

Moreover, CRISPR knock-out of MST3 in a strain expressing endogenously mNEON tagged PKD2, largely removed stationary PKD2 from the distal region. We propose that mastigonemes consist of a 3:1:1 complex of PKD2, SIP and MST3, the latter decorated with MST1. However, mst3 cilia retain PKD2 and SIP in the proximal ciliary region. This indicates the presence of an MST3-independent PKD2 complex in this region. Domain analysis via InterProScan and Alphafold2 identified seven more 5-TMH PKD2-like proteins similar to MST3 and are potential PKD2 partners. Three of these 5-TMH proteins localizes to cilia. Further, these three proteins are strongly reduced in abundance in cilia of pkd2 and sip mutants. We generated knockouts of those 5-TMH proteins, using the endogenously tagged PKD2-mNG background strain. Loss of Cre12.g539650 removed PKD2 from the proximal ciliary region and tagged Cre12.g539650 colocalizes with PKD2 specifically in the proximal cilium. The data suggest that SCV is the binding partner of PKD2 in the proximal region. In scv mst3 double knock-outs, both distal and proximal PKD2 zones were lost and residual PKD2-mNG was highly mobile, putatively indicating the presence of additional PKD2 complexes in Chlamydomonas cilia. We hypothesize that these residual PKD2 complexes are formed by an association between PKD2 and the ciliary 5-TMH protein Cre13.g569550. CTL4, the remaining 5 TMH protein of the four identified in Chlamydomonas cilia, co-localizes predominately to the distal PKD2-mastigoneme region and the distribution of PKD2 and mastigonemes is not affected in clt4 knock-outs. In summary, Chlamydomonas cilia contain at least two, perhaps up to four, biochemically distinct PKD2 complexes. Likely, the unique extracellular and intracellular domains of the 5-TMH protein convey functional and spatial specialization to the PKD2 complexes. Our data reveal an unexpected heterogeneity of PKD2 complexes in cilia of single celled Chlamydomonas. Mammalian PKD2 binds PKD1, which possess 11TMH proteins, of which TMH5 to 11 are

PKD2-like. Chlamydomonas PKD2 partners with 5-TMH proteins, which lack a helix corresponding to that of PKD2 TMH1. SIP complements this missing helix, resulting in the characteristic TRP channel configuration based on 4x 6TMHs. Thus, Chlamydomonas and metazoan used different solutions to partner PKD2 with proteins possessing large ectodomains.

### Results

# 3.3 Proximity labeling identified MST3 as a PKD2-associated protein

To identify proteins involved in establishing the spatial pattern of PKD2 in *Chlamydomonas*, we tagged PKD2 at its C-terminus with the promiscuous biotin ligase miniTurbo. In Chlamydomonas, PKD2 is proteolytically cleaved as it enters cilia (Huang et al., 2007). Antibodies to PKD2 showed two bands of approximately 130 and 100 kDa, representing the Nand C-terminal fragment of PKD2, respectively, in cilia samples obtained from control cell and revealed an upward shift of the C-terminal fragment of PKD2 in the pkd2 PKD2-miniTurbo and the pkd2 PKD2-mNG. Antibodies to BirA/miniTurbo verified the expression of PKD2miniTurbo in the pkd2 PKD2-miniTurbo strain (Fig. 1A). Whole mount negative stain electron microscopy showed the presence of two rows of mastigoneme on pkd2 PKD2-miniTurbo cilia, revealing rescue of the mastigonemes-deficient cilia of the pkd2 mutant strain (Fig. 1B). After adding biotin for 90 minutes to concentrated wild-type and pkd2 PKD2-miniTurbo cells, cilia were isolated and analyzed by western blot analysis with avidin-HRP. Control cilia with and without biotin treatment showed a few background bands, as expected since Chlamydomonas possesses endogenous protein biotin ligases. In the pkd2 PKD2-miniTurbo strain, numerous additional biotinylated bands were visible, especially in the biotin-treated samples (Fig. 1C). Biotinylated proteins were captured for the detergent-soluble membrane and matrix fraction and cold SDS extracts of axonemes from control pkd2 PKD2-miniT cilia, each in eight replicates (consisting of 5 repeats of full length axoneme, 2 repeats of regenerating axoneme and a single sample of membrane-matrix) were subjected to mass-spectrometry (Table S1). PKD2 was detected in all the experimental samples and four of the control samples, albeit with much lower peptide coverage and number in the latter. SIP was identified in two experimental samples with one peptide each. Of all the proteins identified in the experimental samples eight stood out by being present in high coverage in all experimental samples but none of the control samples. This 8572 residue long PKD2-like protein was recently identified as MST3 (Dai et al., 2024) or Mstax (Huang et al., 2024). Here we will use MST3. It possesses 5 TMHs, corresponding to TMH 2 to 6 of PKD2 and an extended N-terminal region. The transmembrane region is predicted to combine with SIP, a single TMH1 protein similar to the TMH1 and TOP domain of PKD2, forming a 3 PKD2:1 MST3:1 SIP channel complex. The N-terminal region forms the core of the mastigonemes and binds to numerous MST1.

# 3.4 MST3 is required for PKD2 localization to the distal cilium

From the *Chlamydomonas* mutant library (CLiP), we obtained eight putative mutants in the genes encoding proteins abundantly found in the experimental samples, including a mutant in *MST3*. Whole mount negative stain TEM showed that of these strains only mst3-2 (CLiP strain LMJ.RY0402.104433) having an insertion of 2.2 KBs cassette lacked the mastigonemes on its cilia; the absence of mastigonemes was previously shown for mst3 (Fig. 2A, B). Accordingly, and as previously shown, the mastigonemes-specific protein MST1 was absent in western blots of *mst3* cilia whereas PKD2 and SIP were present albeit in reduced amounts (Fig. 2C). To localize MST3, CRISPR/Cas9 was used to insert mNeonGreen (mNG) in front of the STOP

codon of MST3. Toward this end, we used a repair template, encompassing mNG, the alpha tubulin TUA1 terminator sequence and a hygromycin resistance gene (Nievergelt et al., 2023). Thus, MST3-mNG is expressed from its native locus but using the 3'-UTR of alpha-tubulin 1. The same repair template was used for the other genes tagged in this study. Endogenous MST3 tagged at its C-terminus with mNG using CRISPR localized to the distal part of cilia (Fig. 2D). By mating g1 MST3-mNG<sup>CRISPR</sup> (mt +) and cc-124 PKD2-mSCV<sup>ISPR</sup> (mt -), we obtained an MST3-mNG<sup>CRISPR</sup> PKD2-mSCV<sup>ISPR</sup> strain, which showed partial colocalization of both proteins in the distal cilium and an MST3-deficient proximal PKD2-mS region. High-resolution in vivo imaging revealed that PKD2 and MST3 were organized into two rows in the distal region; the overlap was not complete as indicated by a Pearson coefficient of ~0.83 (SD=0.05, xx, n=10 cilia) (Fig. 2E, G). A subset of cells had cilia with only one row of PKD2-mS/MST3-mNG complexes. This observation was confirmed by TEM analysis, showing single rows of mastigonemes on some cilia. To test whether the assembly of PKD2 in the distal cilium requires MST3, we generated an endogenously tagged PKD2-mNG strain and knocked-out MST3 using CRISPR. PKD2 was absent from the distal cilium but retained in the proximal cilium (Fig.2 F). Thus, Chlamydomonas cilia contain distally located MST3-dependent PKD-2 complexes, forming the mastigonemes, and MST3-independent PKD2 complexes in the proximal cilium.

3.5 Assembly of PKD2 in the proximal cilium requires the PKD2-like protein Scavenger In *mst3* knockouts, PKD2 remained present in the proximal cilium and western blotting showed that PKD2 and SIP remained present in *mst3* cilia. This suggests the presence of an MST3-independent complex in this region. To identify proteins specific to the proximal PKD2 region, we used a candidate approach. Besides MST3, the *Chlamydomonas* genome encodes seven

additional PKD2-like 5-TMH proteins with extended N-terminal extracellular domains and unstructured C-terminal domains. Structural modeling via Alphafold and InterProScan showed that these 5-TMH proteins can interact with SIP to form a PKD2-like complex with 6 TMHs and a TOP domain resembling that of PKD2. Previous proteomic studies revealed the presence of three of the gene products (Cre13.g569550, Cre12.g539650 and Cre09.g400850) in cilia and a reduction of these proteins in cilia of pkd2 and sip mutant. Using CRISPR, we generated knockouts of the three genes in a strain also expressing endogenously tagged PKD2-mNG; PCR was used to verify the insertion of the hygromycin cassette in the desired location of the target genes. TIRF microscopy revealed largely normal distributions of PKD2-mNG in the Cre13.g569550 and Cre09.g400850 mutants whereas knockout of Cre12.539650 caused a loss of PKD2-mNG specifically from the proximal cilia region. PKD2-mNG was retained in the distal region of Cre12.539650 mutant cilia (Fig. 3a). Next, we tagged endogenous Cre12.539650 at its C-terminus with mNG using CRISPR-CAS9; the tagged protein localized to the proximal region of cilia (Fig. 3b). In Phytozome (<a href="https://phytozome-next.jgi.doe.gov/">https://phytozome-next.jgi.doe.gov/</a>), this 6281-residue long protein is annotated as a polycystin cation channel with a scavenger receptor cysteine-rich domain (SRCR) domain; here we refer to it as SCV-PKD2. Its N-terminal extracellular region is predicted to encompass proline-rich, C-type lectin, IgG-like and SRCR-like domains (Dai et al., 2024). As proximal and distal zone of PKD2 get abrupted in scvand mst3, we generated double knock-out scvmst3 PKD2-mNG and observed via TIRF that the proper formation of the two zones is absent (Fig. 3c). western blot analysis of the cilia of scvshowed the presence of MST1 and expression of PKD2 is almost comparable to wild-type (Fig. 3d). Cilia of double mutant scvmst3 largely lack MST1, PKD2 and SIP observed via western blot (Fig. 3d). Taken together, the data suggest that SCV is the partner of PKD2 in the proximal cilium.

### 3.6 Discussion

We previously showed that *Chlamydomonas* PKD2 anchors mastigonemes, hair-like structures that were thought to be polymers of the secreted glycoprotein MST1, to the ciliary surface and connects them to the axonemal DTM4 and DTM8. However, a distinct population of PKD2-GFP complexes, lacking mastigonemes and showing increased mobility and exchange with cell body PKD2, was observed in the proximal region of cilia. We reasoned that establishing these two distinct populations of ciliary PKD2 likely involves additional proteins. Using immunoprecipitation of tagged PKD2, we identified SIP, a 362 residues 1TMH PKD2-like protein, as putative PKD2 interactor. Cilia of sip mutants lack mastigonemes and are almost completely devoid of PKD2, revealing that SIP is not specific for the proximal or distal PKD2 but rather required to establish PKD2 in cilia. It remained also unclear how PKD2 and SIP interact and organize the mastigonemes. Using PKD2-miniTurbo proximity labeling, we identified a proline-rich PKD2-like protein of 8572 residues as a potential PKD2 interactor. During the cause of this study, this protein, now referred to as MST3 or MSTAX, was also identified in two independent studies by single particle imaging. Mutants in mst3 lack mastigonemes and swim with reduced velocity as previously reported for pkd2, mst1, and sip mutants. MST3 has an extended, proline-rich, glycosylated extracellular domain, to which numerous MST1 associate, suggesting that MST3 determines the length and polarity of the mastigonemes. The predicted transmembrane region of MST3 consists of five TMHs, corresponding to TMHs 2 to 6 of PKD2 in structure. Ultrastructural modeling suggests that MST3 partners with SIP, which is homologous to the N-terminal region of PKD2 including its TMH1, to complement each other to form a PKD2-like transmembrane region and the extracellular top domain characteristic for PKD2. Here, we show that tagged MST3 specifically

localizes to the distal region of cilia, where forms two rows and colocalizes with PKD2. Both proteins frequently move together on IFT trains, suggesting that they enter cilia as a complex. Indeed, CRISPR/Cas9-mediated knockout of MST3 eliminated the PKD2 signal from the distal ciliary region. Together, the data suggest that the mastigonemes consists of PKD2, SIP, MST3, probably in a 3:1:1 heteromeric complex, and multiple MST1 associated to MST3.

However, PKD2-mNG was retained in the proximal region in *mst3* ko cilia, suggesting the presence of an MST3-independent PKD2 complex in this region. The *Chlamydomonas* genome encodes seven additional PKD2-like 5-TMH proteins with extracellular N-terminal domains and unstructured C-terminal domains, ranging from 4105 and 8143 in size, respectively. Three of these (i.e., SCV, CTL4, and Apple) were shown by mass spectrometry to be present in cilia and reduced in *pkd2* and *sip* mutants. In the corresponding knockout strains, the loss of SCV essentially eliminated PKD2-mNG from the proximal ciliary region, whereas a loss of either CTL4 or Apple showed no apparent effect of the distribution of PKD2-mNG. Further, fluorescent protein tagged SCV was essentially restricted to the proximal region of cilia. Because SCV co-localizes with PKD2 in the proximal region and is required for PKD2 assembly in this region, we propose that SCV is the partner of PKD2 in the proximal ciliary region, perhaps forming a 3xPKD2, 1xSIP, 1xSCV complex. Together, the data strongly support the notion that, in *Chlamydomonas* cilia, PKD2 interacts with two distinct 5-TMH proteins.

The extended unstructured C-terminal regions of MST3 and SCV form the unique intracellular parts of the complexes and future work needs to address if these regions are targeting PKD2 complexes to distinct subciliary regions. Similarly, mammalian PKD2 interacts with PKD1 with a 1:3 stoichiometry in cilia of kidney epithelial cells and in other tissues

whereas it partners with PKD1L1 in nodal cilia. PKD1-related polycystins have unique structural regulatory domains that produce channels with distinct properties when they oligomerize with PKD2-related subunits.

In *mst3 scv* double ko cells, residual PKD2-NG complexes, mostly moving by IFT and diffusion, were present along the length of cilia. Such MST3- and SCV -independent PKD2 complexes could present a PKD2 homo-tetramer or a combination of PKD2 with the one of the above mentioned other 5-TMH PKD2-like proteins in *Chlamydomonas*. In the latter scenario, we predict that all PKD2 complexes will contain SIP, which is supported by the near absence of PKD2-mNG from a somewhat leaky *sip* CLiP mutant as well as a *SIP*<sup>CRISPR-KO</sup>. Additional work is needed to determine the extent of PKD2 channel heterogeneity in *Chlamydomonas* cilia and the cell body. Mutants in *pkd2*, *mst1*, *mst3*, *sip* swim with a moderately reduced velocity and other phenotypes were not apparent, raising the question after the function of PKD2 complex heterogeneity in *Chlamydomonas*.

The loss of CTL4 did not affect the pattern of ciliary PKD2-mNG in an apparent manner, indicating that it is not required for the assembly of the distal or proximal PKD2 region. However, CTL4 was reduced in pkd2 and sip mutant cilia and, in many cells, localized to the distal region of cilia, also occupied by the PKD2-mastigoneme complexes. Of note, the distal and proximal PKD2-mNG regions were lost in mst3 SCV double kos, was arguing against a CTL4-PKD2 complex assembled independently of MST3. In this region, CTL4-mNG was organized into two rows, which, however, were not as clearly separated as the rows formed by tagged PKD2 or MST3.

Chlamydomonas MST3, SCV and the other PKD2-like 5-TMH proteins are likely associated with SIP, which substitutes for the TMH corresponding to TMH1 of PKD2 missing in

these proteins. This architecture ensures the formation of a characteristic 4 x 6TMH TRPP channel complex and the formation of the PKD2-specific top domain in combination with an extended extracellular N-terminal region encompassing various ECM motifs. In mammals and other metazoan, PKD2 partners with PKD1, an 11TMH protein with an extended N-terminal extracellular region in which the helices 6 to 11 are PKD2-like and partner with PKD. This suggests a common principle of combining PKD2 with a heterologous PKD2-like protein possessing an uneven number of TMHs and a large ectodomain, but mammals and algae developed distinct ways to achieve such a design. In *Chlamydomonas*, the large number of PKD2-like 5-TMH proteins, each with its individual extracellular and intracellular domains, allow for the formation of spatially and perhaps functionally distinct PKD2 complexes. The extracellular ectodomain is theorized to serve as a mechanical or ligand regulatory domain.

# 3.7 MATERIALS AND METHODS

# Strains, culture conditions and genotyping

Chlamydomonas strains used in this study are enlisted in Table. The wild-type strains cc-124 and cc-125 are availed from the Chlamydomonas resource center. g1( (Pazour et al., 1995) was another wildtype control and pkd2 was a mutant strain outcrossed two times with g1. The original mutant strain of mst3 was obtained from the Chlamydomonas Library Project (CLiP). Cells were grown in modified minimal (M) medium

(https://www.chlamycollection.org/methods/media-recipes/minimal-or-m-medium-and-derivatives-sager-granick/) and maintained at 22°C with a 14-h-light-10-h-dark cycle; large cultures used for cilia isolation were aerated with air enriched with 0.5% CO<sub>2</sub>.

# Transgenic strain generation

To express PKD2-miniTurbo in the *pkd2* mutant, we generated pPD-PKD2-miniTurbo-HYG. The plasmid, pPD-PKD2-miniTurbo-HYG was generated in the following manner. Genomic PKD2 was amplified using primer 1 and 2, miniTurbo tag which is codon optimised for expression in *Chlamydomonas* was amplified using primer 3 and 4, and the vector pBR25 was amplified using primers 5 and 6. All of the three fragments were assembled using NEBuilder® HiFi DNA Assembly kit (New England Biolabs) which resulted into pPD-PKD2-miniTurbo plasmid. For addition of the hygromycin resistance, HYG cassette was amplified with primer 7 and 8, and incorporated at the KpnI site of pPD-PKD2-miniTurbo to produce the complete pPD-PKD2-miniTurbo-HYG. The resulting plasmid was linearized using PsiI cutsmart enzyme and transformed in the *pkd2* mutant by electroporation (Invitrogen Neon<sup>NXT</sup> Electroporation system). Transformants were selected on TAP plates containing 20 μg/ml

hygromycin (Bio Basic). Clones expressing PKD2-miniTurbo protein were identified using whole-mount EM based on the restoration of mastigonemes on the ciliary surface, which was observed in one out of more than 120 transgenic clones analyzed. The ciliary presence of PKD2-miniTurbo in *pkd2* PKD2-miniTurbo-HYG was confirmed by western blot analysis with anti-PKD2 (Huang et al., 2007) and anti-BirA (Agrisera, Product No.AS20 4440) antibodies.

# Ciliary regeneration

Vegetative cells in M medium were deciliated by a pH shock (pH 4.2 for 30 s), transferred to fresh M medium, and allowed cilia to regrow under constant light with agitation. The cells with regrown cilia were further processed by biotin treatment and cilia isolation.

#### Solubilization of biotin

1.22 g of biotin (Therrmo Fischer Scientific) was added to 45 mL of water. Biotin is insoluble in water. So, two to three drops of sodium hydroxide (NaOH) were added for dissolving the biotin. After the proper dissolution of biotin, the pH was adjusted to around 7.5 and the volume of the biotin (in water) solution was brought up to 50 mL to make the stock solution of 100 mM.

# **Biotin assay**

Two to three litre of *Chlamydomonas* culture with a cell density of 2-3 \*10<sup>5</sup> cells /mL was harvested. The cells were resuspended in a total volume of 50 mL fresh M media supplied with 2.5 mM biotin (working concentration). The biotin added *Chlamydomonas* culture was incubated under light for 90 minutes at room temperature with gentle agitation on a rocker. This was followed by the isolation of cilia.

#### Isolation and fractionation of Cilia

To isolate cilia, cells were harvested and washed in 10 mM HEPES (pH 7.4), resuspended in 10 ml of HEPES-Mg2+-sucrose (HMS; 10 mM HEPES, pH 7.4, 5 mM MgSO4, 4% sucrose), and immediately deciliated by addition of 2.5 ml of dibucaine-HCl (25 mM in H2O; Sigma-Aldrich) and vigorous pipetting (Craige et al., 2013). After addition of 20 ml of 0.7 mM EGTA in HMS, the cell bodies were removed via centrifuging (1150 g, 3 min, 4°C; Sorvall Legend XTR, Thermo Fisher Scientific). Next, the supernatant was underlaid with a sucrose cushion (10 ml of 25% sucrose in HMS) and the remaining cell bodies were removed by centrifugation (1700 g, 4°C, 10 min). Cilia in the upper phase were sedimented by centrifugation (27,000 g, 4°C, 20 min; Beckman Coulter, Avanti JXN-26), resuspended in HEPES -Mg2+-EGTA-K+ (HMEK; 30 mM HEPES, 5 mM MgSO4, 0.5 mM EGTA and 25 mM KCl) supplemented with 1% protease inhibitor cocktail (Sigma-Aldrich, P9599) and lysed for 20 min on ice with Triton X-100 or, if phase partitioning was planned, Triton X-114 (each at 1% final concentration). The axonemes were separated from the membrane plus matrix fraction centrifugation (27,000 $\times$  g, 4°C, 15 min). For phase partitioning, the supernatant was incubated at 30°C for 5 min; phase separation is evident by the cloudy appearance of the solution. The micelles were harvested by centrifugation (1700 g; 22°C; 5 min) leading to an upper aqueous phase (matrix fraction) and a detergent phase (membrane fraction). Proteins in the detergent phase were further concentrated by methanolchloroform precipitation.

### Pull down assay of the biotinylated proteins

Fractionated axoneme from g1 and *pkd2* PKD2-miniTurbo rescue strains with as well as without the biotin treatment were solubilized using urea (Sigma-Aldrich). The solubilization buffer

contained 6M urea (final concentration), 50 mM NaCl and 0.1% SDS. The solubilized axoneme was separated from the other non-axonemal proteins by centrifugation at 30,000 g for 20 minutes at 4°C. The supernatant with the solubilized axoneme was diluted with HMEK for bringing down the urea concentration and incubated with Pierce<sup>TM</sup> Streptavidin Magnetic Beads (Thermo Fisher) beads for 1 hour at 4°C using a rotisserie. The bound biotinylated proteins were eluted using SDS sample buffer. The eluate, input and flow-through were analyzed by western blot analysis with anti-HRP avidin antibody and the eluate was subjected to mass spectrometry using an Orbitrap Elite system at the Proteomics and Mass Spectrometry Core Facility at the University of Georgia.

# **Antibodies and western blotting**

Whole-cell samples, isolated cilia or ciliary fractions were incubated for 5 min at 95°C in Laemmli SDS sample buffer, separated by SDS-PAGE using Bio-Rad TGX precast gels, and transferred onto PVDF membrane. Membranes were blocked in TBS supplemented with 0.05% Tween 20, 3% bovine serum albumin and 3% fish gelatin followed by standard immunostaining protocols, i.e. incubation in the diluted primary antibodies for overnight at 4°C with agitation (primary antibodies used in this study are listed in Table 3.3 and incubation in diluted secondary antibodies (anti-mouse-IgG, 1:3000, and anti-rabbit IgG, 1:4000, conjugated to horseradish peroxidase; Invitrogen 31432/AB\_228302 and 31460/AB\_228341, respectively) for ~60 min at room temperature. For visualization, membranes were incubated in chemiluminescence substrate (SuperSignal West Pico PLUS or Atto; Thermo Fisher Scientific) and the images were captured using a Bio-Rad ChemiDoc MP imaging system and the Image Lab software (Bio-Rad).

# Whole-mount negative stain EM

For whole-mount EM, a formvar- and carbon-coated 100 mesh electron microscope grid (FCF100-Cu-50, Electron Microscopy Sciences) was placed on a drop of concentrated cells (~2×10<sup>7</sup> cells/ml in water) on parafilm for 3 min. After removing excess cells using filter paper, the grid was put on a drop of 2% uranyl acetate in water for 1 to 2 min. Finally, the grid was washed with distilled water. Images were collected using a JEOL JEM1011 electron microscope. CC-620 was used as a positive control to screen for sip SIP rescue strains.

# Mating and autolysin preparation

Tap plates of cc-125 (MT+) and cc-124 (MT-) were inoculated and kept under continuous bright light for 7-10 days. The evening prior to the mating day, 10 mL of TAP-N media (Findinier, 2023) was added to each of the plates and the cells were scrapped. The TAP-N media with the cell clumps was transferred to 50mL sterile conical flask and pipetted gently to resuspend the clumps of the cells as much as possible. The two cultures were kept under the light overnight without shaking it. In the morning of the mating day, the cultures were checked for the motility efficiency (50 % of motile cells indicate healthy culture for a successful mating). After ensuring healthily moving cells, both the cultures were mixed and kept under light for 15-30 minutes followed by the centrifugation at 2300 RPM for 3 minutes. The supernatant, which is the autolysin, was collected in a sterile falcon tube and filtered using syringe and 0.45 um filter. The autolysin was frozen using liquid nitrogen and stored at -80 C.

# **CRISPR-CAS9** in *Chlamydomonas*

To tag protein endogenously and generate knockouts of genes in *Chlamydomonas*, we used CRISPR-CAS9 technique. For CRISPR-CAS9 method, the three most inevitable components are guide RNA (sg-RNA), template DNA and cas-9 protein. The guide RNA was generated using CHOPCHOP site and the sg-RNA with highest efficiency was selected. The sequence of plasmid for amplifying the template DNA with m-NEON green or m-scarlet tag having a selective antibiotic resistance are in Fig. S2. The primers for the amplification of template DNA have 20-25 base pair overhang at their 5' end which is homologous to the genomic sequence of the gene of interest. The strain to be transformed was grown in TAP media (https://www.chlamycollection.org/methods/media-recipes/tap-and-tris-minimal/) for 4-5 days in 14-10-hour light -dark cycle. On the day of the CIRSPR-CAS9 experiment, the strain was harvested and incubated in 6 mL of autolysin for 1 hour with a cell density 2-3 \* 10<sup>7</sup>/mL. To evaluate the autolysin treatment on the cell wall, we mixed 0.5% Triton-X 100 and cells in autolysin from the previous step in 1:1 ratio to quantitate the bursting of cells. 70-80% of burst cells implied dissolution of their cell wall which indicates a successful autolysin treatment. After confirming that most of the cells lost their cell wall, the cells were given heat-shock at 40 °C for 30 minutes with gentle agitation. Simultaneously during the heat-shock, we prepared the RNP by mixing 1 uL cas-9 (TrueCut<sup>TM</sup> Cas9 Protein v2, Thermo Fischer Scientific), 2.8 ul IDT DNA duplex buffer and 1.2 uL of sg-RNA, and incubating the mixture for 30 minutes at 37 °C for 30 minutes. After the heat shock, the cells were resuspended in TAP-sucrose (40 mM sucrose in TAP media) with a cell count of 1\*10<sup>8</sup> and kept on ice. 110 ul of the prepared cells mixed with 5 μL of RNP were transformed with 1 μg of template DNA via electroporation (Neon<sup>NXT</sup> Electroporation System, Thermo Fischer Scientific). After the electroporation, the cells were

revived in 16°C for 1 hour and incubated under dim light for 20-24 hours on a rocker with gentle agitation. Towards the end of the 24-hour mark, we plated the cells on a TAP plate supplied with the required selective antibiotic.

### **Endogenous strain and knock-out generation**

Five proteins PKD2, MST3, SCV, CTL4 and 550 were tagged endogenously via CRISPR-CAS9 method in g1. This resulted in the generation of new strains i.e., g1 PKD2-mNG-PARO, g1 MST3-mNG-HYG, g1 SCV-mNG-PARO strains, g1 CTL4-mNG-PARO and g1 SCV-mNG-PARO. We also tagged PKD2 with m-Scarlet at its C-terminus in cc-124 which produced cc-124 PKD2-mSCA-HYG. Primer 35 and 36, primer 10 and 11, primer 13 and 14, and primer 35 and 36 were used to amplify the template DNA for tagging PKD2 with m-Neon Green, MST3 with m-Neon Green, SCV with m-Neon Green and PKD2 with m-Scarlet endogenously. The sg-RNA sequences are enlisted in Table 2.

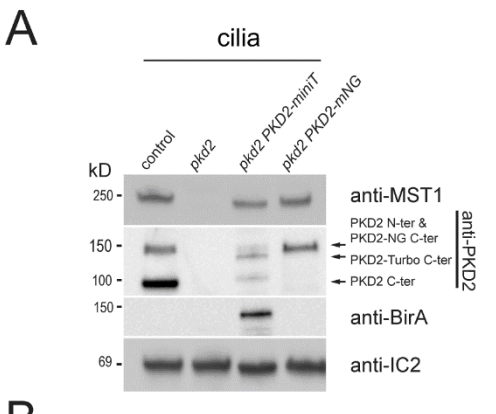
Knockouts in the genes (Cre06.g309951 (MST3), Cre12.g539650(SCV),
Cre13.g569550(POL) and Cre09.g400850(CTL4)) whose gene products are predicted to form
complex with SIP were generated using the g1 PKD2-mNG strain (background strain) via
CRISPR-CAS9. The hygromycin cassette (acted as the template DNA) was inserted in the
aforementioned genes to hinder their expression. Primer 23 and 24, primer 26 and 27, primer 32
and 33, and primer 29 and 30 were used to amplify the Hygromycin cassette (template DNA)
with the gene specific 5' and 3' overhangs (20-25 base pair) for homologous recombination in
the required gene of interest.

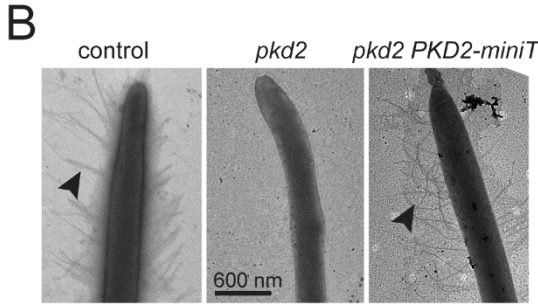
knocking out the (Cre06.g309951 (MST3), Cre12.g539650(SCV), Cre13.g569550(POL) and Cre09.g400850(CTL4) was confirmed by PCR amplification of insertion of the cassette in the

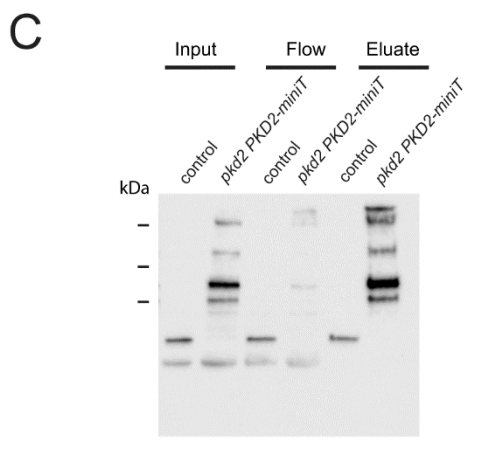
genes at the desired location. Knockouts allowed us to evaluate the role of the genes on PKD2 complex by quickly analyzing the effect of absence of the gene products (proteins) on the localization of endogenous PKD2-mNG. The wild-type PKD2-mNG localization in Cilia is getting arranged into the two rows as proximal mobile and distal stationary zones with a gap (Liu et al., 2020).

Three out of the four knockouts showed wild-type distribution of PKD2 and the one with a new defective PKD2 distribution is the knockout in SCV annotated as *SCV*<sup>CRISPR-KO</sup>. PKD2-mNG in *scv* is disrupted in the proximal but intact in the distal zone.

# 3.8 Figure and Figure legends







miniT rescue strain.

# Figure 3.1) PKD2-miniTurbo rescues mastigonemes in the pkd2 strain

- A) Western blot analysis of cilia isolated from control, *pkd2* mutant, *pkd2 PKD2-miniTurbo* rescue and *pkd2 PKD2-mNG* rescue strains. The membrane was probed with anti-MST1, anti-PKD2, anti-BirA and, as a control for equal loading, anti-IC2, a subunit of the outer dynein arms. In conclusion, PKD2-miniTurbo restores mastigonemes in the *pkd2* mutant.
- B) Analysis of cilia from control, *pkd2*, mutant, and *pkd2* PKD2-miniTurbo rescue cells by whole mount EM. Black arrowheads are indicating mastigonemes.
- C) Input, flow through and eluate of axonemal fractions obtained from control and the *pkd2 PKD2*-

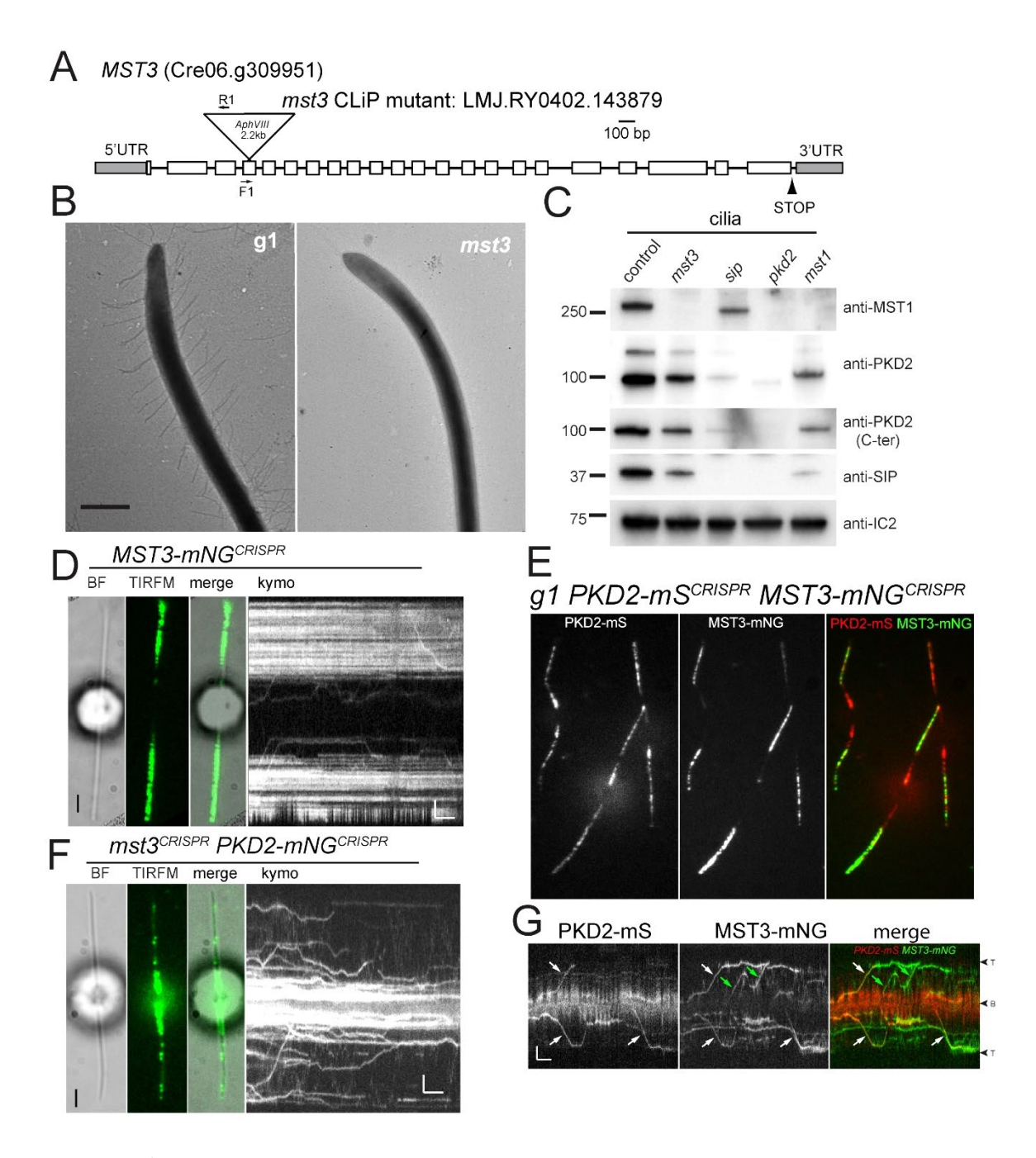


Figure 3.2) MST3 is required for distal PKD2 assembly

- A) Schematic of *mst3* CLiP mutant.
- B) Analysis of cilia from control and mst3 cells by whole mount EM. Arrowheads, mastigonemes. Bar = 600 nm.

- C) Western blot analysis of cilia isolated from control, *mst3*, *pkd2* and *mst1* mutant strains. The membrane was probed with anti-MST1, anti-PKD2 (against the loop region), anti-PKD2 (against the C-terminal), anti-SIP and, as a control for equal loading, anti-IC2, a subunit of the outer dynein arms. Cilia of *mst3* shows the loss of MST1 and a moderate reduction of PKD2 and SIP.
- D) Distribution of MST3-mNG. (Note: presence in distal region)
- E) Distribution of PKD2-mNG. (Note: two PKD2 regions)
- C) Distribution of PKD2-mNG in a *mst3* mutant background. (Note: that residual PKD2 is concentrated in the proximal region.)

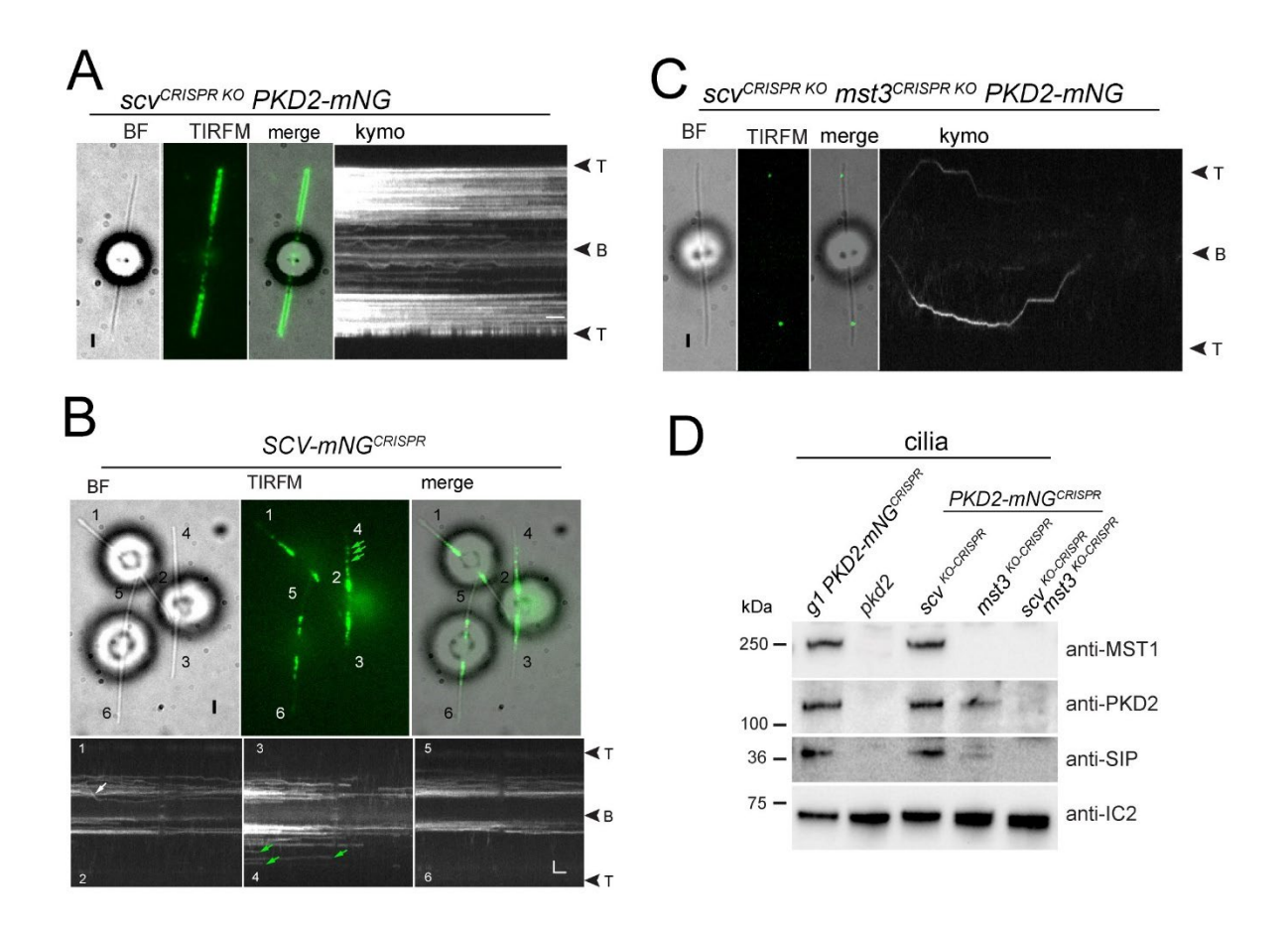


Figure 3.3) Scavenger is required for proximal PKD2 assembly

- A) Distribution of PKD2 in *SCV* KO background. Note that residual PKD2 is concentrated in the distal region.
- B) SCV-mNG localizes in proximal zone of cilia.
- C) Distribution of PKD2-mNG in SCV-KO MST3-KO, double knock-out background. (Note: distal and proximal zones are disrupted)
- D) Western blot analysis of cilia isolated from control, *pkd2*, *scr*, *mst3*, *scvmst3* and *ctl4* mutant strains. The membrane was probed with anti-MST1, anti-PKD2 (against the loop region), anti-SIP and, as a control for equal loading, anti-IC2, a subunit of the outer dynein arms.

# 3.9 Tables

Table 3.1) Strains used in this study.

	Genoytpe	Reference
CC- 125	Nit, nit2,mt-	Chlamydomonas Genetics Centre
CC- 124	Nit, nit2,mt-	Chlamydomonas Genetics Centre
gl (wild-type)	nit1, agg1, mt <sup>+</sup>	(Pazour et al., 1995)
sip <sup>CLiP</sup>	cw15, mini, mt	(Das et al., 2023)
pkd2 PKD2-mNG	pkd2, mt <sup>-</sup>	(Das et al., 2023)
$pkd2$ (progeny selected from $pkd2^{\text{CLiP}}$ backcrossed twice with $g1$ )	cw15, pkd2, mt	(Liu et al., 2020)
mst1 (LMJ.RY0402.052413)	cw15, mst1, mt	Chlamydomonas Genetics Centre
mst1 pkd2 PKD2-mNG	mst1, pkd2	(Liu et al., 2020)
mst3 (LMJ.RY0402.104433)	cw15, mst3, mt	Chlamydomonas Genetics Centre
g1 PKD2-mNG <sup>CRISPR</sup>	nit1, agg1, mt <sup>+</sup> , PKD2-mNG <sup>CRISPR</sup>	This study
CC-124 PKD2-mSCA <sup>CRISPR</sup>	nit1, agg1, mt-, PKD2-mSCA <sup>CRISPR</sup>	This study
g1 MST3-mNG <sup>CRISPR</sup>	nit1, agg1, mt <sup>+</sup> , MST3-mNG <sup>CRISPR</sup>	This study
g1 SPL-mNG <sup>CRISPR</sup>	nit1, agg1, mt <sup>+</sup> , - SPL-mNG <sup>CRISPR</sup>	This study
g1 RPL-mNG <sup>CRISPR</sup>	nit1, agg1, mt <sup>+</sup> , RPL-mNG <sup>CRISPR</sup>	This study
g1 PPL-mNG <sup>CRISPR</sup>	nit1, agg1, mt <sup>+</sup> , PPL-mNG <sup>CRISPR</sup>	This study
g1 PKD2-mNG <sup>CRISPR</sup> MST3 <sup>CRISPR-KO</sup>	nit1, agg1, mt <sup>+</sup> , PKD2-mNG <sup>CRISPR</sup> ,MST3 <sup>CRISPR-KO</sup>	This study
g1 PKD2-mNG <sup>CRISPR</sup> SCV <sup>CRISPR-KO</sup>	nit1, agg1, mt <sup>+</sup> , PKD2-mNG <sup>CRISPR</sup> , SPL <sup>CRISPR-KO</sup>	This study
g1 PKD2-mNG <sup>CRISPR</sup> CTL4 <sup>CRISPR-KO</sup>	nit1, agg1, mt <sup>+</sup> , PKD2-mNG <sup>CRISPR</sup> ,RPL <sup>CRISPR-KO</sup>	This study
g1 PKD2-mNG <sup>CRISPR</sup> POL <sup>CRISPR-KO</sup>	nit1, agg1, mt <sup>+</sup> , PKD2-mNG <sup>CRISPR</sup> ,RPL <sup>CRISPR-KO</sup>	This study

g1 PKD2-mNG <sup>CRISPR</sup> SCV <sup>CRISPR-KO</sup> MST3 <sup>CRISPR-KO</sup>	This Study
PKD2-mSCA <sup>CRISPR</sup> SCV-mNG <sup>CRISPR</sup>	This Study
g1 PKD2-mNG <sup>CRISPR</sup> SIP <sup>CRISPR-KO</sup>	This Study

Table 3.2) list of primers.

Prim er num ber	Primer name	Sequence (5' to 3')			
1	FR- PKD2	5'TCAGCTAGCTTAAGATCCCATCACTAGTGGCCTGGGCGTGAAG AAGC'			
2	RV- PKD2	5'CCTAGGGCGGCGGCGGCGACTAGTCTGGGGCGGGGTCTCA TTCA3'			
3	FR- miniTur bo	5'TGAATGAGACCCCGCCCCAGACTAGTGGAGGTGGTAGTGGAGG AG 3'			
4	RV- miniTur bo	5' CCTCCATTTACACGGAGCGGCCTAGGCTACTTCTCGGCGCT3'			
5	FR-vec	5' ACTAGTCGCCGCCGCCGCCCCTAGGCCGCTCCGTGTAAATGGAGG 3'			
6	RV-vec	5'GCTTCTTCACGCCCAGGCCGGATGGGATCTTAAGCTAGCT			
7	FR- HYG	5' GGTACC CTTTCTTGCGCTATGACACTTC 3'			
8	RV- HYG	5' GGTACC CGCTTCAAATACGCCCAGCCC 3'			
9	REV- NEON	5' ACTGGTGGAAGCCGTAGCCG 3'			
10	FR- MST3	5' CGGCCCCACACCCAAGCGCCGTCAGGCTGGAGACGACGAG GGAGGTGGAAGTGGAGGAGG 3'			
11	RV- MST3	5' CGCTCAGCACCTGACACGTGCCTAAGCACGGCGCGG gagegegegtaatacgactca 3'			
12	FR- MST3- CHK	5' TGGACTCGTTCGGATCCATGA 3'			
13	FR- SDPL	5' ACCGCACGCGCAGTTGCCCTGGATGGCGAGGCCTTC GGAGGTGGAAGTGGAGGAGG 3'			
14	RV- SDPL	5' TGGAGCGCTGCCGGGCGCGCAGGGCGGCAGCGCA gagcgcgcgtaatacgactca 3'			
15	FR- SDPL - CHK	5' AGTTGCAATTGCAGCGAACTC 3'			
16	FR- RDPL	5'CCGACGCTTCGGCGTCGGAGGCCGAGGGCCGCCAaGGAGG TGGAAGTGGAGGAGG3'			
17	RV- RDPL	5'GCTTGCAAAACGCCCGCACTCCTCCAGTCGCATCGCgagcgcgcgta atacgactca3'			

18	FR-	5' CCGCGTCAGTGCCGGCGGCAGT 3'
10	RDPL -	5 cedediendideeddendi 5
	CHK	
19	FR-	5'AGATGAGGAGCAGGGGCGCGGTAGCCGCAGTCACGGCATCGC
	PDPL	A GGAGGTGGAAGTGGAGGAGG 3'
20	RV-	5' CGGATACGCATACGTTCGTTTGCGTACGTGAATCAG
	PDPL	gagegeggtaataegactea 3'
21	FR-	5' GCATGGCAGCTGACGCTGC 3'
	PDPL -	
	CHK	
22	RV-	5' TGAATATGGCTTTGGTAGCT 3'
	HYG-	
	chk	
23	FR-	5'TCGGCCCTGCCGCTGGAACGGCACCATCATCTTCGCCACCTGG
	MST3k	AGGTGGAAGTGGAGGAGG3'
	0	
24	RV-	5' ACGCAGCAGCTGCAGCACGTGGCTGAGGCGCTGCA
	MST3k	gagegegegtaataegaetea 3'
	0	
25	FR-	5' ACGCATGCGTAGCTTCGTGA 3'
	MST3k	
	oCK	
26	FR-	5'TCTGCTGGCACTGCCTCGCCGCAGGGCGGCTTGTTTA
	SDPLko	CTTTCTTGCGCTATGACCACTTCC 3'
27	RV-	5'GCCGCAGCAACAGAGTCAGGTTGCCGGAGCCACCGCCAGAAAGAGGCCA
20	SDPLko	AAATCAACGGA 3'
28	FR-	5' AGCATAACCGCCATCCAGTGT 3'
	SDPLko	
20	CK	51000000000000000000000000000000000000
29	FR-	5'GCCGCGTCGGCGACTGGGCCTACCTCACCGCCGCCCTCTTTCTT
	RDPLk	GACACTTCC 3'
30	RV-	5'CCCCCCTCCCCCACTCCCCTACCTCACCCCCCCCCCTCTTTCTTC
30	RV- RDPLk	5'GCCGCGTCGGCGACTGGGCCTACCTCACCGCCGCCCTCTTTCTT
		GACACTICC 3
31	FR-	5' TCGGCGTGCTTCTGCTTGTGTT 3'
31	RDPLk	
	oCK	
32	FR-	5'CCTACTGCACCACGCGGCTGTGGAGCCTGGAGGTGCTTTCTTGCGCTATG
52	PDPLko	ACACTTCC 3'
33	RV-	5'TTGGGTGCGAGCTGGTCGGGGACACCGCCAGCCAGAAAGAGGCCAAAA
	PDPLko	TCAACGGA 3'
34	FR-	5' ATGAACAGGACCCCAGCACT 3'
	PDPLko	
	CK	
	I	

35	RV- Jonika cassette	5'TGTCGCTGAAAGTGGAGGTC 3'
36	Fr- PKD2- LNK	5'TCCAAGCTGGTGCAGCTGATGAATGAGACCCCGCCCAG GGAGGTGGAAGTGGAGGAGG 3'
37	REV- PKD2- Vec	5'ACGACGCAGAAGCCACCTCCGCATGGACCCCAAGC gagcgcgcgtaatacgactca 3'

Table 3.3) List of antibodies.

Name	Host	Dilution WB	Dilution IF	Reference
Anti-PKD2	rb	1:2000		(Huang et al., 2007)
Anti-SIP	rb	1:2000		(Das et al., 2023)
Anti-MST1	rb	1:2000		(Das et al., 2023)
Anti-IC2	mo	1:1000		(King & Witman, 1990)

#### 3.10 References

- Alessandri-Haber, N., Dina, O. A., Chen, X., & Levine, J. D. (2009). TRPC1 and TRPC6 channels cooperate with TRPV4 to mediate mechanical hyperalgesia and nociceptor sensitization. *J Neurosci*, 29(19), 6217-6228. https://doi.org/10.1523/jneurosci.0893-09.2009
- Bai, C. X., Giamarchi, A., Rodat-Despoix, L., Padilla, F., Downs, T., Tsiokas, L., & Delmas, P. (2008). Formation of a new receptor-operated channel by heteromeric assembly of TRPP2 and TRPC1 subunits. *EMBO reports*, 9(5), 472-479-479. <a href="https://doi.org/https://doi.org/10.1038/embor.2008.29">https://doi.org/https://doi.org/10.1038/embor.2008.29</a>
- Chen, X., Sooch, G., Demaree, I. S., White, F. A., & Obukhov, A. G. (2020). Transient Receptor Potential Canonical (TRPC) Channels: Then and Now. *Cells*, 9(9). https://doi.org/10.3390/cells9091983
- Chung, J. J., Shim, S. H., Everley, R. A., Gygi, S. P., Zhuang, X., & Clapham, D. E. (2014). Structurally distinct Ca(2+) signaling domains of sperm flagella orchestrate tyrosine phosphorylation and motility. *Cell*, *157*(4), 808-822. <a href="https://doi.org/10.1016/j.cell.2014.02.056">https://doi.org/10.1016/j.cell.2014.02.056</a>
- Cohen, M. R., & Moiseenkova-Bell, V. Y. (2014). Structure of thermally activated TRP channels. *Curr Top Membr*, 74, 181-211. <a href="https://doi.org/10.1016/b978-0-12-800181-3.00007-5">https://doi.org/10.1016/b978-0-12-800181-3.00007-5</a>
- Dai, J., Ma, M., Niu, Q., Eisert, R. J., Wang, X., Das, P., Lechtreck, K. F., Dutcher, S. K., Zhang, R., & Brown, A. (2024). Mastigoneme structure reveals insights into the O-linked glycosylation code of native hydroxyproline-rich helices. *Cell*, *187*(8), 1907-1921.e1916. <a href="https://doi.org/https://doi.org/10.1016/j.cell.2024.03.005">https://doi.org/https://doi.org/10.1016/j.cell.2024.03.005</a>
- Das, P., Mekonnen, B., Alkhofash, R., Ingle, A., Workman, E. B., Feather, A., Liu, P., & Lechtreck, K. F. (2023). Small Interactor of PKD2 (SIP), a novel PKD2-related single-pass transmembrane protein, is required for proteolytic processing and ciliary import of Chlamydomonas PKD2. *bioRxiv*. <a href="https://doi.org/10.1101/2023.06.13.544839">https://doi.org/10.1101/2023.06.13.544839</a>
- Delling, M., Indzhykulian, A. A., Liu, X., Li, Y., Xie, T., Corey, D. P., & Clapham, D. E. (2016). Primary cilia are not calcium-responsive mechanosensors. *Nature*, *531*(7596), 656-660. https://doi.org/10.1038/nature17426
- Dentler, W. (2013). A Role for the Membrane in Regulating Chlamydomonas Flagellar Length. *PloS one*, 8, e53366. https://doi.org/10.1371/journal.pone.0053366
- Du, J., Ma, X., Shen, B., Huang, Y., Birnbaumer, L., & Yao, X. (2014). TRPV4, TRPC1, and TRPP2 assemble to form a flow-sensitive heteromeric channel. *The FASEB Journal*, *28*(11), 4677-4685. <a href="https://doi.org/10.1096/fj.14-251652">https://doi.org/10.1096/fj.14-251652</a>
- Findinier, J. (2023). Autolysin Production from Chlamydomonas reinhardtii. *Bio Protoc,* 13(13), e4705. https://doi.org/10.21769/BioProtoc.4705
- Huang, J., Tao, H., Chen, J., Shen, Y., Lei, J., Pan, J., Yan, C., & Yan, N. (2024). Structure-guided discovery of protein and glycan components in native mastigonemes. *Cell*, *187*(7), 1733-1744.e1712. <a href="https://doi.org/10.1016/j.cell.2024.02.037">https://doi.org/10.1016/j.cell.2024.02.037</a>
- Huang, K., Diener, D. R., Mitchell, A., Pazour, G. J., Witman, G. B., & Rosenbaum, J. L. (2007). Function and dynamics of PKD2 in Chlamydomonas reinhardtii flagella. *J Cell Biol*, 179(3), 501-514. <a href="https://doi.org/10.1083/jcb.200704069">https://doi.org/10.1083/jcb.200704069</a>
- King, S. M., & Witman, G. B. (1990). Localization of an intermediate chain of outer arm dynein by immunoelectron microscopy. *J Biol Chem*, *265*(32), 19807-19811.

- Köttgen, M., Buchholz, B., Garcia-Gonzalez, M. A., Kotsis, F., Fu, X., Doerken, M., Boehlke, C., Steffl, D., Tauber, R., Wegierski, T., Nitschke, R., Suzuki, M., Kramer-Zucker, A., Germino, G. G., Watnick, T., Prenen, J., Nilius, B., Kuehn, E. W., & Walz, G. (2008). TRPP2 and TRPV4 form a polymodal sensory channel complex. *J Cell Biol*, 182(3), 437-447. https://doi.org/10.1083/jcb.200805124
- Kottgen, M., Hofherr, A., Li, W., Chu, K., Cook, S., Montell, C., & Watnick, T. (2011). Drosophila sperm swim backwards in the female reproductive tract and are activated via TRPP2 ion channels. *PLoS One*, *6*(5), e20031. https://doi.org/10.1371/journal.pone.0020031
- Liu, P., Liu, Y., & Zhou, J. (2023). Ciliary mechanosensation roles of polycystins and mastigonemes. *J Cell Sci*, 136(3). https://doi.org/10.1242/jcs.260565
- Liu, P., Lou, X., Wingfield, J. L., Lin, J., Nicastro, D., & Lechtreck, K. (2020). Chlamydomonas PKD2 organizes mastigonemes, hair-like glycoprotein polymers on cilia. *J Cell Biol*, 219(6). https://doi.org/10.1083/jcb.202001122
- Nakamura, S., Tanaka, G., Maeda, T., Kamiya, R., Matsunaga, T., & Nikaido, O. (1996). Assembly and function of Chlamydomonas flagellar mastigonemes as probed with a monoclonal antibody [Research Support, Non-U.S. Gov't]. *J Cell Sci*, 109 (Pt 1), 57-62. <a href="http://www.ncbi.nlm.nih.gov/pubmed/8834790">http://www.ncbi.nlm.nih.gov/pubmed/8834790</a>
- Nievergelt, A. P., Diener, D. R., Bogdanova, A., Brown, T., & Pigino, G. (2023). Efficient precision editing of endogenous <em>Chlamydomonas reinhardtii</em> genes with CRISPR-Cas. *Cell Reports Methods*, *3*(8). <a href="https://doi.org/10.1016/j.crmeth.2023.100562">https://doi.org/10.1016/j.crmeth.2023.100562</a>
- Pazour, G. J., Sineshchekov, O. A., & Witman, G. B. (1995). Mutational analysis of the phototransduction pathway of Chlamydomonas reinhardtii. *Journal of Cell Biology*, 131(2), 427-440. <a href="https://doi.org/10.1083/jcb.131.2.427">https://doi.org/10.1083/jcb.131.2.427</a>
- Salas, M. M., Hargreaves, K. M., & Akopian, A. N. (2009). TRPA1-mediated responses in trigeminal sensory neurons: interaction between TRPA1 and TRPV1. *European Journal of Neuroscience*, 29(8), 1568-1578. https://doi.org/https://doi.org/10.1111/j.1460-9568.2009.06702.x
- Samanta, A., Kiselar, J., Pumroy, R. A., Han, S., & Moiseenkova-Bell, V. Y. (2018). Structural insights into the molecular mechanism of mouse TRPA1 activation and inhibition. *J Gen Physiol*, 150(5), 751-762. https://doi.org/10.1085/jgp.201711876
- Smith, G. D., Gunthorpe, M. J., Kelsell, R. E., Hayes, P. D., Reilly, P., Facer, P., Wright, J. E., Jerman, J. C., Walhin, J. P., Ooi, L., Egerton, J., Charles, K. J., Smart, D., Randall, A. D., Anand, P., & Davis, J. B. (2002). TRPV3 is a temperature-sensitive vanilloid receptor-like protein. *Nature*, 418(6894), 186-190. <a href="https://doi.org/10.1038/nature00894">https://doi.org/10.1038/nature00894</a>
- Strübing, C., Krapivinsky, G., Krapivinsky, L., & Clapham, D. E. (2001). TRPC1 and TRPC5 form a novel cation channel in mammalian brain. *Neuron*, *29*(3), 645-655. <a href="https://doi.org/10.1016/s0896-6273(01)00240-9">https://doi.org/10.1016/s0896-6273(01)00240-9</a>
- Tsiokas, L., Arnould, T., Zhu, C., Kim, E., Walz, G., & Sukhatme, V. P. (1999). Specific association of the gene product of <i>PKD2</i> with the TRPC1 channel. *Proceedings of the National Academy of Sciences*, 96(7), 3934-3939. <a href="https://doi.org/doi:10.1073/pnas.96.7.3934">https://doi.org/doi:10.1073/pnas.96.7.3934</a>
- Wang, Y., Yang, J., Hu, F., Yang, Y., Huang, K., & Zhang, K. (2023). Cryo-EM reveals how the mastigoneme assembles and responds to environmental signal changes. *J Cell Biol*, 222(12). https://doi.org/10.1083/jcb.202301066

- Watnick, T. J., Jin, Y., Matunis, E., Kernan, M. J., & Montell, C. (2003). A flagellar polycystin-2 homolog required for male fertility in Drosophila. *Curr Biol*, *13*(24), 2179-2184. https://doi.org/10.1016/j.cub.2003.12.002
- Witman, G. B., Carlson, K., Berliner, J., & Rosenbaum, J. L. (1972). Chlamydomonas flagella. I. Isolation and electrophoretic analysis of microtubules, matrix, membranes, and mastigonemes. *J Cell Biol*, *54*(3), 507-539. https://doi.org/10.1083/jcb.54.3.507
- Xiang, W., zur Lage, P., Newton, F. G., Qiu, G., & Jarman, A. P. (2022). The dynamics of protein localisation to restricted zones within Drosophila mechanosensory cilia. *Scientific Reports*, *12*(1), 13338. <a href="https://doi.org/10.1038/s41598-022-17189-w">https://doi.org/10.1038/s41598-022-17189-w</a>
- Zhao, Y., Wang, H., Wiesehoefer, C., Shah, N. B., Reetz, E., Hwang, J. Y., Huang, X., Wang, T. E., Lishko, P. V., Davies, K. M., Wennemuth, G., Nicastro, D., & Chung, J. J. (2022). 3D structure and in situ arrangements of CatSper channel in the sperm flagellum. *Nat Commun*, *13*(1), 3439. <a href="https://doi.org/10.1038/s41467-022-31050-8">https://doi.org/10.1038/s41467-022-31050-8</a>

#### **CHAPTER 4**

#### CONCLUSIONS AND FUTURE DIRECTIONS

## 4.1 Summary of dissertation

The project's primary goal was to explore the structure of PKD2-mastigoneme complex in the cilia of Chlamydomonas reinhardtii. It was known from previous work that PKD2 forms two zones inside. The two zones are distinct in terms of their position and nature. They are categorized into distal (covering 2/3rd of cilia) and proximal zone. In the distal zone, PKD2 has a stable connection to axoneme making it stationary in nature. In this stationary zone, PKD2 anchors mastigonemes on the surface of cilia. Mastigonemes are a hair-like structures, of which the extracellular glycoprotein MST1 was identified as the main component (Dai et al., 2024; Huang et al., 2024; Liu et al., 2020). In the distal zone, PKD2-Mastigoneme complexes form rows along DMT 4 and 8 of the nine DMTs (Liu et al., 2020). When PKD2 or/and mastigonemes are absent from cilia of *Chlamydomonas*, the cells have a subtle phenotypic defect in motility, indicating a role of PKD2-mastigoneme complexes in high velocity swimming. The proximal PKD2 is more mobile in nature and PKD2 particles can be observed hopping on and off the axonemes and moving by IFT or diffusion. This arrangement suggests the presence of PKD2hetero complexes with unique interactors in in different regions of *Chlamydomonas* cilia. This formed the most alluring question about PKD2: "How are the zones of PKD2 rows in the ciliary membrane established?". To answer this question, delving into the complex was necessary.

# 4.2 SIP: A novel single pass transmembrane protein

This led us to undertake the first strategy of immuno-purifying PKD2-mNG complexes from the Chlamydomonas cilia. We used control, pkd2 PKD2-mNG (rescue) and mst1 pkd2 PKD2-mNG strains for isolating the PKD2 complexes. pkd2 PKD2-mNG has intact PKD2 zones intact, whereas mst1 pkd2 PKD2-mNG has diminished distal zone. With the usage of these two test strains, we hoped to distinguish between the PKD2 complexes in the distal and proximal zones. This strategy led to the discovery of novel single-pass transmembrane protein small interactor of PKD2 (SIP). SIP has structural homology with the TMH1 and initial part of the extracellular TOP domain of PKD2. sip mutants lack mastigonemes and swim slow. In these mutants, PKD2 is nearly absent from cilia, indicating that SIP is involved in the establishment of both the PKD2 zones. Further, defect in SIP expression causes disruption in PKD2 stability and impacts its proteolytic processing (Das et al., 2023). While SIP is a component of the PKD2mastigoneme complex, it not specific to either PKD2 zone but a common factor of both zones. It is further unclear how the 1TMH protein SIP could contribute to the formation of mastigonemes on PKD2. In conclusion, we expect additional PKD2-associated proteins to participate in the formation of distinct PKD2 zones.

## 4.3 MST3: A 5-TMH protein of distal PKD2 complex

To determine the proteins which are distinct in both the complexes. Thus, we incorporated our second strategy of proximity labelling. When cilia are fractionated into membrane-matrix (MM) and axoneme, PKD2, being a transmembrane protein, gets majorly separated into the MM fraction but a reasonable amount also stays attached to axoneme.

Conceivably, a protein critical for PKD2 localization could remain attached to the insoluble axonemal fraction. Therefore, proximity labelling, using BioID with PKD2-miniTurbo, was our second strategy. Seemed a promising approach to catch the whole of the PKD2 interactome. Pull-down of biotinylated proteins from the cilia of pkd2 PKD2-miniTurbo enabled detection of another novel 5-TMH protein named MST3. Endogenous tagging of MST3 showed that it localizes in the distal part of cilia similar to the stationary PKD2. Tagging endogenous PKD2 with mNeon Green in mst3 knock-out strain showed the near absence of PKD2 in the distal zone. This indicated that MST3 is a part of the distal PKD2 complexes. During the course of these studies, MST3 was also discovered independently via cryo-electron microscopy as the backbone protein of the mastigoneme structure (Dai et al., 2024). Around 82 copies of MST1 are attached to the extracellular N-terminal domain of MST3. Structural analysis of MST3 revealed that it has an incomplete 5-TMHs PKD2-like domain lacking the first transmembrane domain. Structural modeling showed that SIP, which has structural homology with the first transmembrane domain of PKD2, beautifully completes the PKD domain of MST3. Thus, PKD2, MST3 and SIP form complex in the distal cilia with stochiometric ratio of 3:1:1 respectively, which together with MST1, constitutes the PKD2-mastigoneme complex.

# 4.4 Generation of an In-vivo Tool / Generation of PKD2-mNG (CRISPR) – A Biological tool

Data mining via structural predictions showed that the *Chlamydomonas* genome encodes seven additional MST3-like 5-TMH proteins and three of them are present in cilia, based on Mass-Spec data. Alphfold2 predictions of the protein domains indicated that SIP interacts with each of them to complete their incomplete 5-TMH PKD domain. Therefore, the three ciliary proteins looked like potential PKD2 interactor and the genes are Cre12.g539650, Cre13.g569550

and Cre09.g400850.To access the potentiality of these gene products to be in ciliary PKD2 interactome, an endogenously tagged PKD2-mNG (g1 PKD2-mNG (CRISPR)) strain via CRISPR-CAS9 was generated. This strain played an essential role of a biological tool because it allowed us to easily observe the impact of defects in the aforementioned three genes on PKD2-mNG in cilia. Thus, we generated single and double knockout strains for the three ciliary 5-TMH proteins and analyzed the distribution of PKD2-mNG in their cilia.

## Distribution of CTL4-mNG and Knock-out of ctl4

Endogenously tagged CTL4-mNG was observed in both the proximal and distal PKD2 zone. The distal CTL4-mNG mostly stationary in nature and is organized into two interrupted rows. while it was more mobile in the proximal zone, as observed for tagged PKD2 and SCV as well as moves by IFT or diffusion. Its amount and distribution in cilia varied strongly between cells with a notable subset of cells showing CTL4-mNG enriched in the distal zone. Knock-outs of CTL4 showed a normal distribution of PKD2-NG in cilia and TEM analysis revealed the presence of mastigoneme rows. This showed that defect in CTL4 brings no change to PKD2-mNG indicating that either CTL4 is not a PKD2 interactome (the obvious one) or CTL4 is redundant for other protein(s) in the complex.

## Distribution of SCV-mNG and knockout of SCV

Endogenous tagging of SCV with mNG showed SCV-mNG in proximal cilia forming two rows and was observed to move by IFT as well as diffusion as seen in the case of proximal PKD2 too. One unique observation of SCV-mNG was that it is strictly restricted in the proximal

region without any distal signal. SCV stood out because in *scv*knockout endogenous PKD2-mNG localization was disrupted due to obliteration of the proximal PKD2 zone which was exactly opposite to *mst3* knock-out. These data are strong suggestive of SCV being a partner of PKD2 in the proximal zone and that it is required for the establishment of proximal PKD2 rows.

# scv mst3 PKD2-mNG (Double knock-out)

Generation of double knock-out *scvmst3* PK2-mNG, showed the disruption of proximal as well as the distal zones, as was expected from the observation of the respective single knock-out strains. This indicates that SCV and MST3 are primarily required for the formation of the proximal and distal zone formation of PKD2, respectively. However, the double knock-out *scvmst3* does have ciliary PKD2-mNG present as random dots moving via IFT and diffusion, in addition to occasionally docked signals. This suggests that additional MST3 and SCV independent PKD2 complexes could be present in cilia. Besides either a possible PKD2 homotetramer or a heterotertramers with one of the 5-TMH proteins is an attractive option. Thus, presence of PKD2-mNG in cilia when all of the three proteins are missing indicates that either more PKD2 heteromer(s) or PKD2 homomer also exist in the cilia independent of the aforementioned three heterocomplexes and, absence would confirm that we have determined all the three hetero-complexes of PKD2 in *Chlamydomnasi* cilia. Therefore, we successfully discovered four novel proteins: SIP, MST3, PIP and 550 that are in the PKD2 interactome.

#### Knockout of 550

With the possibility of exploring the presence of more PKD2 heteromers, we studied the remaining 5-TMH protein too. Knockout of 550 had no effect on the proximal and distal ciliary PKD2-mNG and ciliary PKD2-mNG seemed unimpacted. Kymogram analysis of 550 PKD2-mNG showed wildtype PKD2-mNG presence.

## Knock-out of SIP

To explore the possibility that SIP is an obligate requirement for the PKD2 transport and complex assembly in cilia, we generated *SIP*<sup>CRISPR-KO</sup>. TIRFM images of the strain showed the obliteration of the PKD2 zones and presence of random PKD2-mNG dots. It is possible that in absence of SIP, a very negligible PKD2-mNG is entering the cilia and possibly is forming either homo-tetramer or a complex with other 5-TMH proteins. Kymogram analysis showed that the PKD2-mNG in *SIP*<sup>CRISPR-KO</sup> PKD2-mNG is stationary in nature. This again opens a new direction to examine the PKD2-mNG complexes in absence of SIP by mass-spec and structural studies.

## 4.5 TRP Proteins in Sub Ciliary Compartments

There are several lines of evidence of different TRP proteins localizing in cilia with proximal and distal domain markings. For example, the cilia of chordotonal neurons of *Drosophila* have mechanosensory TRP channel, NompC in the distal region near ciliary cap and heteromeric TRPV channels in the proximal region (Inactive/Nanchun) (Xiang et al., 2022). Similar to these, the PKD2 orthologue AMO is located near the tip of sperm cilia. (Kottgen et al.,

2011; Watnick et al., 2003). TRP11 in *Chlamydomonas* is reported to localize in the proximal end of cilia and possibly aids in mechanosensation, but it is absent in the cell body (Fujiu et al., 2011). In the head of sperm there is a presence of septin ring which might work as a barrier to regulate the localization of proteins and maintain a separation between the midpiece and principal piece of sperm. Our protein of interest Chlamydomonas PKD2 also localizes in proximal and distal zones separated by a gap region (Liu et al., 2020). There is either a possibility of marker proteins distinguishing between the proximal and distal zones of PKD2 or the protein themselves are the marker.

Here, we successfully discovered the PKD2 zonal markers in cilia of *Chlamydomonas*, which is formed by the outshining pair of my project i.e., MST3 (**distal marker**) and SCV (**proximal marker**). we are proposing a common design principle for PKD2. The interactors of PKD2 are transmembrane protein with an extended N-terminal domain as in mammals PKD2 interacts with PKD1 and in green algae PKD2 interacts with a complex of SIP and 5-TMH protein.

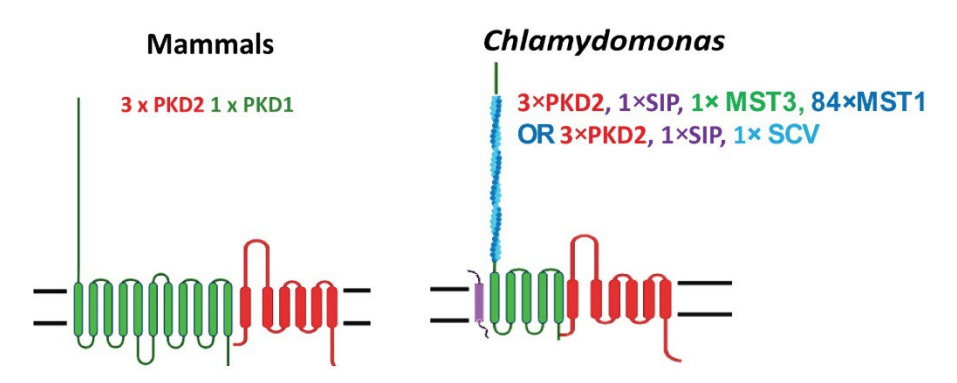


Figure 4.1) Proposed design principle of PKD2: In mammals PKD2 interact with PKD1 and in Chlamydomonas PKD2 interact with a complex of SIP and 5-TMH proteins.

# 4.6 Future directions for PKD2 complexes

The ciliary PKD2 complexes has been explored completely. But, the mass-spec data also showed the presence of four more 5-TMH proteins with possible cell body localization. In the cell body of *Chlamydomonas*, PKD2 localizes in the apical region and accumulates in discrete dots on the peripheral surface. Thus, characterization of these proteins via endogenous tagging and pull-down assays will enable in verifying their connection with the hetero-PKD2 complex of cell body. Exploring non-ciliary PKD2 can reveal how PKD2 behaves differently in cell body from cilia. *pkd2* mutants, likely lacking all complexes of the 3x PKD2 1x 5-TMH/SIP type, swim with moderately reduced velocity and no other phenotypical defects have been identified. This suggests that a functional analysis of these complexes will be challenging.

As shown by CRISPR-CAS9 endogenously tagged SCV, MST3 and CTL4 localize in distinct PKD2 zones of cilia. MST3 and often CTL4 localize in the distal PKD2 area whereas SCV remains strictly restricted in the proximal area. It is intriguing to find the answers of: "how is the localization of these PKD2 interactors determined distinctively?" and "What demarcates the proximal area and the distal area without any membranous separation?" Clearly, the unstructured and heterogenous C-terminal domains of the 5-TMH proteins are attractive candidates as drivers of PKD2 complex targeting. In the postulated complexes, the C-termini of the 5-TMH proteins give individuality on the intracellular surface of the channel complexes. We hypothesized that the c-termini of the 5-TMH proteins interact directly with the axoneme and are the reason behind the compartmental separation of the PKD2 complexes. To explore this possibility, we are planning to undertake two approaches: first of deleting the C-termini of both MST3 and SCV and, second of exchanging the c-termini of MST3 with SCV as well as vice-a-versa. We hypothesize that the deletion of C-terminus of MST3 can lead to establishment of

multiple mastigoneme rows instead of the typical two and exchanging the C-terminus of MST3 with that of SCV also can lead to encroachment of distal mastigoneme rows into the proximal region. Deletion of the C-terminus of SCV can also change the location of the proximal PKD2. These experiments hold a strong ground to give a clear understanding of the importance of C-termini of the 5-TMH proteins in creating the zones of PKD2.

## 4.7 References:

- Dai, J., Ma, M., Niu, Q., Eisert, R. J., Wang, X., Das, P., Lechtreck, K. F., Dutcher, S. K., Zhang, R., & Brown, A. (2024). Mastigoneme structure reveals insights into the O-linked glycosylation code of native hydroxyproline-rich helices. *Cell*, *187*(8), 1907-1921.e1916. https://doi.org/https://doi.org/10.1016/j.cell.2024.03.005
- Das, P., Mekonnen, B., Alkhofash, R., Ingle, A., Workman, E. B., Feather, A., Liu, P., & Lechtreck, K. F. (2023). Small Interactor of PKD2 (SIP), a novel PKD2-related single-pass transmembrane protein, is required for proteolytic processing and ciliary import of Chlamydomonas PKD2. *bioRxiv*. https://doi.org/10.1101/2023.06.13.544839
- Fujiu, K., Nakayama, Y., Iida, H., Sokabe, M., & Yoshimura, K. (2011). Mechanoreception in motile flagella of Chlamydomonas. *Nature Cell Biology*, *13*(5), 630-632. <a href="https://doi.org/10.1038/ncb2214">https://doi.org/10.1038/ncb2214</a>
- Huang, J., Tao, H., Chen, J., Shen, Y., Lei, J., Pan, J., Yan, C., & Yan, N. (2024). Structure-guided discovery of protein and glycan components in native mastigonemes. *Cell*, *187*(7), 1733-1744.e1712. <a href="https://doi.org/10.1016/j.cell.2024.02.037">https://doi.org/10.1016/j.cell.2024.02.037</a>
- Kottgen, M., Hofherr, A., Li, W., Chu, K., Cook, S., Montell, C., & Watnick, T. (2011). Drosophila sperm swim backwards in the female reproductive tract and are activated via TRPP2 ion channels. *PLoS One*, *6*(5), e20031. https://doi.org/10.1371/journal.pone.0020031
- Liu, P., Lou, X., Wingfield, J. L., Lin, J., Nicastro, D., & Lechtreck, K. (2020). Chlamydomonas PKD2 organizes mastigonemes, hair-like glycoprotein polymers on cilia. *J Cell Biol*, 219(6). https://doi.org/10.1083/jcb.202001122
- Watnick, T. J., Jin, Y., Matunis, E., Kernan, M. J., & Montell, C. (2003). A flagellar polycystin-2 homolog required for male fertility in Drosophila. *Curr Biol*, *13*(24), 2179-2184. https://doi.org/10.1016/j.cub.2003.12.002
- Xiang, W., zur Lage, P., Newton, F. G., Qiu, G., & Jarman, A. P. (2022). The dynamics of protein localisation to restricted zones within Drosophila mechanosensory cilia. *Scientific Reports*, *12*(1), 13338. <a href="https://doi.org/10.1038/s41598-022-17189-w">https://doi.org/10.1038/s41598-022-17189-w</a>